Evaluation of CRPV-based cell systems for the therapeutic studies of papilloma virus associated head and neck cancer

Dissertation

zur

Erlangung des Doktorgrades

der Naturwissenschaften

(Dr. rer. nat.)

dem

Fachbereich Pharmazie

der Philipps-Universität Marburg

vorgelegt von

Ghazala Ambreen

aus **Sargodha, Pakistan**

Marburg/Lahn **2021**

Erstgutachter: **Prof. Dr. Udo Bakowsky**

Zweitgutachter: **Prof. Dr. Robert Mandic**

Eingereicht am **10.11.2020**

Tag der mündlichen Prüfung am **13.01.2021**

Hochschulkennziffer: 1180

Ich versichere, dass ich meine Dissertation

"Evaluation of CRPV-based cell systems for the therapeutic studies of papilloma virus associated head and neck cancer"

selbständig ohne unerlaubte Hilfe angefertigt und mich dabei keiner anderen als der von mir ausdrücklich bezeichneten Quellen bedient habe. Alle vollständig oder sinngemäß übernommenen Zitate sind als solche gekennzeichnet.

Die Dissertation wurde in der jetzigen oder einer ähnlichen Form noch bei keiner anderen Hochschule eingereicht und hat noch keinen sonstigen Prüfungszwecken gedient.

Marburg, den 10.11.2020

……………………

Ghazala Ambreen

AUTHOR'S DECLARATION

I declare that this thesis titled

"Evaluation of CRPV-based cell systems for the therapeutic studies of papilloma virus associated head and neck cancer"

has been written entirely by myself and is a record of work performed by myself. The research was carried out at the Institut für Pharmazeutische Technologie und Biopharmazie, University of Marburg, at the campus Ketzerbach 63 (old location) and Robert-Koch-Straße.4 (new location) and the Klinik für Hals-, Nasen- und Ohrenheilkunde, Universitätsklinikum Gieβen und Marburg under the supervision of Prof. Dr. Udo Bakowsky and Prof. Dr. Robert Mandic.

This thesis has not been submitted in any form elsewhere for a higher degree

Marburg, 10.11.2020

…………………….

Ghazala Ambreen

Die vorliegende Arbeit entstand auf Anregung und unter Leitung von

Herrn Prof. Dr. Udo Bakowsky

Und

Herrn Prof. Dr. Robert Mandic

am Institut für Pharmazeutische Technologie und Biopharmazie der Philipps-Universität Marburg

Universitätsklinikum Gießen und Marburg, Philipps-Universität Marburg

Table of Contents

CHAPTER NO 4

Construction, and validation of CRPV E6 & E7 recombinant plasmids and their transient expression analysis in eukaryotic cells *63*

CHAPTER NO 1

Introduction

1.1   *Animal model systems for human head and neck squamous cell carcinoma (HNSCC)*

Head and neck squamous cell carcinoma (HNSCC) is ranked as the sixth most common form of diagnosed cancers in the world and responsible for 1-2% of all cancer death [1] [2] . At the time of diagnosis, approximately 50% of all patients with HNSCC have life expectancy of 5 years [3] . With increasing rate of head and neck cancer cases, there is much need of model system that should be anatomically and pathophysiologically sufficient to study head and neck cancer. Literature reveals designing and use of animal model that closely mimic histopathology and molecular pathogenesis of human HNSCC would be an attractive option for better understanding of complex histological, molecular & genetic changes in disease and also in assessing the feasibility of treatment strategies against HNSCC [4] .

Different types of preclinical HNSCC animal models were designed and developed to study various genetic, molecular and immuno-regulatory processes leading to neoplastic transformation of head and neck cancer. These models include

    i.   Naturally occurring animal models (rare) i.e. sheep ear squamous cell carcinoma (SCC) [5] and bovine ocular SCC [6]

    ii.   Chemically (carcinogen) induced models like mouse/rat SCC [7] [8] and hamster cheek pouch carcinoma [9]

    iii.   Model induced by transplantation of animal carcinoma tissue into immunocompetent [10] [11] or human tissue into immunodeficient [12] animals

    iv.   Transgenic mouse models [13]

    v.   Models induced by inoculation of transplantable cell lines includes prostrate derived SCC in Fischer rat [14] and skin SCC in Wag-Rij rat [15]

Each of the these animal models has its own advantages and disadvantages [16]. Limitations to use of models include death of experimental animals caused by carcinogen toxicity, non-functional host immune response, a very little or no lymph node metastasis in case of nude mice, transgenic mouse models don't reflect human anatomic and physiological conditions and lack of syngeneic strains contributes to tissue rejection [16] [17]. Lack of true representation of clinical data must limit interpretation of studies using such models.

1.1.1 Papilloma virus associated animal as a model for HNSCC

Despite designing various animal models induced by application of carcinogen or transplantation of carcinoma tissue, naturally occurring papilloma virus associated animal tumor appears to be a good choice to study human papillomavirus (HPV) associated HNSCC [18]. Cottontail rabbit papilloma virus (CRPV) is a natural pathogen of the rabbit. In comparison to rodents and mice, rabbits are convenient sized animals, easy to handle. CRPV induced rabbit papilloma is distinctively comparable in etiology and mechanism with many naturally occurring lesions induced by papilloma viruses [19]. The life cycle deregulation of the cell induced by CRPV has some resemblance with that of high-risk human papilloma virus, which are implicated in the pathogenesis of HNSCC [20]. CRPV like HPV, induces papillomatosis and carcinogenesis of the squamous epithelium and metastasize to regional lymph nodes, mimicking the natural pattern of HPV associated human HNSCC [21]. Therefore CRPV tumor models are suitable systems to study HNSCC [22].

1.1.2 CRPV associated VX2 carcinoma in rabbits

1.1.2.1 Historical Background

Cottontail rabbit papilloma virus is one of animal papillomaviruses and was discovered in Cottontail rabbits in Midwestern United States. A case reported in the 1930s in which hunters found unusual animals with strange, horn like protrusions on the face and neck of shot rabbits lead to the discovery of cottontail rabbit papilloma virus by Richard Shope, therefore it is also known as the Shope papilloma virus (SPV) and being involved in the formation of skin tumors [19].

Cottontail or Shope papilloma virus was characterized for the first time in 1933 as a transmissible agent by Shope and Hurst [16] [18] [21]. Shope inoculated the isolated virus particles from hunted wild rabbits to a group of 10 domestic rabbits and observed papilloma formation leading to invasive and metastatic malignant carcinoma in seven animals carrying papilloma for more than 200 days [23]. These carcinomas can be transmitted both to wild rabbits and domestic rabbits, however domestic strain cannot transmit carcinoma to domestic rabbit [16].

In 1936, Kidd et al reported the first successful transplantation of carcinoma tissue on Dutch belted rabbits and designated as "V1" but on second transfer, papilloma growth was not remarkable [24]. Successful transplantation and propagation of squamous cell carcinoma derived from virus induced rabbit papilloma was observed in 14 successive groups of rabbits and was called as "Carcinoma V2" [25]. Thenceforth, V2 squamous cell carcinoma was reported to be successfully transplanted and grew rapidly not only in different rabbit species but also in guinea pigs, mice, hamster and rats [26]. This propagated carcinoma "V2" was renamed as "VX2" carcinoma after World War II [27]. There were observations about sera derived from animals carrying VX2 carcinoma in its 46th generation failing to neutralize the virus, therefore tumor lost ability to immunize rabbit against papilloma virus [27].

1.1.2.2 Biology of CRPV and Its role in oncogenesis

Papilloma viruses are double stranded DNA viruses causing induction of cutaneous and mucosal epithelial proliferations in humans and animals. These lesions persist and can progress to invasive carcinomas. CRPV is a member of Papillomaviridae family. CRPV and HPV1a are found to be the most related papillomaviruses (PV), as both of viruses target squamous cell epithelia of the skin. Also, sequencing of Shope papilloma virus genome in 1984 showed substantial similarities to HPV1a [28]. Further structural analysis of the papillomavirus capsid was illustrated using electron microscopy and confirmed that CRPV and HPV type 1 have identical structures [29].

The cottontail rabbit papilloma virus induces papilloma formation and these papillomas can progress to skin carcinomas. The life cycle of papillomaviruses begins with infections of cells in the basal and parabasal layers of epithelium. For completion of the viral life cycle, the differentiation of cells is essential. The life cycle of PVs can be divided into early and late phases. The initiation of the early phase takes place in basal and parabasal layers containing actively proliferating cells. In the early phase, viral transforming proteins along with viral replication proteins also known as regulatory proteins are responsible for induction of papilloma formation and for maintaining low copy numbers of episomal viral genome. The late phase of the viral life cycle occurs during differentiation of the infected basal/parabasal cells [30] [31].

CRPV encodes early proteins (E1, E2, E4, E5, E6 & E7) and late proteins (L1 & L2) **(Figure 1)**. E1 and E2 are early viral proteins and involved in viral genome replication as well as also in viral

transcriptional regulation [32]. E4 is correlated with viral DNA amplification and there are certain findings that the productive phase of the CRPV life cycle in New Zealand white (NZW) and cottontail rabbits is dependent on the expression of full length CRPV E4 protein because in its absence onset of DNA amplification and L1 expression were abrogated [33]. L1 and L2 are late viral proteins and are responsible for viral assembly. CRPV E8 showed little transforming activity in vitro [34]. The role of CRPV E8 in papilloma growth but papilloma formation has been reported [35]. CRPV encodes three transforming proteins; LE6, SE6 and E7. Each of these proteins is responsible for epithelial proliferation and viral DNA replication.
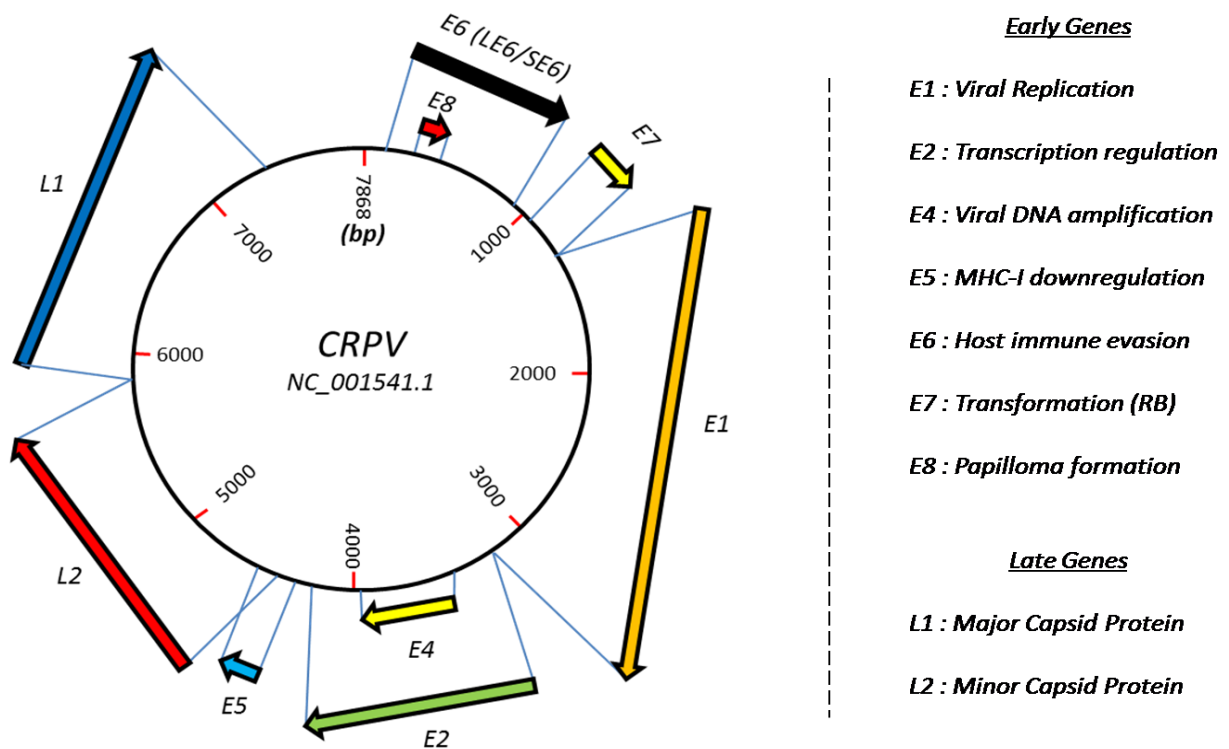
Figure 1. Genomic Organization of CRPV genome. Schematic representation of CRPV genome showing location of early (E) and late (L) genes (modified from Christensen et al., 2017) [36]

In comparison with other papillomavirus strains, the E6 protein in CRPV is almost twice the size. Studies on CRPV E6 and E7 proteins in rabbit keratinocytes showed that CRPV E7 protein like the HPV E7 protein binds to the tumor suppressor protein pRb while CRPV E6 protein neither degrades p53 nor binds to E6AP [37].Based on immunostaining and in situ hybridization results, the CRPV E4 protein was detected in intermediate epithelial layers whereas CRPV E6 and E7 proteins were found to be more expressed in lower basal layers of the epithelium, CRPV L1 protein was detected in terminally differentiated layers [33]. Similarly as observed for HPV associated HNSCC

tumors, the CRPV related oncogenes E6 and E7 are implicated in transformation, tumor growth and progression and therefore are considered as major therapeutic targets.

1.1.2.3   VX2 auricular carcinoma

For nearly 20 years, the auricular VX2 carcinoma of New Zealand white rabbits serves as a model system for head and neck squamous cell carcinomas [38] [39] and was originally designed by van Es et al [40]. The VX2 auricular model resembles morphologically and pathophysiologically with human HNSCC and can be deployed in the evaluation of novel anticancer therapies as well as diagnostic procedures [41] [28].

VX2 carcinoma cells can be considered as an equivalent to HPV positive HNSCC cells. From this perspective, it is of paramount importance to establish a VX2 cell line using standard cell culture techniques which would allow to perform *in vitro* studies, thereby helping to reduce animal experiments.

1.1.2.4   In vitro generation of a VX2 cell line

From the mid-sixties, literature revealed establishment of *in vitro* cell line from VX2 carcinoma [42]. The idea behind generating VX2 cell line was to maintain tumor in culture for in vitro studies and also to avoid frequent freezing, thawing and storage of the tumor. By developing and maintaining a VX2 cell line in culture, there would be no need of serial transplantation of tumors in rabbits, thereby reducing the number of animals for experimental purposes.

For testing the potential of preventive and therapeutic agents, as well as for further understanding of the biological mechanisms of carcinogenesis and progression, such a cell line would be a good alternative to the animal experiments. The cell lines represents the experimental models for assessing the cell viability, toxicity and drug efficacy in the tumor cells and would also help in reduction of direct animal use and associated administration formalities like getting permission grants from animal ethics committee.

Before development of VX2 cell lines, scientists used different methods for storage of VX2 tissue or VX2 cell suspension for serial transplantation of VX2 tumor in rabbits. Galasko and coworkers observed after using different techniques for preservation of the tumor that repeated freezing of tumor cell suspensions resulted in major loss of cell viability and in some cases tumor growth became slower, no metastases were seen [43] [44].

From the literature, there are several reports about generation of *in vitro* cell lines derived VX2 carcinoma. In 1967, Osato and Ito tried to develop a VX2 cell line from minced VX2 carcinomas but unfortunately lost the cell line at its 10th passage. After this, Osato developed another cell line named as VX7 but it was less anaplastic than VX2 [45]. Voelkel in 1975 and Yoenda in 1985 reported about the isolation of clonal strains from the VX2 tumor. These clonal strains named as EVX2 and VX2-L, were generated only for in vitro studies of prostaglandin E2 synthesis and calcium metabolism respectively and not for re-implantation purposes [46] [47].

Easty in 1982 in his research had given a detailed description about cell culture conditions required for the establishment of a VX2 cell line that could be maintained in culture for several months [42]. In 1985, there were reports about two CRPV associated VX2 cell lines (VX2-T & VX2-R), that were generated on basis of their keratinocyte differentiation, tumorigenicity and transplantability potential [48]. At the moment, VX2 carcinoma cells are available as frozen tissue or serially transplantable VX2 tumor suspension [49]. Despite single reports about VX2 carcinoma derived cell lines, the few sources that can be found are either discontinued (e.g. ATCC® CRL-6503™), not readily available or show limited characterization. Therefore, the intention of current study is to generate and characterize a VX2 cell line from fresh VX2 tumor.

1.2   *Photodynamic therapy (PDT) as a treatment regimen*

The standard regimen for the treatment of cancer includes surgery, chemotherapy and radiation. The side effects of these treatments can result in structural deformities, scars and hyperpigmentation [50] [51]. To reduce the toxicity and avoid side effects, alternative treatment strategies have been proposed. Photodynamic therapy is one of less invasive modalities that can be used instead of conventional therapies.Papillomaviruses belong to a group of tumor viruses that have been associated with multiple cancers including cervical, anogenital and a major subset of head and neck squamous cell carcinomas (HNSCC) which constitute about 4.5% of all solid

tumors [52]. HNSCC is ranked as the sixth most common form of cancer being responsible for 1-2% of all cancer deaths [1] [2]. PDT is considered as a well suited therapy in the treatment of head and neck squamous cell carcinomas because of its little effects on the underlying tissues [50].

Disease recurrence is the major issue associated with HNSCC and further additional anticancer treatments (surgery or chemotherapy) cannot be salvaged by patients, therefore in that cases, PDT seems to be great alternative treatment. Literature reveals that PDT has an efficacy similar to conventional therapies in the treatment of early head and neck cancer and 75% of treatment response sustained for 2 years after photodynamic therapy [53]. Studies are also being conducted to evaluate the palliative effects of PDT in advanced stages of head and neck cancers and 58-70% of patients showed positive response to palliative effects. Therefore, PDT has been considered an effective approach in treatment of head and neck cancer.

The advantages of photodynamic therapy include limited tissue damage as illuminated light is restricted only to the photosensitized area, no major long-term systemic side effects are seen. Additionally, PDT has no interaction with chemo and radiotherapy and can be repeated as needed without destructive effects [54] [55]. In this thesis, photodynamic therapy as a treatment modality was addressed.

1.2.1 History of PDT

For more than three thousand years, light has been used by ancient Egyptians, Indians and Chinese to treat diseases like rickets, psoriasis and skin cancer [56] [57]. This therapy was re-emerged in the late 18th and the early 19th century and rediscovered by Arnold Rikli, Niels Finsen, Oscar Raab and Herman von Tappeiner [58].

In 1898, Oscar Raab in his research for the first time showed the cytotoxic effects of acridine and light, when used in combination, on paramecium caudatum [59]. Arnold Rikli is known as pioneer of modern phototherapy- light only. He was the first in the 19th century to introduce sunbathing as treatment of chronic diseases [60]. Niels Finsen used red light for prevention of small pox pustules formation and ultraviolet light for treatment of cutaneous tuberculosis [54].

In 1904, Prof Hermann von Tappeiner, one of the pioneers of photobiology from the University of Munich introduced the term "photodynamic therapy" and reported "presence of oxygen" as

necessary element for photosensitization [61]. Herman von Tappeiner and A.Jesionek treated skin tumors using eosin and white light. Friedrich Meyer Betz was among the first to investigate PDT along with porphyrins in humans. In 1975, Thomas J. Dougherty, a developer of modern photodynamic therapy, treated cancer for the first time in preclinical models. Thomas Dougherty and his coworkers found that a combination of HPD (hematoporphyrin derivatives) and red light causes eradication of mammary tumor growth in mice [62]. J.F.Kelly and his coworkers in 1976 reported tumor destruction in bladder carcinoma using red light activated HPD derivatives [63]. In 1994, the FDA approved PDT with photofrin for the palliative treatment of esophageal cancer [57].

1.2.2   Components of PDT

Photodynamic therapy (PDT) has two major components

i)   Photosensitizer

A photosensitizer is a substance that can be activated upon exposure of light such as UV or visible light. The photosensitizers can be administered to the targeted site through topical application or systemic routes. An ideal photosensitizer possesses no dark toxicity, high photo activity, low manufacturing cost, stability, rapid clearance from the normal tissues and the strong absorption at wavelength range of 630-800nm [64]. A number of naturally occuring and synthetic compounds are used as photosensitizers as mentioned in **Table 1**.

Table 1. A list of natural and synthetic photosensitizers

Natural Photosensitizer [65]	Synthetic dyes [66]
Curcumin, Chlorine e6, Indocyanine green, Hypericin, Riboflavin, Porphyrin derivatives	Methylene blue, Toluidine blue, Rose Bengal, Squaraines

Photofrin, ALA and its ester derivatives are the clinically approved photosensitizers for the treatment of breast, esophageal, bladder, cervical and ovarian cancers [67]. A large number of studies have been conducted to achieve targeted PDT by attaching moieties having greater affinity toward

cancer cells. These targeted moieties include monoclonal antibodies [68], proteins like transferrin [69], epidermal growth factor [69] and somatostatin[70]. Photodynamic therapy in combination with chemotherapeutics like doxorubicin, paclitaxel, mitomycin and cisplatin can potentially induces more antitumor effects and have been studied in preclinical studies [71].

ii)   Light source

The light source with appropriate wavelength is the second major component of photodynamic therapy that is used to activate the photosensitizer to produce the desired therapeutic effect. There are three types of light systems for the photodynamic therapy [72].

a-   diode laser systems

b-   non-coherent light sources such as tungsten filament, halogen and phosphor coated sodium lamps, preferentially for the treatment of large areas

c-   light emitting diodes

The choice of light source depends on the type , location of photosensitizer and the dose of light to be delivered. Lamps are suitable for superficial tumors i.e skin and oral cavity. Diode lasers are lighter, portable and cheap. The light can be focussed and penetrated deep into the target tissue by coupling diode laser to optical fibres through specially designed illuminator tips such as microlens, or a cylindrical or spherical diffuser. Microlens are suitable for flat surfce treatments like PDT of skin. Diffusing tips can be utilized in interstitial PDT [73]. Diffuser ballons can be used for the irradiation of interior tissues such as pleural cavity, larynx or esophagus [74].

1.2.3 Mechanism of action of PDT

Photodynamic therapy (PDT) is a promising non-invasive therapeutic procedure involving administration of nontoxic photosensitizers (PS) followed by application of light with specific wavelengths for activation of these photosensitizers [75] [76]. After exposure to light, PS absorb photons and are transformed from a ground state to an excited triplet state. The excited triplet can undergo two different types of reactions; Type I and Type II reaction as illustrated in **Figure 2**.

In Type I reaction, the excited photosensitizer can react directly with cellular molecules (lipids, proteins and nucleic acids) to transfer one electron to the substrate leading to formation of radical

species and these radicals react with oxygen to generate reactive oxygenated products (ROS).In Type II reaction, the excited photosensitizer may generate excited state singlet oxygen ($^1O_2$) after transferring directly its energy to ground state molecular oxygen [77]. The resulting singlet oxygen is highly reactive and very toxic. In the biological systems, the singlet oxygen is $< 0.04\mu s$. Both Type I and Type II occurs at the same time, the ratio between Type I and Type II reactions depends on PS type being used, concentration of substrate and oxygen and also binding affinity of PS with substrate. Due to high reactivity and short life of oxygen radicals, the effects of PDT are restricted only to the area of PS localization, usually within radius of 20nm [78].
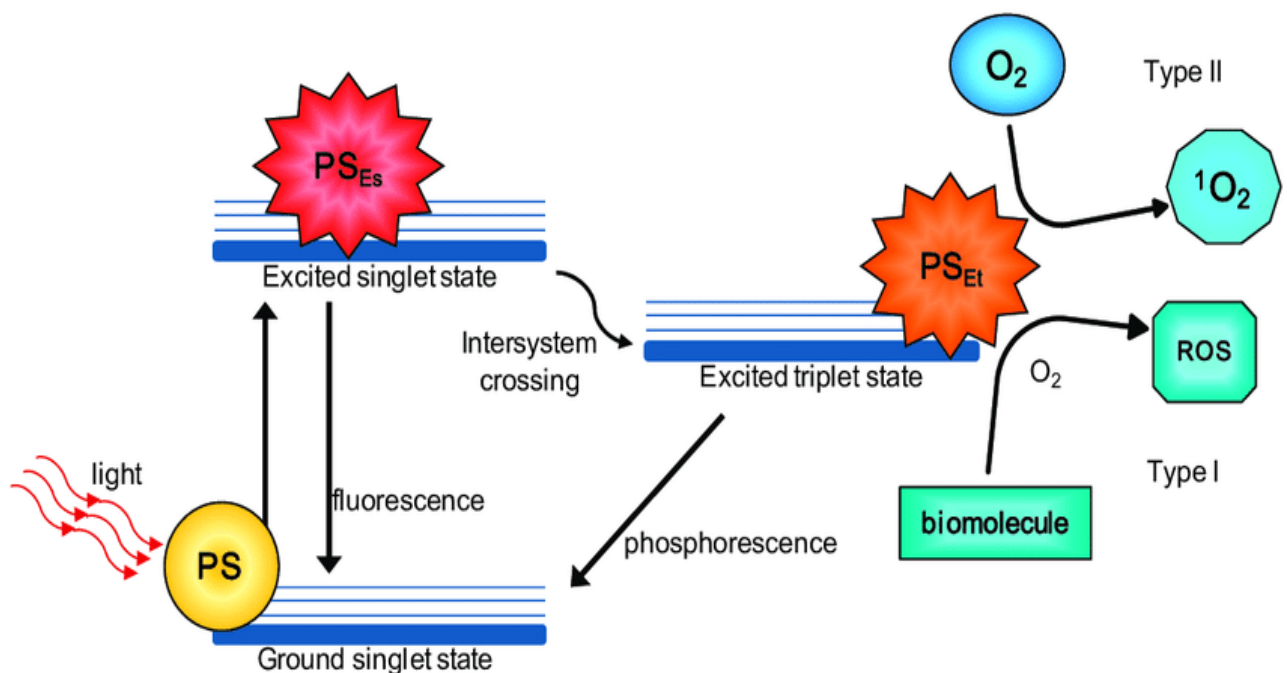
Figure 2. Schematic illustration of Type I and Type II reaction in PDT [79]. PS: photosensitizer, PS_{Es}: photosensitizer in excited singlet state, PS_{Et}: photosensitizer excited triplet state, ROS: reactive oxygen species

1.2.4 PDT induced effects on tumor

In photodynamic therapy, the light exposure causes damages to the cell membrane and is manifested as swelling, formation of blebs, vesicles shedding that contains various lysosomal and cytosolic enzymes, depolarization of cell membrane, increased PS uptake, increased chromate and cytosolic enzymes, inhibition of plasma membrane enzymes (ATPase), down-regulation of surface antigen, lipid peroxidation and damage to multidrug transporters [80].

There are the three mechanisms as illustrated in **Figure 3,** through which PDT mediates tumor cells destruction that involve ROS generation, tumor associated vasculature damage or immune response activation against the tumor. In response to ROS generation, oxidation of cellular and sub cellular organelles induce apoptosis, necrosis or autophagy [80] [81]. Adequate supply of the nutrients through the blood vessels is very essential for survival of the tumor, so the most promising approach for killing of tumor cells is to target the microvasculature resulting in hypoxia.
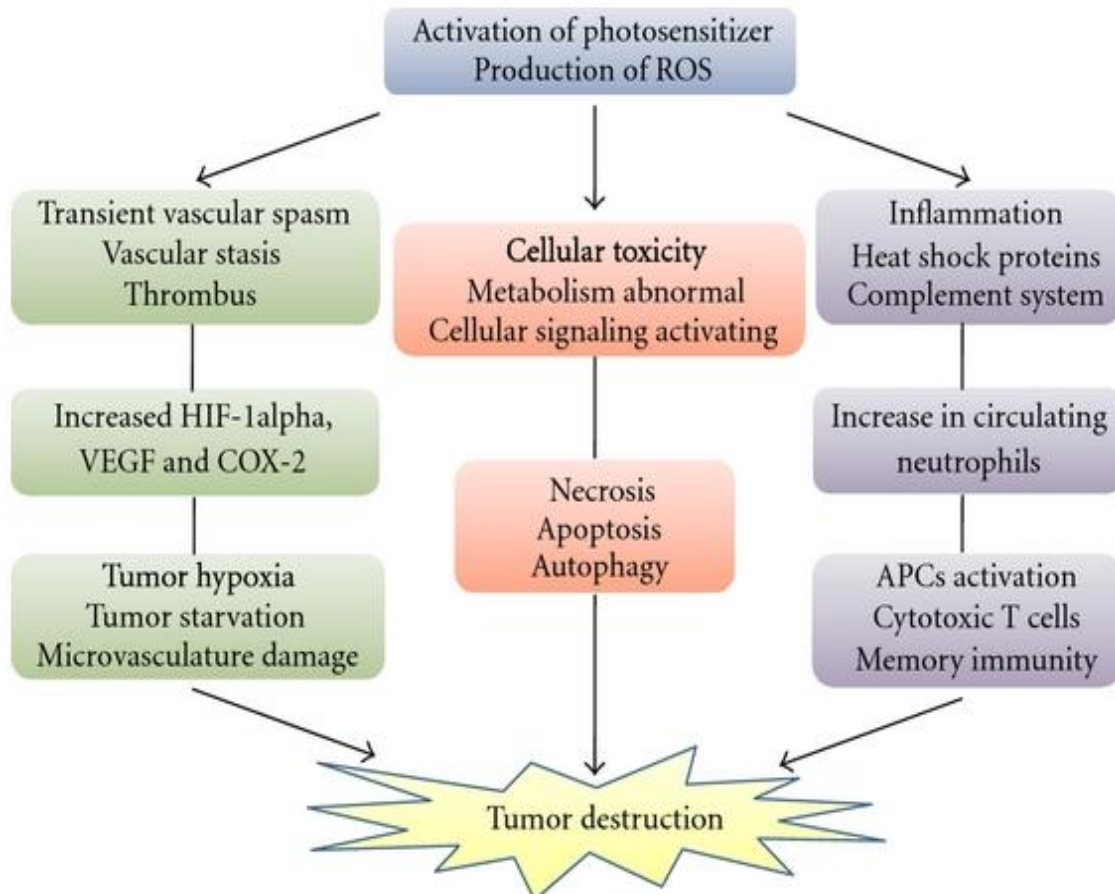
Figure 3. Mechanisms underlying PDT induced anti-tumor effects [82]

Studies have shown that photodynamic therapy with PS like Photofrin [83], benzoporphyrin derivatives (BPD)[84] causes vascular constrictions, thrombus formation leading to tumor growth inhibition. Following PDT treatment, infiltration of lymphocytes, macrophages and leukocytes leads to immune response activation [85]. The inflammatory process is mediated by several factors like complementary cascades, cytokines, growth factors and immune regulators. in 1996, during *in vivo* study, Wil de Vree clearly noticed a retardation of tumor growth after PDT induced neutrophil accumulation [86] and in absence of neutrophils, PDT showed no effect on tumor [86].

1.2.5   Curcumin as Photosensitizer

Since the last two decades, the use of naturally occurring compounds exhibiting anticancer properties has been gaining much attention as compared to conventional anticancer drugs. So during this research project, one of the naturally occurring substances i.e curcumin has been selected as therapeutic agent.

Curcumin (diferuloylmethane), a naturally occurring yellowish poly-phenolic compound extracted from rhizomes of turmeric (Curcuma longa) is cultivated in Southeast Asia. Turmeric contains a class of compounds called as curcuminoids, consisting of curcumin, demethoxycurcumin and bisdemethoxycurcumin. Curcumin constitute 2-5% of turmeric and is responsible for yellow color and therapeutic effects of turmeric. Apart from being used as flavoring agent , it is also used for the treatment of various conditions and diseases such as skin diseases, sprains, aches, pains, wounds and liver disorders [87].

Curcumin has identified as anticancer agent and has been studied in multiple carcinoma such as head and neck, breast, colon, prostrate and ovarian cancers [88] [89] [90]. Its anticancer activity is based on multiple mechanisms including targeting cell growth regulatory processes, transcription factors, signaling proteins, stimulation of apoptosis, inhibitory effects on tumor angiogenesis and metastasis [88]. Studies have shown that curcumin suppresses growth of head and neck carcinomas *in vitro* and *in vivo* [91]. Moreover, a report from the National Cancer Institute states that a curcumin formulation named Lipocurc[TM] has shown chemoprevention activity without any toxicity in Phase I clinical trials [92]. An oral dose of 8.0 g/day of curcumin is required for pharmacological effect and various studies have proven that no toxicity occurred at doses of 10g per day [93].

Curcumin in combination with irradiation (350-500nm) showed significantly better antitumor activity than curcumin alone; therefore it is used as photosensitizer in photodynamic therapy [94] [95]. Despite its numerous therapeutic effects, the clinical benefits are limited due to poor aqueous solubility (<0.125mg/L), low bioavailability, rapid metabolism and rapid systemic elimination [96]. Since last years, much effort has been employed to overcome this barrier (poor absorption and low solubility) by using different strategies such as liposomes, emulsions, solid dispersions, microspheres and nanogels. Among all drug carriers, liposomes have been broadly studied and showed significantly promising effects [97]. Liposomes are popular choice for drug delivery because of their close resemblance to biological membrane and their ease of optimization.

1.2.6 Liposomes as a potential carrier for curcumin

Liposomes were discovered for the first time by English hematologist Alec Bangham in 1961 [98] and proposed as delivery vehicles for drugs by Gregoriadis and Ryman in 1972 [99]. DOXIL®, DAUNOXOME® and AmBisome® were approved as first nanoscale drug carrier in 1995 for clinical use [100].

Liposomes are artificially generated spherical vesicles consisting of one or more phospholipid bilayers and are considered as promising carrier systems for transporting both hydrophilic and hydrophobic drugs [101]. Hydrophobic drugs fit themselves inside the lipid bilayer while the hydrophilic drugs get entrapped within aqueous core of the liposomes. Entrapment of drugs (hydrophilic and hydrophobic) into liposomes bypass the non-specific toxicity associated the drug to the normal tissues and thereby increases therapeutic index of drug. The encapsulation of drug into liposomes make it inaccessible to the metabolizing enzymes and thus improves bioavailability, stability and circulation time [97]. The lipids forming liposomes may be natural or synthetic, thus making the liposomes biocompatible and biodegradable [101]. Liposomes can be prepared by several techniques but thin film method by Bangham *et al* [102] is the most widely used for the preparation of liposomes in which lipid component with or without drug are dissolved in the organic solvents. The solvent will be evaporated using rotary evaporator followed by rehydration of film.

For successful drug delivery, stability of liposomal formulation is one of the main concerns. Liposomal formulation must be stable during its preparation, storage and even after delivery into body. In order to increase stability of liposomes, conventional lipids were coated with polymers, cholesterol was incorporated within bilayers of lipids but sufficient stability was not achieved. While the stability studies of tetraether lipids provide a wide range of their application as drug delivery system [103]. During this study, curcumin tetraether liposomal formulation by Duse *et al* [104] was selected as delivery system for curcumin **(Figure 4)**.

Curcumin (PS)   Liposomes   Curcumin Liposomes
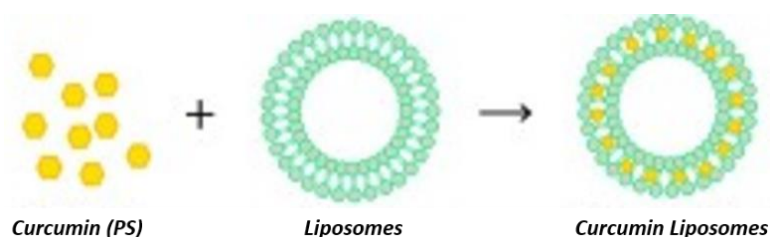
Figure 4. A graphical abstract of curcumin liposome formation [104]

1.3 *Molecular Cloning*

Molecular cloning involves biological techniques to allow in vitro generation of DNA constructs carrying a gene of interest and in vivo propagation of such recombinant DNA to induce the expression of the gene and resulting gene products. Cloning procedures were developed in 1970s after the discovery of restriction enzymes by Linn and Arber in late 1960s [105]. Later in 1970, Hamilton Smith isolated restriction enzyme from "Haemophilus influenza" for the cutting of DNA [106]. Much like the discovery of enzyme for cutting of DNA, it was also necessary to have enzyme that can bind DNA, so Gellert, Lehman, Richardson, and Hurwitz laboratories discovered enzyme "DNA ligase" for binding of DNA [107]. Without propagation and isolation of newly constructed DNA, cloning was impossible, so Griffth was first who demonstrated the transformation ability of bacteria [108]. In 1973, Cohen, Boyer and Chang laid the foundation for molecular cloning process by executing construction of functional bacterial plasmids *in vitro* [109]. Further research over the next decades led to discovery of new tools, techniques and methodologies for improving the efficiency of molecular cloning.

Molecular cloning has a diverse range of applications including development of recombinant antigens, vaccines, production of new antibiotics and development of diagnostic probes. For example the early diagnosis of hereditary disease is made possible by development of gene probes, expression of desired gene of interest and studying morphological, physiological and metabolic functions is one of the main applications of the recombinant DNA cloning. During this research project, cloning has been done for the generation and expression of recombinant CRPV oncogenes.

1.3.1 Basic Steps of cloning

The basis workflow for cloning as shown in **Figure 5** involves following steps

i.   PCR amplification of DNA containing gene of interest (GOI) and addition of restriction site sequences using custom designed primers [110].

ii. Isolation of DNA containing the GOI from PCR amplicons by gel extraction.

iii. Restriction enzyme digestion of amplicon DNA and the representative backbone vector to produce sticky ends

iv. Ligation of amplicon into the backbone vector.

v. Transformation of the ligated product into competent bacteria.

vi. Colonies formation on agar plates by overnight incubation of transformed bacteria.

vii. Screening for positive clones (containing GOI).
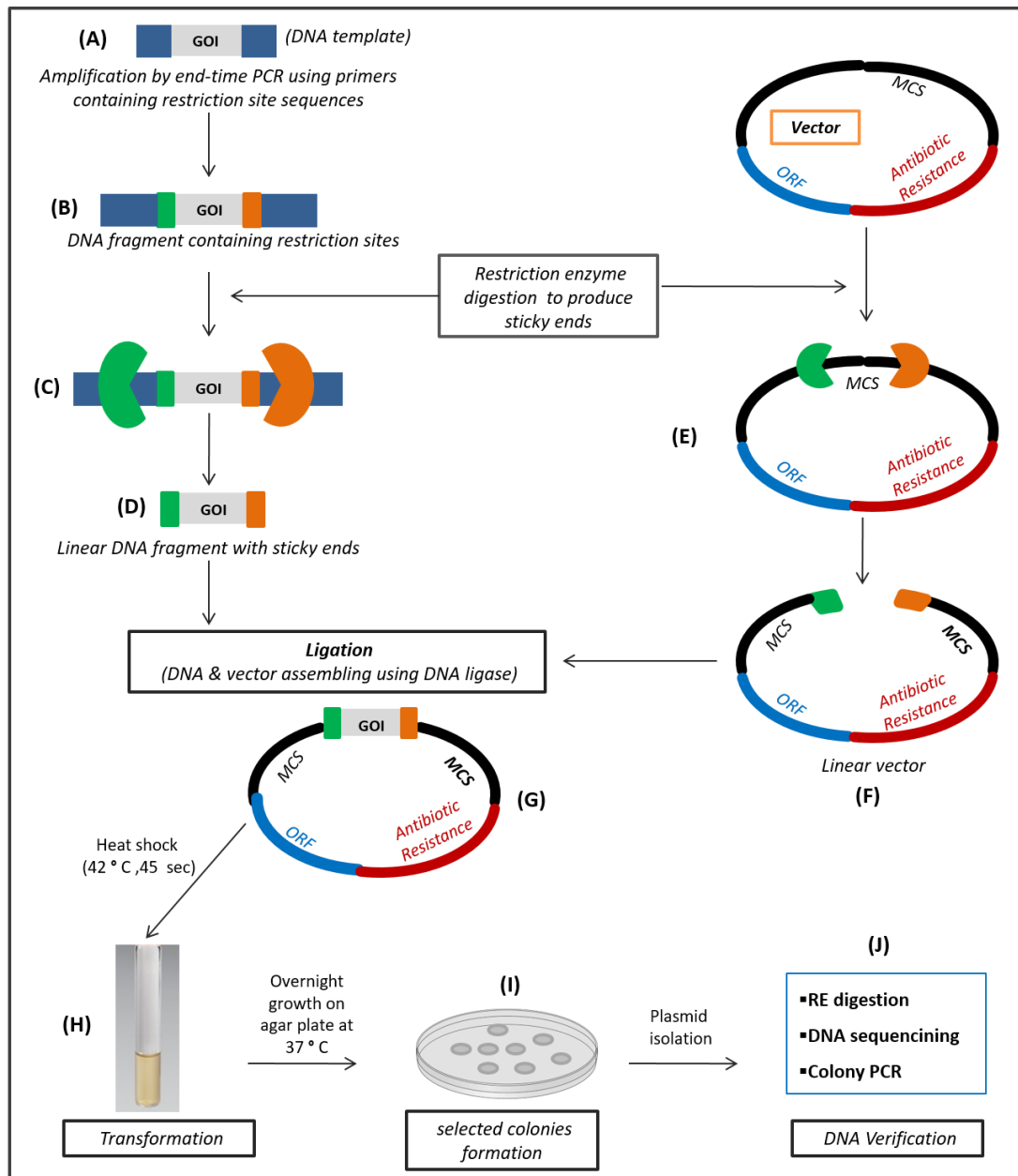
Figure 5. Schematic workflow of cloning process. Addition of different restriction sites (blue & orange color) (B) to both ends of double stranded DNA (dsDNA) containing (GOI) gene of interest by PCR amplification (A) followed by digestion with corresponding restriction enzymes (REases) (C) to produce linear dsDNA with sticky ends (D). Cleavage of plasmid vector using compatible REases (E) to

produce linear plasmid vector with sticky ends (F). Ligation of linear DNA fragment containing gene of interest into linear plasmid vector to produce recombinant DNA (G). Introduction of recombinant DNA into competent cells (42°C, 45s) for the replication of DNA termed as transformation (H). Only the transformed bacteria harboring recombinant plasmids with antibiotic resistance gene survived after exposure to selective antibiotic (I). Verification of selected clones for presence of desired DNA construct by different experimental methods (J).

1.3.2   Expression Vectors

An expression vectors are also known as expression constructs are designed to express gene of interest (GOI) in the cellular context. These are used to introduce gene of interest into the target cells and initiate protein synthesis utilizing host cellular machinery. The vectors are designed to contain regulatory sequences like promoter and enhancers for efficient transcription of gene of interest carried on vectors. Expression vectors consist of following elements **(Figure 6)** :

   i.   An inducible promoter, where RNA polymerase binds and starts transcription

  ii.   Origin of replication (ori) for propagation of genetic material

 iii.   Selectable markers as antibiotic resistance genes

 iv.   Multiple cloning site (MCS) also known as polylinker containing around 20 restriction sites, that can be cleaved allowing for integration of genes of interest

  v.   Transcription initiation sequences

 vi.   Elements for initiation of translation such as Kozak sequences

 vii.   Purification tag may or may not be added to cloned genes (such as His tag)

viii.   Fusion protein inserts or reporter genes like GFP or RFP which may be used in studying protein expression by cellular imaging

 ix.   Poly-adenylation signal: an element that contains poly-A necessary to produce a protein

Vectors are broadly categorized into viral and non-viral [111]. Non-viral vectors are preferred upon viral vectors because of less toxicity, reduced immunogenicity, low cost and their ease of production [112]. Since 1970, the use of plasmids as non-viral vectors have been identified [113]. Because of strong physiochemical characteristics and improved safety as compared to viral vectors, non-viral vectors has gained much attention in clinical trials [114] [115]. Therefore non-viral vectors as an expression vector were preferred during this study.
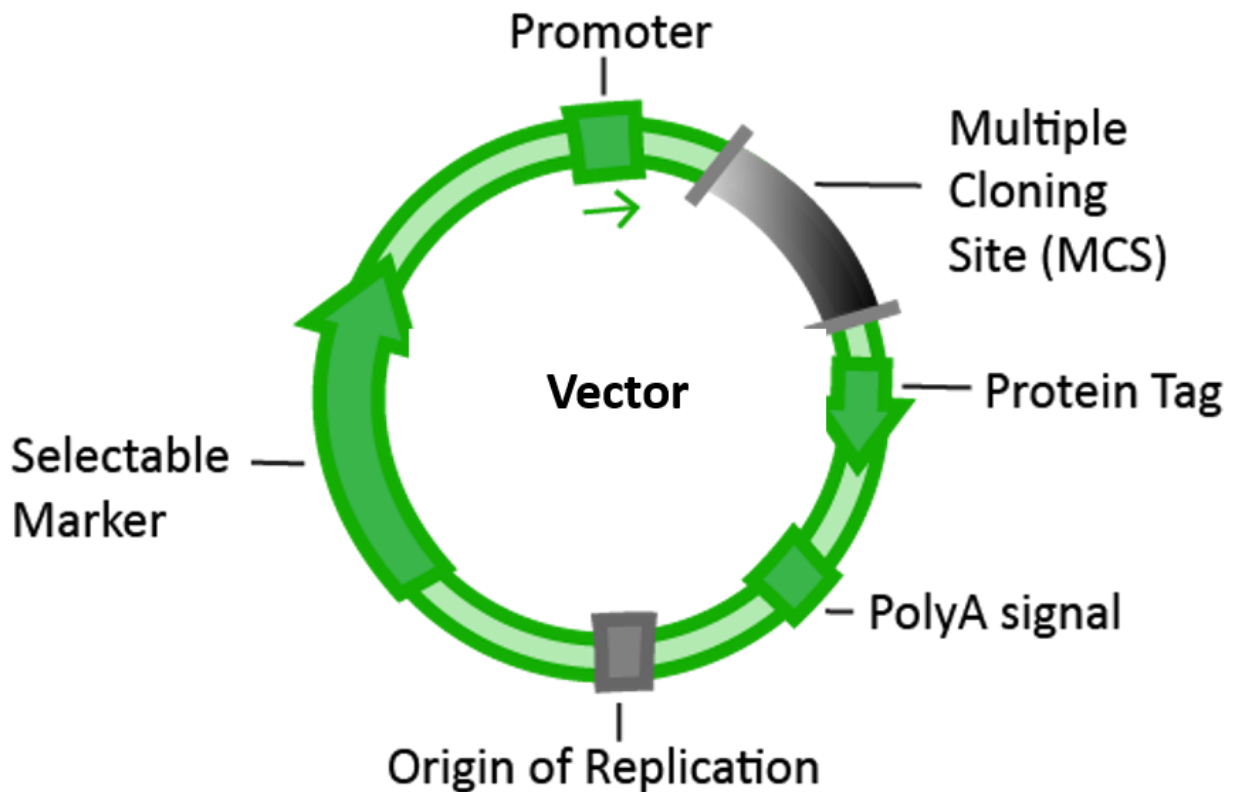
Figure 6. Elements of cloning vector [116]

1.3.3   Expression systems for gene expression

The expression of foreign genes in appropriate expression systems is executed for studying and understanding of gene expression and function. There is variety of expression systems used as a host for the expression of foreign DNA including prokaryotic cells, yeast, insect cells, mammalian cells, in vitro expression systems, transgenic animals and plants [117].

1.3.4   Mammalian expression systems

Although prokaryotic cells can express high levels of recombinant proteins [118] but due to foreign DNA toxicity, generation of unstable proteins because of differences in folding and unfolding mechanisms and particularly lack of post translational modifications in bacteria, prokaryotic cells are frequently inappropriate hosts for protein expression [119] [120]. Therefore non-prokaryotic

expression systems such as most preferentially mammalian expression systems serve as suitable hosts for the expression of gene of interest. The mammalian cells having ability to perform proper post translation modifications are usually used as hosts for recombinant protein expression [121] [122] [123]. Examples of such mammalian cells include African monkey kidney (COS, VERO), Chinese hamster ovary (CHO), Human embryonic kidney (HEK 293), Murine myeloma and Human embryonic retinoblast [124]. The choice of the expression system depends on the aims of the study. For transient gene expression, COS cell lines are more appropriate and convenient cell systems that yield high protein expression levels[125].

1.3.5   Gene Delivery systems

To achieve successful and efficient gene expression, the most crucial step is the selection of appropriate, effective and safe gene delivery systems. An efficient gene delivery system possessing the property to condense DNA, delivers the gene of interest into the cell, aids its release and thereby leads desired gene expression with subsequent protein production. A variety of viral and non-viral delivery systems has been used for gene delivery as listed in **Table 2**.

Viral gene delivery systems consist of modified viruses having no ability to replicate but possess ability to deliver DNA (gene) for expression. Although viral gene delivery systems possesses natural ability to invade cell, provide efficient transfection levels, constant expression but due to difficulty in production, limited repeated administration due to acute inflammation, high immunogenicity, toxicity observed during clinical trials[126] [127], various genome integration issues and lack of optimization, use of viral delivery systems is limited [128] [129].

Therefore in recent years, much attention has been drawn towards non-viral delivery systems alternative to viral delivery systems. Non-viral delivery systems utilizes various physical or chemical means to deliver gene through cell membrane to cell. The chemical means includes natural or synthetic materials for the formation of particle that delivers gene into the cell by endocytosis. Non-viral delivery systems have several advantages like less immune responses, unrestricted packaging capacity, are easy to synthesize, are cost effective and have an improved targeting potential by using modified ligands specific to targeted cells [130] [131].

Table 2. A list of viral and non-viral gene delivery systems

Delivery system	Types	Sub-types	Examples
Viral[132]	Biological		Lentivirus [133], Herpes simplex virus [134], Adenovirus [135], Retrovirus [133]
Non- viral[13]	Chemical	Polymers [136]	Polyamides, Dextran, Chitosan, DOTAP, DOTMA, DCChol, PEI, lipofectamine, Calcium phosphate
		Liposomes [137]	
		Dendrimers [138]	
		Cationic lipid compatible systems [139]	
	Physical	Gene gun [140]	Perfluoropropane loaded albumin microbubbles, gold, silver or tungsten microparticles, ultrasound contrast agent,
		Electroporation[141]	
		Ultrasound [142]	
		Hydrodynamic [143]	

1.3.6   Lipopolyplexes as a non-viral gene delivery system

Lipopolyplexes, a second generation non-viral gene delivery system possesses high transfection efficiency and size range (100-200 nm) with improved biocompatibility and stability [144]. Lipopolyplexes (LPP) are ternary complexes formed by combination of nucleic acid, polymers and negative or neutral lipids. Lipopolyplexes possess combined properties of lipoplex (lipid based delivery carriers) and polyplex (polymer based delivery carriers). Encapsulation of polyplex (DNA/polymer) with combination of various lipids (liposomes) reduces immunogenic risk, cytotoxicity and premature nucleic acid dissociation associated with polyplex and lipoplex only [145]. Intracellular trafficking of nucleic acid is improved by the polyplex portion of LPP, while lipids enhance cellular uptake of lipopolyplexes [146] [147].

LPP has shown promising transfection efficiency in vitro. Moreover, the performance of LPP depends on various factors like chemical structure of lipid and polymer and molar ratios of DNA, lipid and polymers. Lipopolyplex formulations contain lipids with different combinations like DOPE:DPPC:Cholesterol, DPPC:DSPE:PEG, possess higher transfection efficiencies in various cancer lines [148]. During this research project, PEI based lipopolyplexes [149] were used as transfecting agents **(Figure 7)**.
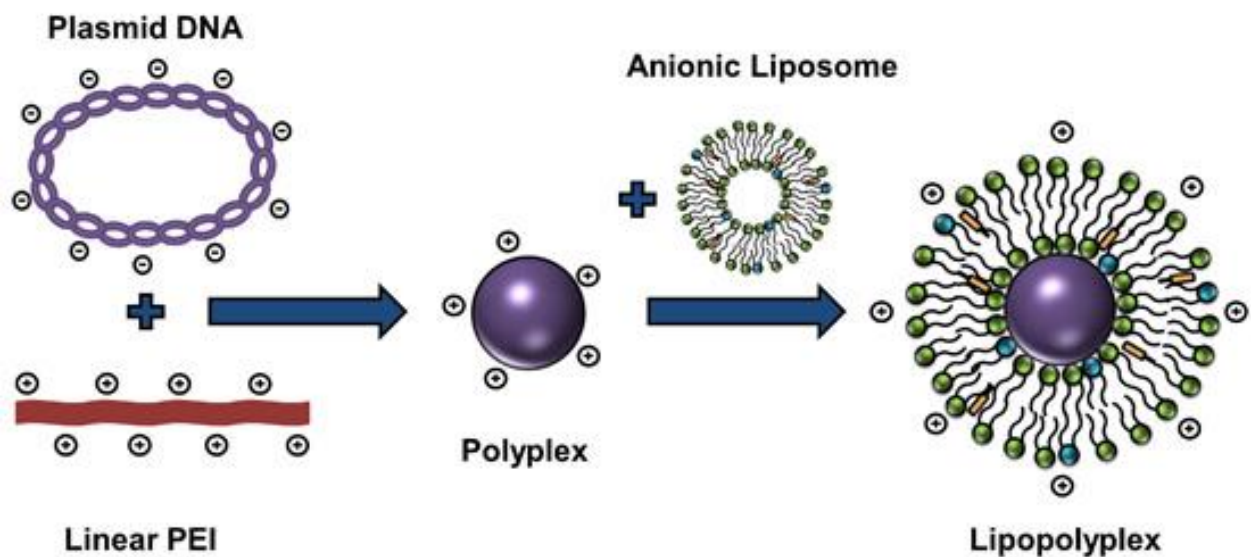
Figure 7. A graphical abstract of lipopolyplex formation [149]

1.3.7   Gene expression via transfection

A successful delivery of cloned genes via most appropriate gene delivery systems is required for most efficient gene expression. Transfection mediated gene expression helps in studying various biochemical and physiological processes such as gene function, protein expression and different signaling pathways.

Transfections can be performed in two ways:

i.   Transient gene expression (TGE) via transient transfection

In transient transfection, the foreign DNA or gene is introduced into cells for a limited time period. This transiently expressed gene is not a part of the genome and will not replicate during cell

division. This transient gene typically will be expressed for 24-96 hours in transfected cells, after which the transiently expressed gene will dilute out due to nuclease degradation after cell division and finally will no longer be detectable. Fusion of reporter genes or tags along with the gene of interest may help in assessing the transfection efficiency and the level of gene expression. Some reporter genes possess visual characteristic of fluorescence or luminescence. Most common reporter genes are GFP or RFP. Transiently transfected cells are used to study gene functions various biological processes associated with short-term gene over expression or gene inhibition e.g RNA but can also be deployed for the production of recombinant proteins on a small scale.

ii.   Stable Transfection

During stable transfection, foreign DNA or genes are imported into the cell by transient transfection first followed by use of selective markers, which identify and select cells containing gene of interest (plasmid). In stable transfection, the foreign gene becomes an integral part of the genome and is replicated during cell division. Generation of stably transfected cells is time consuming. Stable cell transfection is more advantageous in case of large scale production of recombinant proteins but is also suitable for long term studies of gene function.

In the present study, transient gene expression was the preferred method used.

1.3.8   Cottontail rabbit papilloma virus (CRPV) E6 and E7 oncogenes as therapeutic targets

As already stated earlier, the CRPV associated auricular VX2 carcinoma is considered as preclinical model for the study of HPV-associated HNSCC and therefore could provide *in vivo* platform not only for studying pathogenesis and disease progression associated with PV but also model for designing and developing therapeutic modalities against PV associated malignancies.

CRPV E6 and CRPV E7 proteins are found to be responsible for anchorage independent growth in immortal cell lines. Unlike HPV E6, CRPV E6 proteins (le6, se6) neither bind to E6-AP nor degrade rabbit p53 but still contribute to immortalization [150]. While CRPV E7 like HPV-16 E7 binds to retinoblastoma protein (pRb), causes disruption of complex between pRb and transcription factor (E2b), transactivate E2 promoter and causes transformation of fibroblasts (rodent) as seen by growth in soft agar [151]

E6 and E7 are the major oncogenes of cottontail rabbit papilloma virus (CRPV). The molecular functions of these oncoproteins involve viral replication, transformation and disease progression and therefore represent the potential therapeutic targets. Based on the role of these major CRPV oncogenes, particular emphasis has been laid on the generation of CRPV E6 and E7 recombinant clones and their expression during this project.

1.4   *Aims and Scopes*

For last two decades, CRPV associated VX2 carcinoma NZW rabbit serves as animal model for human HNSCC, therefore this research study was aimed at *in vitro* **i)** development of CRPV based cell systems and **ii)** therapeutic evaluation of PDT on CRPV cell system.

Development of CRPV based cell systems

The aim was to develop two types of CRPV based cell systems

i-   A synegenic VX2 cell line was derived from VX2 carcinoma tissue and was cultured under standard laboratory conditions. The resulting cell line was characterized on the basis of oncogenes. Another major objective of establishing VX2 carcinoma derived cell line was the provision of unlimited number of cells for conducting various *in vitro* studies and also for *in vitro* screening of various treatment strategies

ii-   The second CRPV based cell system alternative to cell line was the construction, validation of CRPV E6 & E7 recombinant clones and assessment of their transient expression in different eukaryotic systems.

Investigation of treatment efficacy on CRPV system

After establishing and characterizing the cell line derived from VX2 carcinoma, the next step was to investigate the efficacy of various treatments. Non-invasive treatment such as photodynamic therapy using curcumin loaded liposomes was selected during this study. Could the same photodynamic therapy be employed in the other papilloma virus associated human cell lines such as UDSSC-2 and Hela, was also addressed in the thesis.

CHAPTER NO 2

Establishment and characterization of a CRPV (Cottontail Rabbit Papillomavirus) associated cell line

2.1 *Aims and objectives*

The aim of this chapter was to establish and characterize a VX2 carcinoma derived cell line as *in vitro* experimental model that could be used for evaluating the efficacy and toxicity of new treatment modalities and also act as preclinical model to treat head and neck cancer.

VX2 tumor from the ear of New Zealand White rabbit was used as a source for generation of VX2 cell line. After the generation of VX2 cell line, different methodologies like immunocytochemistry, flow cytometry, western blot were used to characterize and validate the cell line. Real time polymerase chain reaction was performed to check the presence of endogenous CRPV E6 and E7 oncogenes.

2.2 *MATERIALS AND METHODS*

2.2.1 Auricular VX2 Tumor Tissue

Fresh VX2 tumor tissue from adult New Zealand White (NZW) rabbits (Oryctolagus cuniculus; female) was generously provided by Prof. Dr. Michael Bette, Institute of Anatomy and Cell Biology, University of Marburg, Germany. The generation of VX2 tumors in NZW rabbits was approved by the regional board Giessen, Germany (V54-19c20-15 h01 MR 20/26 Nr. 83/2015) according to the German Animal Protection Law. A list of all used materials is mentioned in the appendix.

2.2.2 Induction of the auricular tumor

The implantation of an auricular VX2 carcinoma was done as described elsewhere [152]. Briefly, for the inoculation of solid auricular VX2 carcinoma tissue, the animals were first sedated with 5mg/kg body weight Rompun®. Then using a cannula, a pocket of air was injected s.c. into the auricle followed by injection of freshly collected VX2 tumor cell suspension (containing 1×10^7 cells in volume of 200µl). Tumor growth was checked and monitored on a daily basis. Typically, 2 weeks after cell inoculation, a tumor nodule of >2000mm^3 was formed. Thereafter, this VX2

tumor would be used for cell culture, molecular analysis and for the generation of syngeneic VX2 cell line.

2.2.3   Generation of a VX2 Carcinoma derived cell line

The protocol for establishing a VX2 cell line **(Figure 8)** was as previously reported with some modifications [47] [153]. The VX2 tumor nodule was surgically removed from the ear and was carefully prepared by removing fatty and necrotic regions of the tissues. The dissected tumor tissue was washed 3-4 times with sterile PBS and growth media under sterile conditions.

The tumor tissue was then minced into small pieces of approximately 2-3mm diameter size using a sterile scalpel followed by transferring 4-5 pieces into $10mm^2$ cell culture dishes (Sarstedt, Numbrecht, Germany) containing 10ml of Dulbecco's modified Eagle medium and Ham's F12 media (DMEM/Ham`s F-12, 1:1) with 2 mmol/L L-Glutamine (Capricorn Scientific, Ebsdorfergrund, Germany) supplemented with 10% FBS (fetal bovine serum) (Biochrom AG, GmbH, Germany), 50 μg/ml gentamicin (Biochrom AG, GmbH, Germany), 100 U/ml penicillin/streptomycin (Capricorn Scientific, Ebsdorfergrund, Germany) and 50 μg/ml amphotericin B (Biochrom AG, GmbH, Germany).

The tissue fragments were allowed to propagate for 2 weeks in the same media at $37^{\circ}C$ in humidified atmosphere of 5% CO2. During this period, the cell culture dishes were checked and monitored to prevent them from for any kind of contamination. Outgrowing cells from the VX2 tumor pieces became adherent to the cell culture plate. After reaching confluency, the cells were trypsinized with a solution of 0.05% trypsin/EDTA solution (Biochrom AG, GmbH), centrifuged at 250 g for 5 min. The cells were washed with sterile PBS and transferred to new cell culture dishes containing DMEM/F-12 media.

2.2.4   Characterization of a VX2 Carcinoma derived cell line

2.2.4.1   Immunocytochemistry

Immunocytochemistry (ICC) is a laboratory technique used to anatomically visualize the location of a specific cellular protein deploying specific primary antibodies directed against this protein.

VX2 cells from early (4th to 8th) passages and late (40th to 50th) passages were used for characterization studies. Cells were grown in monolayers on 18 mm glass cover slips in 6 well plates. For fixation of cells, the medium was carefully removed from the wells and washed with cold PBS (with Ca^{2+} & Mg^{2+}) .Cells were fixed for 5 min in 100% pre-chilled (-20°C) methanol. After fixation, cells were treated with 3% BSA and 0.3% NP40 in PBS (blocking buffer) for 30 min to block all non-specific binding sites. The cells were exposed to primary mouse antibody, vimentin (clone V9, dilution 1:100, DAKO, CA, USA) at room temperature for 1 hour in the abovementioned blocking buffer.

After incubation with the primary antibody, the coverslips were washed 3 times with blocking buffer for 5 min each and also with PBS 3 times for 5 min each and then incubated with the secondary antibody (goat anti-mouse IgG-TR, 1:100, Santa Cruz Biotechnology, CA, USA) in the dark for 1 hour at RT. Cells were then washed three times with PBS and counterstained with 4'6-diamidino-2-phenylindole (DAPI, 1 µg/ml final concentration in H_2O) for 10 min to visualize nucleus followed by mounting cover slips in fluorescent mounting media (Dako, CA, USA). The signals were analyzed by confocal laser scanning microscopy (Leica TCS SP2, Leica Microsystems AG, Wetzlar, Germany).

2.2.4.2   Cell sorting and Flow cytometry

VX2 cells from culture dishes were dislodged using 0.05% trypsin/EDTA in PBS and re-suspended in ice cold Ca^{2+} and Mg^{2+} free PBS. The VX2 cell suspension was then filtered through 40µm nylon mesh (Becton Dickinson, Heidelberg, Germany) to remove large aggregates. All sample tubes containing re-suspended cells, collection tubes and 96 well plates pre-coated with FBS were kept on ice during subsequent procedures. 5×10^6 cells/ml were used for flow cytometric sorting deplyoing MoFloTM Astrios cell sorter, Summit 6.3 software (Beckman Coulter, Indiana, USA). Forward (FSC) versus side scatter (SSC) gating was used to identify different subpopulations on the basis of cell size and granularity **(Figure 8A)**.
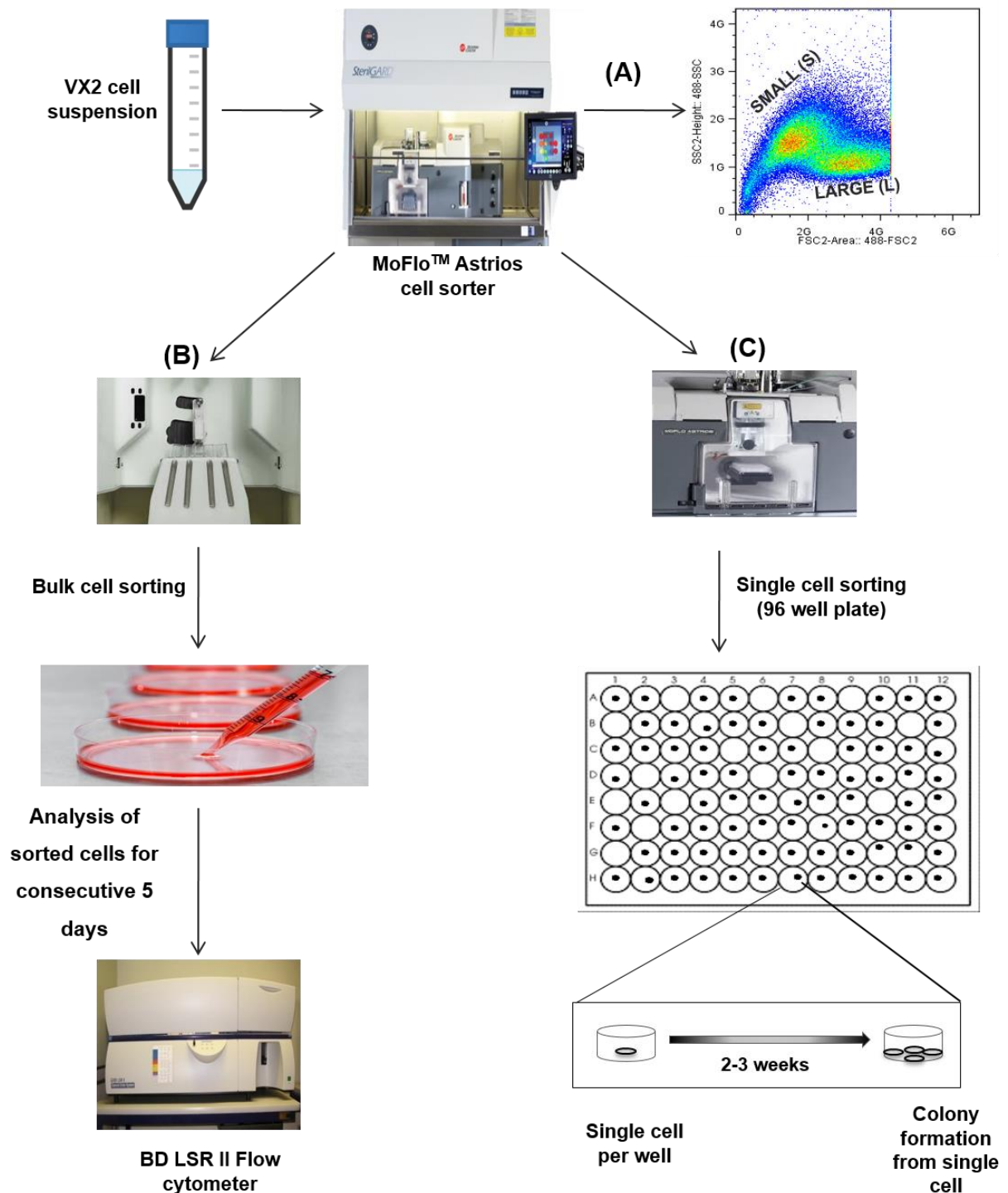
Figure 8. Schematic representation of cell sorting of VX2 cell line derived from VX2 carcinoma

(A) Two populations of VX2 cells based on different phenotypes were observed after FACS analysis. One was termed small (S) and other large (L) based on their different cell size and granularity *(B)* Bulk cell sorted VX2 cells were analyzed using LSR II flow cytometer to check changes in cell populations. *(C)* Single cell sorting of VX2 cells into 96 well plates was performed to exclude the possibility of having different cell lines as mixture.

2.2.4.2.a   Bulk Cell Sorting Assay

For bulk cell sorting **(Figure 8B)**, two different cell populations (small and large) were collected separately into 15ml falcon tubes pre-coated with FBS. Afterwards, sorted cells were incubated separately in 10ml culture dish at 37°C with 5% CO_2 and were analyzed for any change in subpopulations for consecutive 5 days using BD LSR II, FACS DIVA software (Becton Dickison, San Francisco, USA).The data was analyzed using the BD CellQuest and FlowJo softwares

2.2.4.2.b   Single Cell Sorting Assay

In this assay, single sorted cells were cultured in separate wells of a 96-well plate **(Figure 8C)**. Each well already contained 100µl of complete media (DMEM/F-12). This assay was performed to determine viability, proliferation and colony formation potential of single sorted cell. Cells sorted into 96 well plates were spin down for 40-60 sec and incubated at $37°C$ with 5% CO_2. After sorting, all plates were scanned for the presence of a single cell per well under the microscope and the cells were incubated for 2-3 weeks to expand the clonal population. The plates were continuously monitored by visual inspection using a Leica DM IL LED microscope (Leica Microsystems, Wetzlar, Germany) and scored as a cell not showing any growth or a cell that continued to divide, grow and make colonies.

2.2.4.3   Immunoblotting analysis

2.2.4.3. a   Preparation of cell lysates

Whole cell proteins from VX2 carcinoma tissue, unsorted VX2 cells and FACS sorted VX2 cells from small and large populations were extracted to evaluate protein expression levels as depicted in **(Figure 8)**. Directly after sorting, cells were subjected to lysis by incubating samples at $4°C$ for 1 hour in lysis buffer (2mM EDTA, 1% NP40, 137mM NaCl, 20mM Tris-Cl pH8.0, 10% glycerol) supplemented with protease and phosphatase inhibitors (Sigma-Aldrich, Saint Louis, MO, USA).Thereafter, lysates were centrifuged at $12,000 \times g$ for 15 min at 4°C. The supernatant was gently removed and stored in separate tubes (on ice). The protein concentration of the supernatant

was determined with Bio-Rad protein assay kit. Cell lysates along with the lysis buffer and 4×SDS sample buffer were incubated for 10 min at 95°C for complete protein denaturation prior to loading samples on SDS polyacrylamide gel.

2.2.4.3. b   SDS-PAGE

Proteins can be easily separated on basis of their molecular weights in SDS-polyacrylamide gel electrophoresis under denaturing conditions [154]. For the preparation of SDS-polyacrylamide gels, the casting chamber was used to prepare vertical gels in between two glass plates having an internal space of 1.5mm. The gels were composed of two layers; a separating gel used to separate proteins on basis of their sizes and a stacking gel to ensure entry of proteins at the same height into the separating gel. The composition of both gels is shown in **Table 3**.

Table 3. SDS-PAGE composition for gel electrophoresis

Ingredients (ml)	Stacking Gel 6 %	Seperating Gel 12 %
Polyacrylamide	4	16.4
1.5 M Tris-HCl pH 8.8	-	10
0.5 M Tris-HCl pH 6.8	5	-
10% SDS	0.2	0.4
10% APS	0.2	0.4
TEMED	0.02	0.04
Water	q.s to make 20	q.s to make 40

SDS-PAGE was performed under standard conditions using a discontinuous 12% polyacrylamide gel. Thirty μg of whole cell lysate protein was loaded per lane. The Precision Plus Protein™ Standard (161-0373) from Biorad (Hercules, CA, USA) was used for size comparison. SDS PAGE was done using 70-75V for 30 min through stacking gel followed by 100V for 1 hour through

separating gel. Western blotting was first developed by Renart and Towbin in 1979 [155] [156]. After SDS-PAGE, the proteins were transferred to nitrocellulose membranes at 85V for 1hr. Subsequently, for the detection of protein of interest, the membranes were blocked with 3 % nonfat dry milk in PBS (blocking buffer) and incubated overnight with continuous agitation at 4°C with the primary antibody diluted in blocking buffer. After overnight incubation, the membranes were washed thrice in blocking buffer for 10 min and incubated with an HRP-coupled secondary antibody for 1 h at room temperature. After incubation and three washes, immune stained proteins were visualized on X-ray film (Agfa, Cologne, Germany) using the enhanced chemiluminescence (ECL) method (Amersham Biosciences, Buckinghamshire, United Kingdom).

2.2.4.3.c   Antibodies

Rabbit monoclonal anti-Zyxin (clone EPR4302, 1:500, Epitomics); mouse monoclonal anti-Vinculin (clone V9131, 1:500, Sigma-Aldrich); mouse monoclonal anti-ERK1/2 or anti-Mitogen Activated(MAP) Kinase (clone MAPK-YT, 1:500, Sigma-Aldrich); rabbit polyclonal anti-EGFR1005 (SC-03, 1:500, Santa Cruz Biotechnology); rabbit polyclonal anti-TRKB (SC-12, 1:500, Santa Cruz Biotechnology); rabbit monoclonal anti-Pin1-Phospho-Serine16 (clone EP1480Y, 1:500, Abcam); rabbit polyclonal anti-Pin1 (PC270, 1:500, Calbiochem); mouse monoclonal anti-PCNA PC10 (SC-56, 1:500, Santa Cruz Biotechnology); rabbit monoclonal anti-CXCR4 (clone Ab24824, 1:500, Abcam) were used as primary antibodies for western blot analysis. Mouse-IgGk BP-HRP, (SC-516102, 1:2000, Santa Cruz Biotechnology); rabbit-IgGk HRP, (SC-2004, 1:2000, Santa Cruz Biotechnology) were used as secondary antibodies for western blot.

2.2.4.4   Molecular Biological Analysis

2.2.4.4.a   RNA Extraction

For isolation of total RNA from VX2 tumor tissue, approx. 30 mg of minced tumor was transferred to a Precellys tube followed by addition of RLT buffer (RNeasy FFPE Kit, Cat.73504, Qiagen, Hilden, Germany) followed by subsequent homogenization in a Precellys tissue homogenizer at 6,000 rpm at 1×20 s. All other steps were performed according to the manufacturer's protocol

(RNeasy FFPE Kit). For extraction of RNA from cells (rabbit keratinocytes and VX2 cells derived from the VX2 cell line), QIAshredder columns (Qiagen, Hilden, Germany) and RNeasy Mini Kit (Cat.74106) (Qiagen, Hilden, Germany) were used. RNA concentration was measured with the NanoPhotometer® NP80 system (IMPLEN, Munchen, Germany). RNA was stored at -80°C or used directly for cDNA synthesis.

2.2.4.4.b   Reverse Transcription

The Transcriptor First strand cDNA synthesis kit (Roche diagnostics, Mannheim, Germany) was used for cDNA preparation according to manufacturer's protocol. Oligo dT primers were used to transcribe 1.0 µg RNA from each sample using the TProfessional Thermocycler (Biometra, Gottingen, Germany). In the first reaction step **(Table 4***)*, the following reagents were mixed.

Table 4. Reaction setup for cDNA synthesis in 1ˢᵗ step

Reagents	Volume	Final conc.
Water	q.s to make 13µl	-
Total RNA	variable	1µg (10ng - 5µg)
Anchored oligo (dT)$_{18}$ primer	1µl	2.5 µM

The mixture prepared in the 1ˢᵗ step was heated for 15 min at 65°C to denature secondary RNA structures followed by cooling at 4°C and proceeding to step 2 in **Table 5**.

Table 5. Reaction setup (Mastermix) for cDNA synthesis in 2ⁿᵈ step

Reagents	Volume	Final conc.
Transcriptor RT Reaction Buffer	4 µl	1x
Protector RNAse	0.5 µl	20 U
Deoxynucleotide Mix (10mM each)	2 µl	1 mM each
Transcriptor Reverse Transcriptase	0.5 µl	10 U

After addition of the master mix in the 2nd step, the reaction mixture was subjected to reverse transcription at 50$^{°}$C for 60 min followed by enzyme inactivation at 85$^{°}$C for 10 min and subsequent cooling to 4$^{°}$C. The resulting complementary DNA was either used directly for PCR or stored at -20$^{°}$C until used for further use.

2.2.4.4. c   Real time Polymerase Chain Reaction

The expression pattern of CRPV associated oncogenes in the VX2 carcinoma, VX2 cell line and rabbit keratinocytes was evaluated by RT-PCR using gene specific primer pairs. VX2 tumor tissue and normal rabbit keratinocytes were used as a positive and negative control, respectively. Real time PCR analysis was done using PowerUp^{TM} SYBR^{TM} Green Master Mix (Applied Biosystems, Darmstadt) according to the manufacturer's instruction as depicted in **Table 6**.

Table 6. PCR Reaction setup

Reagents	Volume
PowerUp^{TM} SYBR^{TM} Green Master Mix	5 µl
Forward and reverse primer (300-800nmol/L)	2 µl
DNA template (1-10ng)	2 µl
Water	q.s to make 10 µl

Table 7. Standard cycling conditions for RT-PCR

Steps	Temerature	Time	
UDG activation	50°C	2 min	
DNA polymerase	95°C	2 min	
Denature	95°C	15 sec	
Anneal	55-60°C	15 sec	40 cycles
Extend	72°C	1 min	

The reaction was carried out in a total volume of 10µl in 96 well plates using QuantStudio® TM 5 system (Thermo Fisher Scientific, CA, USA). Standard cycling parameters for RT-PCR are shown in **Table 7**

2.2.4.4.d   Primers for RT-PCR

For RT-PCR, primers specific for CRPV E6 & E7 oncogenes and primers for housekeeping genes of the rabbit were designed using NCBI/Primer-BLAST **Table 8**. The primers were purchased from Invitrogen and used to detect the specific gene product. Rabbit *GAPDH* and *RPL32* were used as housekeeping genes to normalize oncogenes expression in each sample. Samples were run in triplicate. The $2^{-\Delta\Delta CT}$ method was used for relative mRNA quantification of the sample [157]. The results were analyzed using QuantStudio™ design & Analysis software v1.3.1 and Microsoft Excel.

Table 8. A list of oligonucleotide primer pairs for RT-PCR

Primer Pair	Direction	Sequence (5'-3')	GenBank No
Rabbit _GAPDH (378-485)*	Forward	CTGCACCACCAACTGCTTAG	NM_0011082253
	Reverse	GTCTTCTGGGTGGCAGTGAT	
Rabbit _RPL32 (93-208)*	Forward	TAAGCGTAACTGGCGGAAAC	NM_001171505.1
	Reverse	GCATGTGCTTGGTCTTCTTG	
CRPV_E6 (63-142)*	Forward	GGACTTGCCGTTTGGTTGTA	NC_001541.1
	Reverse	ATAGCCCCGTGCATTTGA	
CRPV_E7 (67-171)*	Forward	CATTGCGACGAAGCATTAGA	NC_001541.1
	Reverse	CTTACATGGCACGGACACTG	

(*) numbers refers to the primer location in the reference sequence

2.3   RESULTS & DISCUSSION

2.3.1   Establishment and characterization of VX2 carcinoma derived cell line

After isolated tumor fragments adhered to the culture dish and within 4-5 days, outgrowths of epithelial cells and some fibroblastic cells were clearly noticed. After introduction of lag period of 15 days, cells started attaching to culture plate and manifest polygonal shape and grew as a monolayer, adherent cells. In early passages, fibroblasts were still dominated but started declining with increased passage numbers **(Figure 9)**. The outgrowing cells were periodically sub-cultured in fresh VX2 culture media to provide fresh nutrients and enough space for proliferating cells. Due to its high proliferation rate, VX2 cells reached 70-80% confluency after sub-culturing at a ratio of 1:3, which was normally carried out twice a week. The VX2 cells remained in culture as a cell line for approximately 150 passages over period of 18 months.
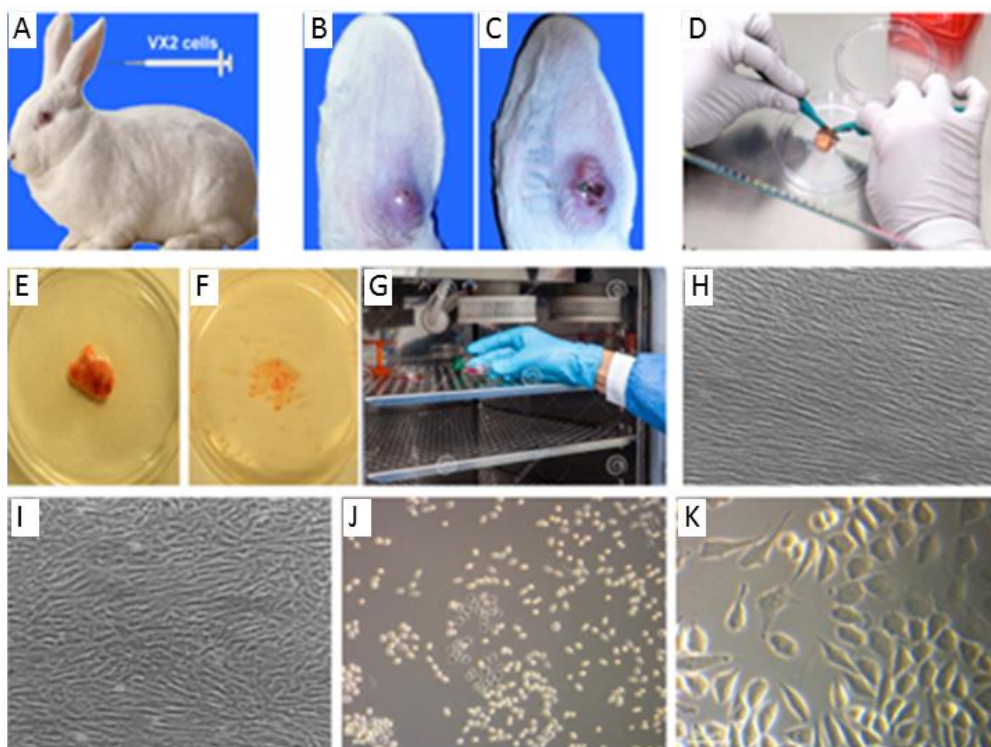
*Figure 9. Schematic representation of VX2 cell line development from rabbit VX2 tissue. (A)*The auricle of New Zealand White Rabbit (NZWR) is inoculated with a VX2 carcinoma cell suspension with daily follow up of tumour growth *(B, C)*. Mincing of VX2 tumour tissue after excision from the rabbit ear *(D, E, F)*, followed by incubation of cells *(G)*. Fibroblasts dominancy appeared in early passages *(H, I)*. Fibroblasts start declining after several passages *(J)*. VX2 cells survived for a period of 18 months with (~150) passage numbers *(K)*.

2.3.2   Immunocytochemistry

Immuno-cytochemical examination was deployed to help characterizing the phenotype of cultured VX2 cells. In early passages, fibroblasts were present and identified based on their spindle shaped morphology while in late passages, fibroblasts disappeared. In addition to visual examination, the presence of fibroblasts was further confirmed by vimentin staining of the cells.
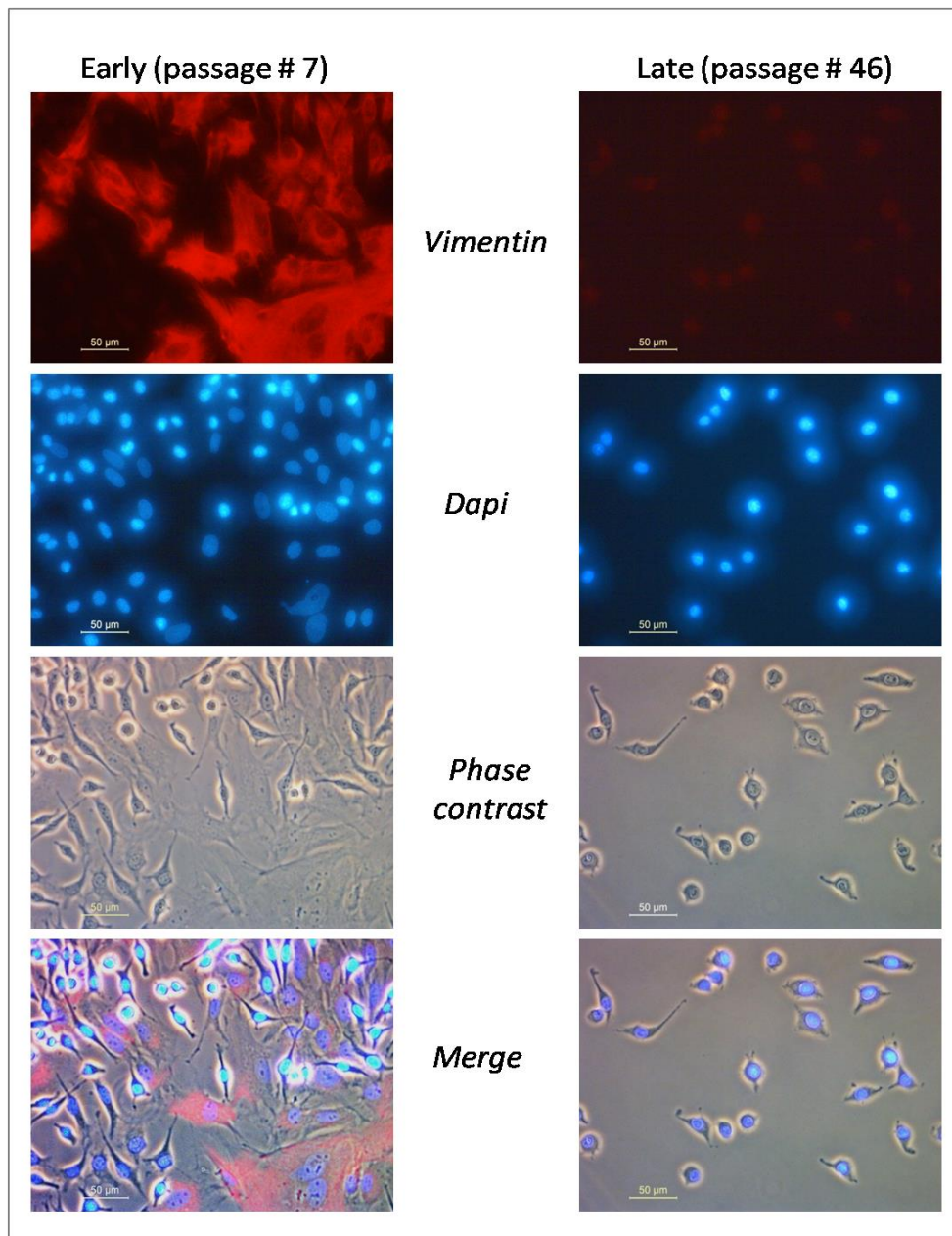
Figure 10. Immunofluorescent staining of cultured VX2 carcinoma derived cells. Immunofluorescence analysis of VX2 cultures with early (p # 7) and long (p # 46) passage numbers revealed vimentin expression only during early but not in high passage number, potentially representing tumour-associated fibroblasts.

Immunofluorescence staining of VX2 cells as depicted in **Figure 10** revealed that in early passages (passage # 7), a large number of cells is vimentin positive as compared to cells with higher passage numbers (passage # 46). Presence of vimentin expression in VX2 cells at early passages (passage # 7) shows the presence of tumor associated fibroblasts [158] [159]. While loss of vimentin expression in VX2 cells at late passage (passage # 46) demonstrating the progressive loss of tumor associated fibroblasts that became senescent with cell culture duration. Thereafter VX2 cell culture contained only highly proliferative cells. Vimentin expression in early passages indicated the cells to carry mesenchymal phenotype.

2.3.3   Flow cytometry

Flow cytometry is a technique used for detection and measurement of physical characteristics of populations of the cells or particles. Flow cytometrey is commonly used for cell sorting, cell counting and for determining the characteristic and function of the cells. During cell sorting, the flow cytometer detects and sorts cells on the basis of different parameters like cell size, morphology. During flow cytometry, the heterogenous mixture of the cells passed through the laser light and this laser light scatters upon interaction with cells. The scattered light is measured as forward scatter (FSC) and side scatter (SSC) using two optical detectors. FSC intensity refers to the diameter (size) of the cell and SSC refers to cells with complexity (granularity).
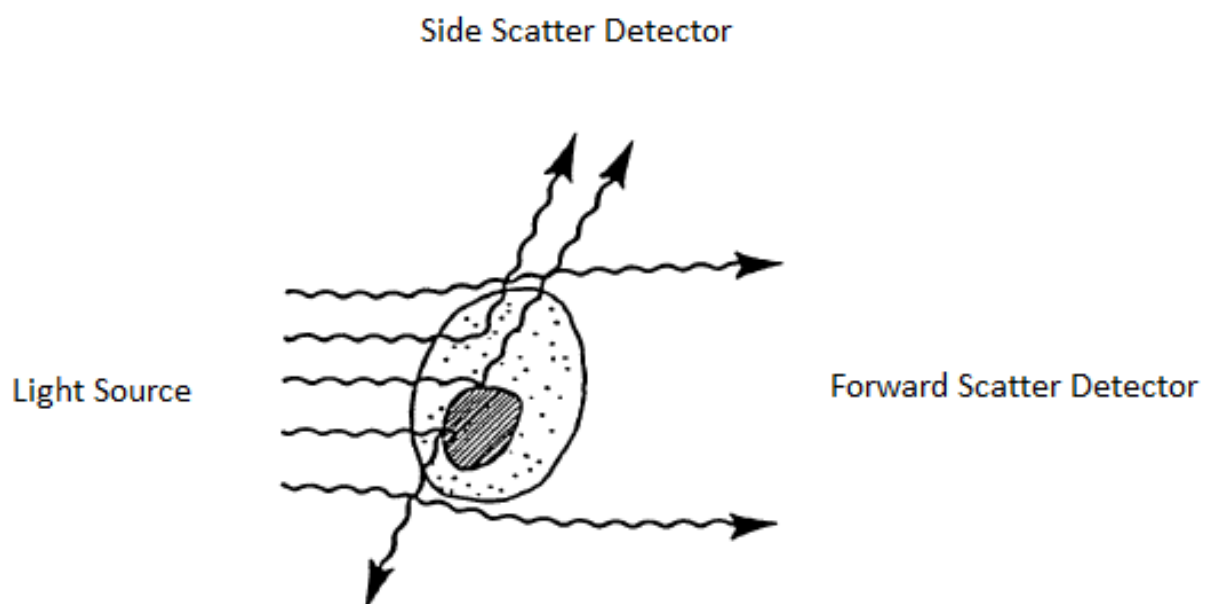
Figure 11. Scattering properties of light after interaction with a cell [160]

During flow cytometry of cultured VX2 cells, two different cellular phenotypes (cell size) were observed on the basis of forward and side scattering, one was named as 'small cell population' and the other was 'large cell population' **(Figure 12)**.

The presence of two different populations with large and small size implied the possible presence of two different cell lines. Therefore, it was assumed that there was a mixing of two different cell lines. In order to resolve this query, single cell sorting in 96 wells plates and bulk cell sorting in 15ml tubes was done from each of two subpopulations (small and large).
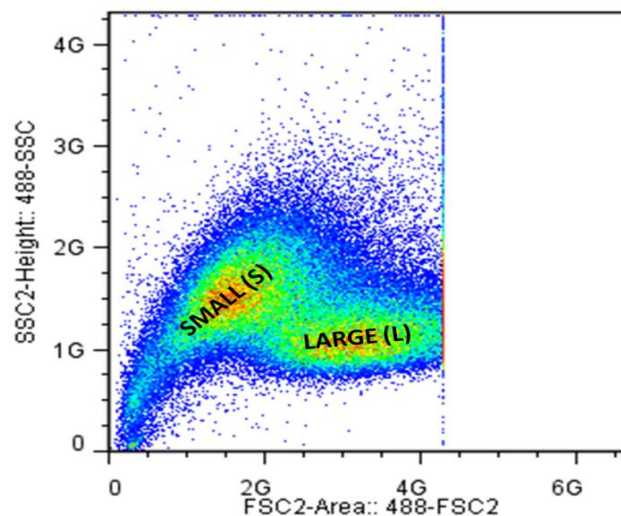
Figure 12. Evaluation of cultured VX2 carcinoma derived cells by flow cytometry. Two subpopulations (small cell population and large cell population) were observed according to cell size and granularity.

2.3.3.a   Bulk Cell sorting

Cells derived from the large cell subpopulation (L.C.P) and small cell subpopulations (S.C.P) were sorted in bulk and cultured separately in 100 mm cell culture dishes under standard laboratory conditions and were analyzed for changes in population (large and small) for consecutive 5 days. During continuous monitoring of VX2 cells on LSRII, it was observed **(Figure 13A)** that both cell populations (large & small) reappeared from sorted L.C.P. While from sorted S.C.P, large population disappeared on 4th day and both population disappeared on 5th day. This concludes that the small cell population could not survive alone in the absence of large cell population.
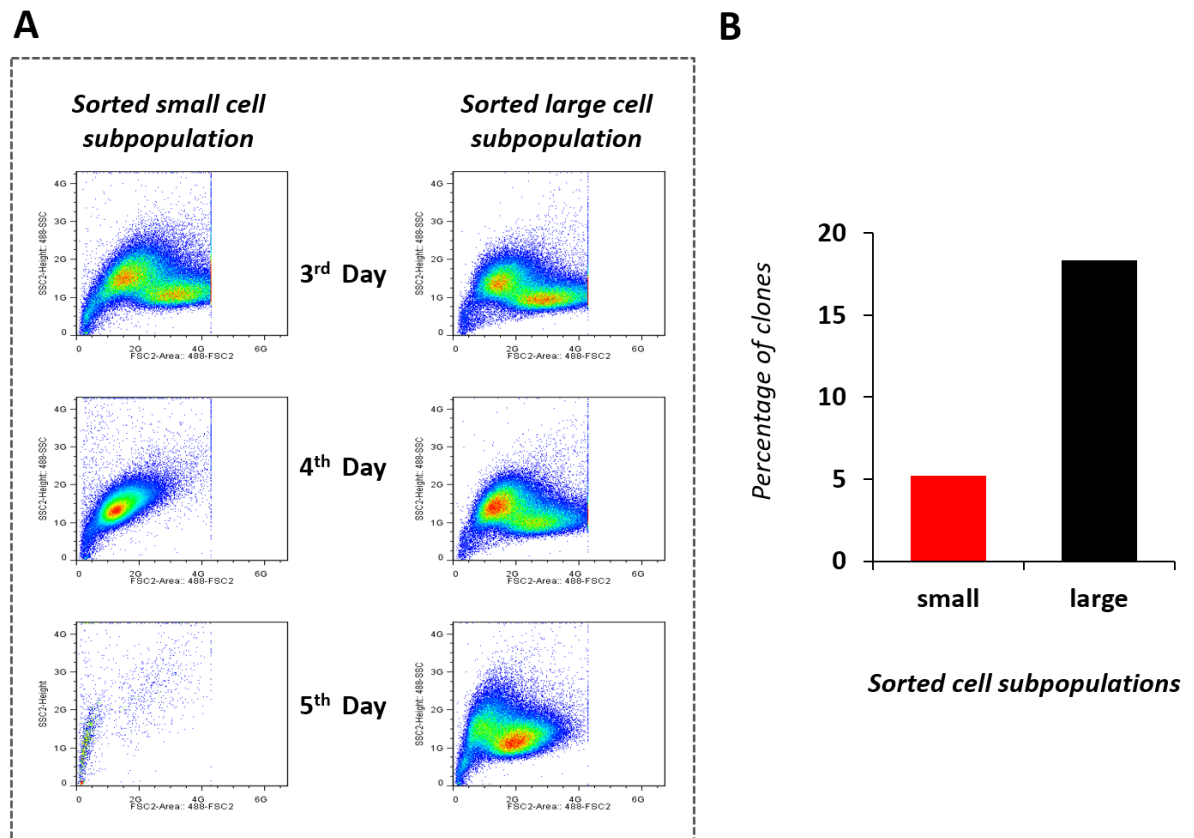
Figure 13. Flow cytometry detects 2 distinct populations in VX2 carcinoma cells. (A) Bulk cell sorting of small and large subpopulations of VX2 cell line and were monitored for consecutive 5 days. ***(B)*** Percentage of viable clones after single cell sorting of small cell population and large cell subpopulation of VX2 cells in 96 well plates to clear doubt about accidental mixing of both populations.

2.3.3.b   Single Cell sorting

To account for a possible leakage of single cells from one population to the other during bulk sorting, single cell sorting was performed into 96 well plates. After 2-3 weeks, the formation of colonies from single cells were observed. It was noted that a higher percentage of viable colonies was found in the sorted large cell population as compared to the sorted small cell population (**Figure 13B**). Repeated flow cytometry of colonies demonstrated both cell populations to reappear, thereby proving that both subpopulations belong to one and the same cell line.

Parallel assessment of results from bulk cell sorting and single cell sorting demonstrated that re-appearance of both cell populations from sorted large population (bulk sorting) referred to a high percentage of surviving clones (**Figure 13B**) during single cell sorting into 96 wells plate from

L.C.P. While disappearance of both populations in sorted small population conferred to underlying reason for less percentage of survived clones during single cell sorting from S.C.P. Therefore the presence of a L.C.P. correlates with a higher proliferative VX2 cell line. This supports the hypothesis that the larger cell population not only supports the survival of smaller cell population but also contributes in the proliferation of VX2 cell line.

2.3.4   Western blot analysis

Immunoblotting was performed to evaluate the expression of certain protein markers **(Figure 14).** TrkB (Tropomyosin receptor kinase B) is EMT mediator, promote invasiveness and found to be expressed in more than 50% of HNSCC tumor [161]. Vinculin, one of the focal adhesion molecules is involved in cell-cell and cell–ECM linkages and endorse tumor cells progression, migration and invasive potential [162] [163]. Zyxin is suggestive to be correlated with migration and invasive ability of HNSCC cells [164]. Similarly expression of Erk1/2, PCNA, CXCR4 and Pin-1-phospho can be related to migration and the invasive nature of the tumor cells. High expression of PCNA (proliferating cell nuclear antigen), phosphorylated (active) Erk1/2 correlates with tumor progression [165].

Western blot analysis of protein lysates derived from VX2 carcinoma tissue and the VX2 carcinoma derived cell line was performed to characterize VX2 cells. VX2 carcinoma tissue was used as control. Western blot results showed expression of protein markers (proliferative, EMT) both in the VX2 tumor and the VX2 carcinoma derived cell line.VX2 cells express the epidermal growth factor receptor (EGFR) thereby demonstrating the cells to be of epithelial origin. Surprisingly, the "large" subpopulation of the VX2 carcinoma cell line exhibits higher levels of phosphorylated (active) Erk1/2 as well as higher PCNA and Pin1-phospho Serine 16 levels compared with the respective "small" subpopulation.

All tested proteins are implicated in cell proliferation and cancer progression thereby pointing to the "large" population as the more proliferative one and having a more pronounced cancer cell phenotype. Furthermore, the EMT (epithelial mesenchymal transition) and metastasis related protein Zyxin is found less expressed in the "small" subpopulation indicating that the "large" population possibly is in a more mesenchymal stage than the "small" one [166] [167].
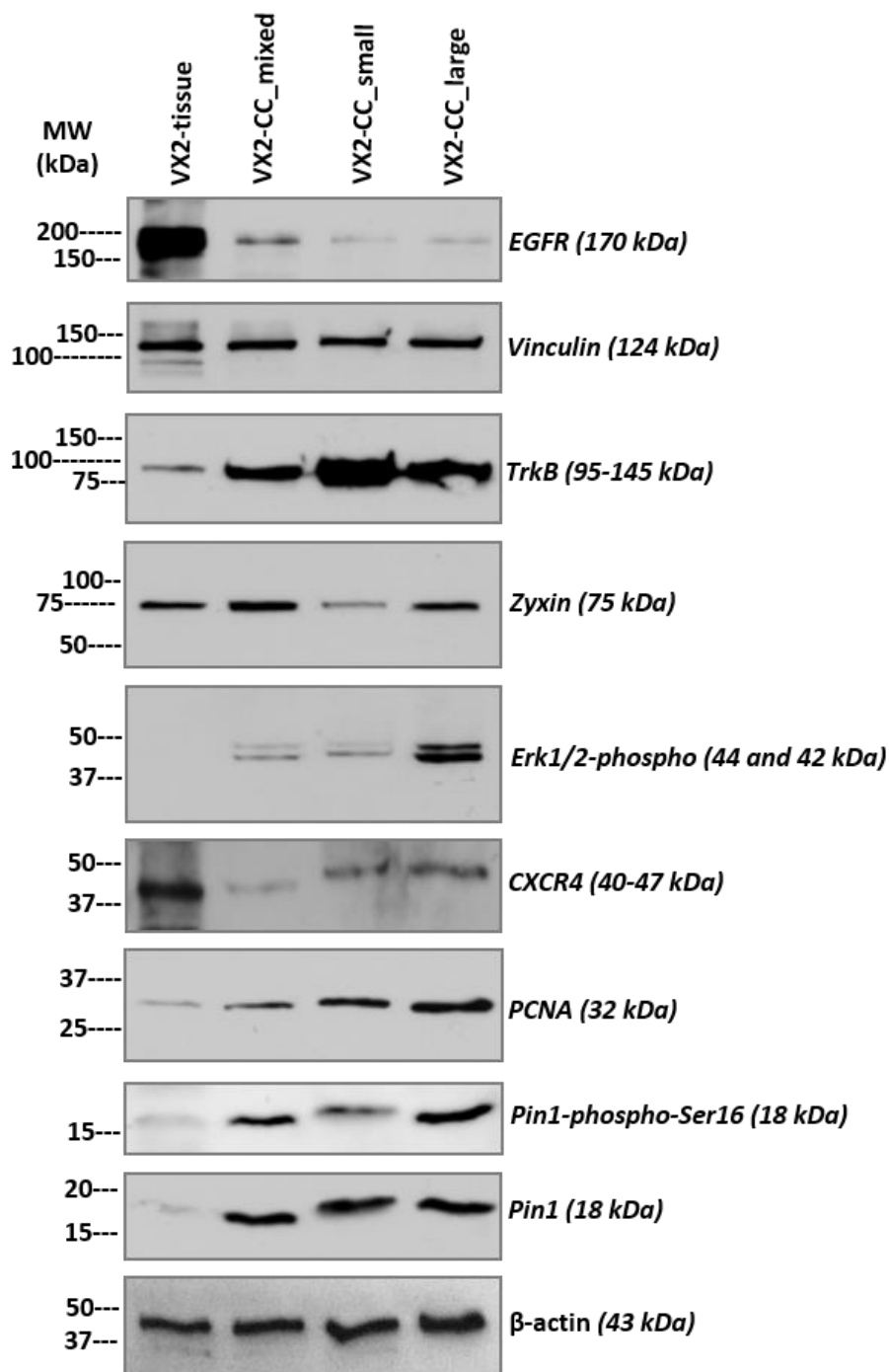
Figure 14. Western Blot of VX2 tissue, VX2 cells (unsorted), VX2 small and VX2 large (sorted cells on the basis of their FSC and SSC). Expression of EGFR (epidermal growth factor receptor), Vinculin (cell matrix adhesion moleculr), TrkB (neurotrophic marker), Zyxin (actinin 1 marker), Erk1/2-phospho (cell proliferation marker), CXCR4 (cell proliferation and differentiation marker), PCNA (proliferating cell nuclear antigen marker), Pin1-phospho-Ser16 , Pin 1 cell cycle progression markers, negative regulators of mitotic entry).

2.3.5   Molecular Biological characterization of VX2 tumor and VX2 carcinoma derived cell line

Quantitative real time PCR was performed to measure CRPV E6 and E7 oncogene transcripts using primers mentioned in **Table 8**. The results demonstrate detectable transcript levels of CRPV E6 and E7 oncogenes in the VX2 carcinoma and VX2 carcinoma derived cell line when compared to healthy rabbit skin keratinocytes **(Figure 15).** VX2 carcinoma derived cell line showed significant levels of CRPV E6 and E7 mRNA expression with fold change ~ 70.7 (**** $p < 0.0001$, n=9) and ~ 52.3(****$p < 0.0001$, n=9) respectively, while VX2 carcinoma (used as positive control) showed highly significant E6 & E7 mRNA levels with fold change of ~ 3925.5 (**** $p < 0.0001$, n=9) and ~ 8563.4 (****$p < 0.0001$, n=9) respectively, Contrary to these, rabbit keratinocytes (negative control) did not show any expression of CRPV E6 and E7 transcripts and had a fold change of 1 for baseline.
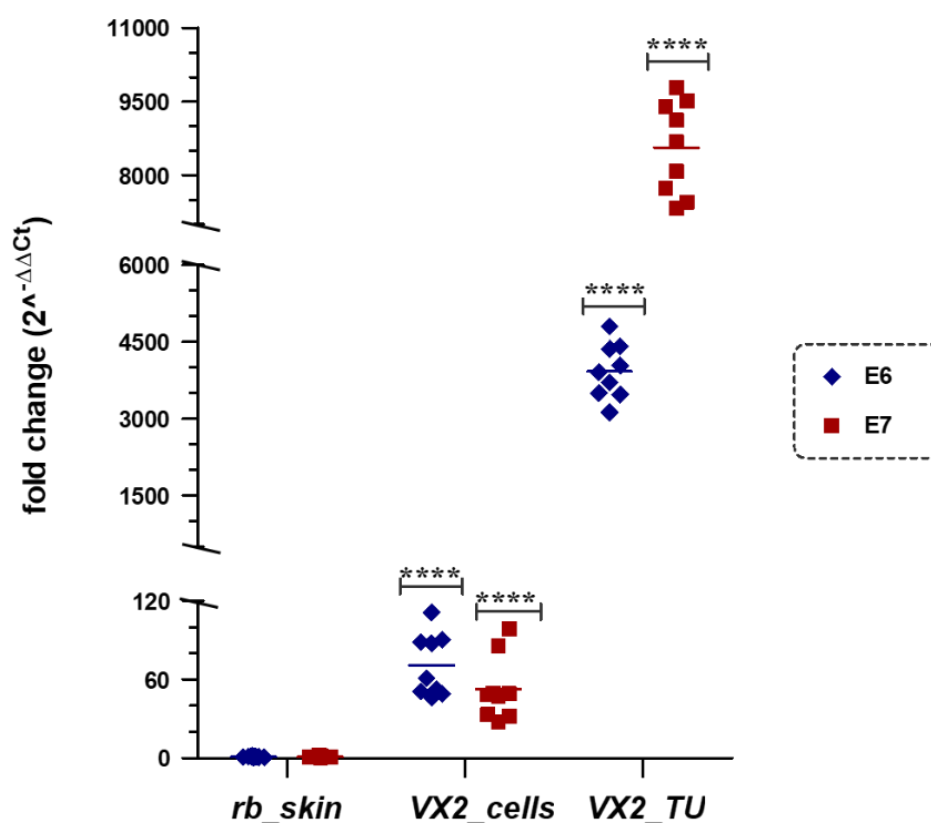
Figure 15. mRNA expression of CRPV E6 & E7 oncogenes expression in VX2 cells. VX2 tumour tissue was used as a positive control and rabbit keratinocytes as a negative control. The relative expression level was normalized using GAPDH and RPL32 housekeeping genes. Data are shown as mean $\pm$ SD (n=9), **** (p < 0.0001).

43

CHAPTER NO 3

Investigation of Photodynamic therapy effects on VX2 carcinoma derived cell line

3.1 *Aims and Objectives*

PDT has been identified as a promising therapeutic tool for the treatment of papilloma virus associated cervical cancers and head and neck cancers [168] [169]. The objective of this study is to evaluate the effects of PDT in combination with curcumin loaded liposomes in papilloma virus positive (PV+) cell lines. A set of three PV+ cell lines has been selected. Next to the transiently growing cottontail rabbit papilloma virus (CRPV) positive cells derived from the VX2 carcinoma of the New Zealand White (NZW) rabbit, which serves as an animal model for human HNSCC [22] [170], we also included HPV-18 positive cervical cancer cell line HeLa and the HPV-16 positive HNSCC cell line UD-SCC-2. The purpose of including HeLa and UD-SCC-2 cells in addition to VX2 cells was to observe how the same therapy (PDT) respond to human cell lines. Naturally occurring photosensitizer (curcumin) was selected for this study. The aims include

i.   Delivery of curcumin in the form of encapsulated liposomes to enhance its bioavailability and stability.

ii.   Toxicity studies (MTT assay) were conducted on cells using different curcumin liposomal concentration and various light fluences.

iii.   Selection of optimal dosages (conc) of curcumin liposomes and light irradiation for further studies.

iv.   Study of curcumin encapsulated liposomal effects on cells proliferation or migration abilities by scratch assay (wound closure) and clonogenic survival.

v.   To observe the death pathways through SYTO9/PI, Annexin-FITC/PI.

All abovementioned effects were analyzed using light irradiation only, curcumin liposomes with and without irradiation. These three treatment groups were selected to see which therapy works better on cells and is the most effective.

3.2 *MATERIALS AND METHODS*

3.2.1   Reagents

Curcumin was purchased from Sigma Aldrich (Taufkirchen, Germany). 1,2-distearoyl-sn-glycero-3-phosphocholine (DSPC) and 1,2-distearoyl-sn-glycero-3-phosphoglycerol (DSPG) were provided by Lipoid GmbH (Ludwigshafen, Germany). 3-(4,5-dimethylthiazol-2-yl)-2,5-diphenyltetrazolium bromide (MTT) was purchased from Sigma Aldrich Chemie GmbH (Taufkirchen, Germany). Dimethyl sulfoxide (DMSO) was obtained from Carl Roth GmbH & Co. (Karlsruhe, Germany). Organic solvents including methanol (MeOH), ethanol (EtOH) and chloroform ($CHCl_3$) were purchased from VWR International (Pennsylvania, USA). Phosphate buffered saline (PBS) pH 7.4 (with and without Ca^{2+}/ Mg^{2+}) was freshly prepared, sterilized and filtered using 0.2 µm polyethersulphone filters for all experiments. A list of all used materials is mentioned in the appendix.

3.2.2   Cell Culture

Transiently growing VX2 cell line derived from the VX2 carcinoma of New Zealand White (NZW) rabbits (as described in 2nd chapter) was used and sub-cultured in DMEM/Ham's F-12 (1:1) media containing 2 mmol/L L-Glutamine (Capricorn Scientific GmbH, Germany) supplemented with 10% FBS, 50 µg/ml gentamicin (Biochrom GmbH, Germany), 100 U/ml penicillin/streptomycin (Capricorn Scientific, Germany) and 50 µg/ml amphotericin B (Biochrom GmbH, Germany).

The cervical cancer derived HeLa and the HNSCC derived UD-SCC-2 (kindly provided by Prof. Dr. H. Bier, University of Düsseldorf, Germany) cell lines were grown in Dulbecco's Modified Eagle's Medium (DMEM) supplemented with 10% FBS (fetal bovine serum), 2 mmol/L L-Glutamine (Capricorn Scientific GmbH, Germany), 50 µg/ml gentamicin (Biochrom GmbH, Germany), 100 U/ml penicillin/streptomycin (Capricorn Scientific GmbH, Germany) and 50 µg/ml amphotericin B (Biochrom GmbH, Germany).

All three cell lines were cultured at 37°C, 5% CO_2 in a humidified incubator. Cells were grown as a monolayer until reaching app. 80% confluency.

3.2.3   Curcumin liposomes: preparation and characterization

Curcumin liposomes (cur.lipo) were generated as described previously by Duse et al [104] and are based on the thin-film hydration method [171].Briefly, liposomes were formulated by mixing lipids (DSPC : DSPG; 80:20 molar ratio dissolved in chloroform:methanol 2:1; v/v) and curcumin (dissolved in methanol) in a round bottom flask. Curcumin was added to the lipid mixture in a ratio of 1:30. The solvents were evaporated to obtain a thin film using a Laborota 4000 rotary evaporator (Heidolph Instruments, Schwabach, Germany) equipped with a vacuum pump (KNF Neuberger GmbH, Freiburg, Germany). 20 mmol/L HEPES buffer solution (pH 7.4) was used to rehydrate the film followed by sonication in a bath-type sonicator (Elmasonic P30 H, Elma Hans Schmidbauer, Singer, Germany) at 56 $^\circ$C to obtain liposomal dispersion. The liposomes were then extruded using polycarbonate membrane filters (Nuclepore track-etch membrane, Whatman GmbH, Germany) through 200 nm using Avanti mini-extruder® (Avanti Polar Lipids, Alabama, USA). The extruded liposomes were stored at 4 $^\circ$C until further use.

The hydrodynamic diameter and zeta potential of liposomes were measured by dynamic light scattering (DLS) and laser Doppler velocimetry (LDV) respectively using Zetasizer Nano ZS (Malvern Panalytical GmbH, Kassel, Germany) equipped with a 10 mW HeNe laser at $\lambda = 633$ nm with scattered light detection at an angle of 173°. Prior to the measurements, liposomes were diluted (1:100) with 20 mmol/L HEPES buffer (pH=7.4) and placed in a clear disposable folded capillary cell (DTS1060, Malvern Instruments) for determining particle size and zeta potential. The curcumin concentrations were measured as previously described by Duse et al [104].

3.2.4   Photodynamic therapy

A low power LED (light emitting diode) device (Lumundus GmbH, Eisenach, Germany) was specifically designed to fit multiwell plates. The device is equipped with two different LEDs of 457nm (blue) and 652nm (red) wavelengths. It is supplied with the functions to control setting for wavelength, current (mA) and irradaiation time (s) as per energy requirement. The device is able to deliver 220.2 W/m^2 irradiance at a current of 100 mA and a wavelength of 457nm. The light dose (J/cm^2) supplied to the cell is equal to irradiance (W/cm^2) times the irradiation time (s).

For all PDT treatments, HeLa, UD-SCC-2 and VX2 cells were incubated with curcumin liposomes for 4 h at 37 ºC, 5% CO_2. Subsequently, cells were washed with PBS followed by addition of fresh

media. Cells were then exposed to different light fluences and incubation was continued for 24 h. The cells were irradiated by light with a wavelength of 457 nm (blue) for 45, 136 and 227 s at a light fluence of 220.02 W/m^2 (100 mA) corresponding to 1, 3 and 5 Jcm^{-2} respectively of the total light energy delivered.

3.2.5   Assays

3.2.5.1   Cell viability and irradiation experiments

The MTT assay [172] was deployed to assess the viability of cells treated with curcumin liposomes alone, PDT alone or a combination of curcumin liposomes with PDT. Cells were seeded at ~1×10^4 (HeLa and VX2) or ~6×10^4 (UD-SCC-2) cells per well (0.35 cm^2) in a 96 well transparent microtiter plate (Nunclon Delta, Thermo Fischer Scientific GmbH, Dreieich, Germany). Twenty four hours after seeding, cells were incubated with curcumin bound liposomes or free curcumin (dissolved in DMSO) in different concentrations ranging from 0-100 µmol/L for 4 h. Afterwards, cells were washed twice with PBS followed by addition of fresh medium.

The cells were irradiated with light fluences of 1, 3 and 5 Jcm^{-2}. The irradiated plates were incubated for 24 h at standard conditions (37 °C, 5% CO_2). Non-irradiated plates (dark) were used as a control. After 24 h, MTT solution (final dilution in medium: 2 mg/ml) was added to the cells and incubation was continued for another 4 h. Subsequently, the resulting formazan crystals were dissolved with DMSO and the absorbance (Ab) was measured at 570 nm using the FLUOStar Optima plate reader (BMG Labtech, Ortenberg, Germany). Cell viability was calculated using the following formula:

$$Viability\ of\ cells\ (\%) = \frac{Ab\ (sample) - Ab\ (blank)}{Ab\ (control) - Ab\ (blank)} \times 100$$

Ab (sample) represents absorbance of cells treated with sample (cur.lipo or curcumin alone) and Ab (control) shows absorbance of cells without any treatment. Whereas Ab (blank) stands for absorbance of wells containing media only.

3.2.5.2   Flow cytometric assay using Annexin-FITC/PI staining

Flow cytometry was performed to determine cell death mechanism using Annexin V-FITC /PI kit (Annexin V-CFS, R&D Systems, Minneapolis, Canada) [173]. Apoptosis and necrosis are the two main mechanisms involved the death of cells. During apoptosis, there is a translocation of membrane phosphatidylserine (PS) from inner to outer side of membrane precedes loss of membrane integrity. Annexin V binds specifically to phosphatidylserine so labelled Annexin V can be used to detect apoptotic cells. The integrated cell membrane excludes propidium iodide in viable and early apoptotic cells, whereas necrotic cells are permeable to propidium iodide. Therefore dicrimination between live, early apoptic, late apoptotic and necrotic cells on applying various treatments to the cells was made through FACS analysis using Annexin V-FITC /PI kit.

Briefly HeLa, UD-SCC-2 and VX2 cells were seeded in 6 well plates overnight at a density of 5-10×10^5 cells per well. Upon reaching a confluency of 70-80%, cells were exposed to different treatments (cells treated with curcumin liposomes only, cells treated with light irradiation only and cells treated with both curcumin liposomes and irradiation). Cells without any treatment were used as a control.

Twenty four hours after treatment, cells (1×10^5) were harvested, washed in ice cold PBS and re-suspended in 100 µl of (1x) binding buffer (1.4 mol/L NaCl, 0.1 mol/L HEPES (pH 7.4), 2.5 mmol/L $CaCl_2$). The cells were incubated with 10 µl of fluorescein-conjugated Annexin V reagent for 15 min at room temperature in the dark. Thereafter, 400 µl of (1x) binding buffer containing 5 µg/ml PI (which stains late apoptotic and necrotic cells) was added to each tube and placed on ice.

The sample measurements were performed using a BD LSR II flow cytometer (Becton Dickinson, New Jersey, USA) and data analysis was performed with the FlowJo 10.6.2 software (Flowjo, LLC, Ashland, OR, USA). Early apoptotic, late apoptotic and necrotic cells were estimated as the percentage of the total number of cells using the BD FACSDiva 7.0 software. Curcumin liposomes were incubated for 4 h and light fluence was set to 3 Jcm^{-2} (IC_{50} at 3 Jcm^{-2}: 9.52 µmol/L for HeLa, 7.88 µmol/L for UD-SCC-2 and 20.70 µmol/L for VX2 cells).

3.2.5.3   Live/dead staining assay

The live/dead staining assay was performed on HeLa, UD-SCC-2 and VX2 cells to evaluate the toxicity of the different treatments (exposure of cells to curcumin liposomes only, exposure to light irradiation only and exposure to a combination of curcumin liposomes and PDT). The cells were incubated with curcumin liposomes for 4 h followed by irradiation. After 24 hours of treatment, cells were washed with PBS (containing Ca^{2+}/Mg^{2+}) and stained with a solution containing 2 μmol/L of SYTO9 (S34854, Invitrogen, Thermofischer Scientific) and 4 μmol/L of PI (81845, Sigma-Aldrich Co). The cells were incubated at 37 °C, 5% CO_2 for 30 min, washed in PBS and analyzed under a microscope (CKX-53 Olympus, USA). Curcumin liposomes were incubated for 4 h and light fluence was set to 3 Jcm^{-2} (IC_{50} at 3 Jcm^{-2}: 9.52 μmol/L for HeLa, 7.88 μmol/L for UD-SCC-2 and 20.70 μmol/L for VX2 cells).

3.2.5.4   Clonogenic survival assay

A colony formation assay was performed to evaluate the ability of cells to proliferate after being exposed to the different treatment modalities [174]. HeLa, UD-SCC-2 and VX2 cells were plated in six well plates at a density of 150 cells per well. Following different treatment procedures (PDT only, curcumin liposomes only, curcumin liposomes with PDT), cells were incubated for two weeks at 37°C and 5% CO_2 without media change. After completing the 14 days incubation period, cells were washed with ice-cold PBS (containing Ca^{2+}/Mg^{2+}) and subsequently fixed with pre-chilled methanol for 10 min followed by another wash in PBS. Staining with 0.1% crystal violet dye was done to detect colony formation. Colonies with at least 50 cells were considered and counted. Curcumin liposomes were incubated for 4 h and light fluence was set to 3 Jcm^{-2} (IC_{50} at 3 Jcm^{-2}: 9.52 μmol/L for HeLa, 7.88 μmol/L for UD-SCC-2 and 20.70 μmol/L for VX2 cells).

3.2.5.5   Scratch cells migration assay

The scratch (wound closure) assay was deployed to analyze the migratory ability of cells after exposure to various treatment procedures [175]. HeLa, UD-SCC-2 and VX2 cells were seeded in 6 well plates at a density of 5×10^5 cells/well and cultured until cells reached 90% confluency. After cells were subjected to different treatments (PDT only, incubation of cells with curcumin

liposomes in dark and in light), a linear scratch was made using a 10 µl sterile pipette tip followed by washing of cells with PBS and addition of fresh medium. The images were captured at t = 0 h to record the initial area of the scratch and at t = 24 h to evaluate effects of different treatments on the migratory ability of cells towards the scratch area. The images were photographed with the CKX53 microscope system (Olympus, USA). ImageJ analysis software [176] (MRI_wound healing tool: written by V. Baecker; collaborators: N. Cahuzac and V. Georget; (c) 2010-2017, INSERM) was used to quantify the area of the scratch. The images were photographed using microscope (CKX-53 Olympus, USA). The migration of cells towards the scratch was expressed as percentage of scratch cell migration [177]

$$Scratch\ cells\ migration(\%) = \frac{Area(t = 0hr) - Area(t = 24hr)}{Area(t = 0hr)} \times 100$$

Curcumin liposomes were incubated for 4 h and light fluence was set to 3 Jcm^{-2} (IC$_{50}$ at 3 Jcm^{-2}: 9.52 µmol/L for HeLa, 7.88 µmol/L for UD-SCC-2 and 20.70 µmol/L for VX2 cells).

3.2.5.6   Lysosomal disruption

Hela, UDSSC-2 and VX2 cells were plated at a seeding density of 5-10$\times$10^5 cells per well in 6 well cell culture plates containing sterile coverslips(15mm diameter) and cultured at 37°C and 5% CO$_2$ until cells reached 70-80% confluency.

The cells were treated with curcumin liposomes only, PDT only and curcumin liposomes with PDT followed by incubation for 24h. Then the cells were incubated with 100nmol/L of LysoTracker® red DND-99 (Thermo Fischer Scientific, Dreieich, Germany) in the dark for 30 min at 37°C to stain the lysosomes. After completion of the incubation period, cells were washed with 500µl PBS with Ca^{2+}/Mg^{2+} followed by fixing the cells in 4% formaldehyde solution. DAPI (0.1µg/ml) was used to counterstain the nucleus.

Non-fluorescent glycerol based mounting medium (FluorSave^{TM}, Calbiochem Corp, La Jolla, USA) was used to seal coverslips on glass slides. The cells were analyzed using a confocal laser scanning microscope (Zeiss Axiovert 100 M, Carl Zeiss microscopy GmbH, Jena, Germany). Incubation period of 4h for curcumin liposomes (9.52µmol/L for Hela, 7.88µmol/L for UD-SSC-2 and 20.70µmol/L for VX2 cells) was used and light fluence was set to 3 Jcm^{-2}.

3.3 *RESULTS & DISCUSSION*

3.3.1   Physicochemical properties of curcumin liposomes

The stability, safety, efficacy of drug delivery systems depend on various physical attributes such as particle size and the polydispersive index. The mean size distribution of liposomes was assessed by photon correlation spectroscopy (PCS) using Zetasizer Nano ZS (Malvern Panalytical GmbH, Kassel, Germany). By this method, the particle size (hydrodynamic diameter), zeta potential and polydispersity index (PDI) can be determined. The data was expressed as the mean ± standard deviation derived from measurements of three independent experiments **(Figure 16)**.
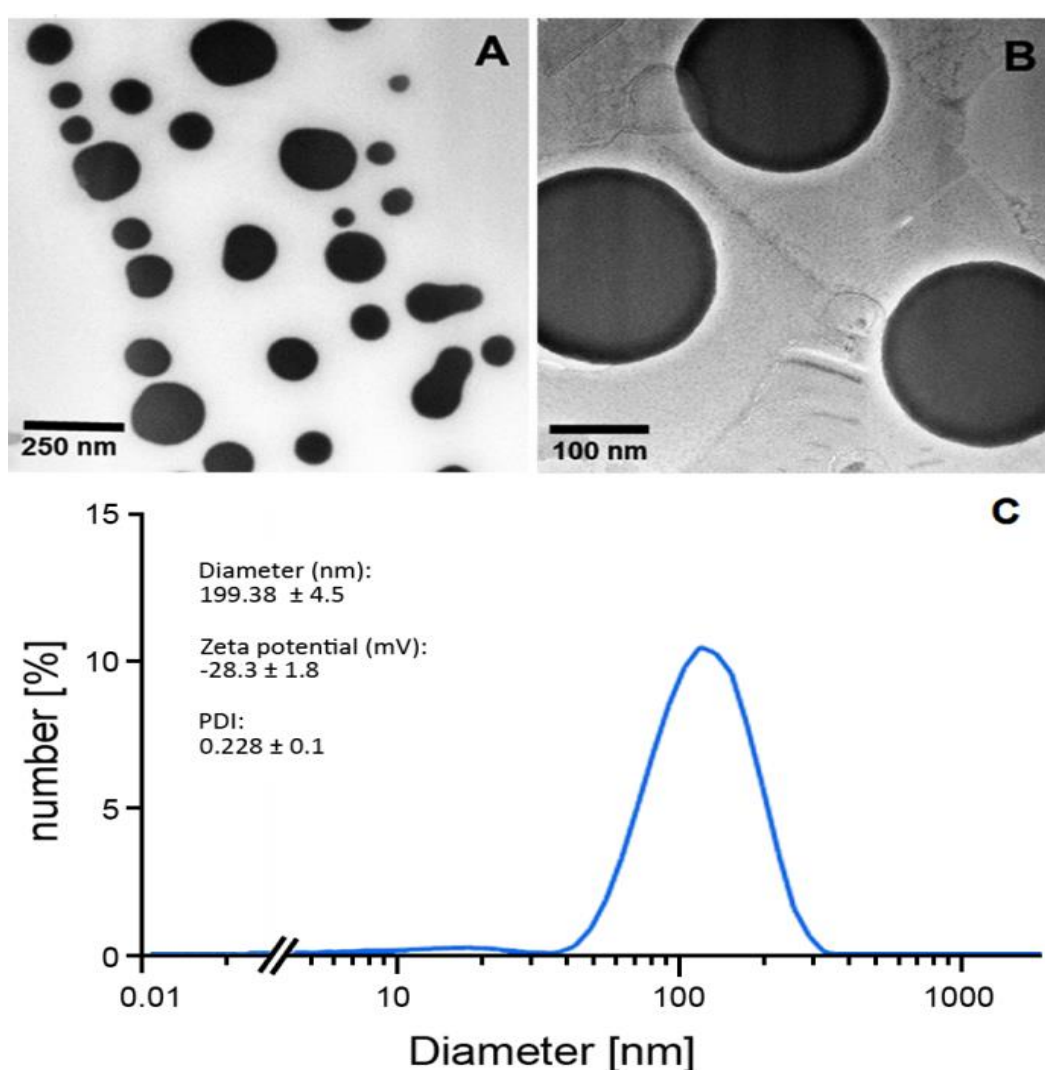
*Figure 16. Physicochemical characteristics of curcumin liposomes.* Transmission electron microscopical images depicting the morphology and size variance of curcumin liposomes *(A, B)* were generated as previously described by Duse et al [104]. Shown are characteristical features of the used curcumin liposomes such as diameter (size) distribution, zeta potential and polydispersity index (PDI) *(C)*.

The dynamic light scattering analysis showed a PDI > 0.2 suggesting the presence of a polydispersed liposome formulation [104]. The curcumin liposome formulation used here is as reported by Duse et al [104]. In the study by Duse et al. the authors extensively described the generation and characterization of curcumin liposomes and particularly evaluated the effects of curcumin liposomes in conjunction with PDT on ROS generation, blood coagulation, haemolysis and the microvasculature of the chicken chorioallantoic membrane. In addition, using the MTT viability assay, the authors looked at cytotoxic effects in the human ovarian carcinoma cell line SK-OV-3 and in primary human coronary artery endothelial cells treated with curcumin loaded liposomes together with PDT.

The present study is building on and extending the work of Duse et al. by in addition to evaluating cellular viability, looking into the biological effects of curcumin loaded liposomes and PDT on other tumor associated features such as apoptosis, ability of cells to form colonies and tumor cell migration. For this, three papillomavirus associated cell lines were deployed since PDT previously was found to effectively treat HPV positive cervical intraepithelial neoplasia (CIN) and vulvar HPV-16 positive cell lines [169] [178]. In particular, we also included two papillomavirus positive squamous cell carcinoma cell lines derived from the head and neck area since, next to cervical cancer of the uterus, head and neck cancer, specifically in the oropharyngeal region, is highly associated with HPV type 16.

3.3.2 Evaluation of cell viability after dark-toxicity and phototoxicity of curcumin liposomes

MTT assay was first described by Mosman T et al [179]. This is a colorimetric method based on the reduction of yellow tetrazolium salt (3-(4,5-dimethylthiazol-2-yl)-2,5-diphenyltetrazolium bromide or MTT) by nicotinamide adenine dinucleotide phosphatase (NADPH)-dependent oxidoreductase enzymes in the viable cells to purple formazan cyrstals. Therefore MTT assay is used to measure cell viability, cellular proliferation and cellular toxicity during application of any treatment strategy to cells.

MTT assays were performed to evaluate the dark toxicity (no light exposure) and phototoxicity of curcumin liposomes and free curcumin in HeLa, UD-SCC-2 and VX2 cells 24 h after exposure. It was carried out by incubation of cells with different concentrations (0-100 µmol/L) of curcurmin liposomes and free (dissolved in DMSO) curcumin for 4 h followed by subsequent exposure to

different light fluences (1, 3 and 5 Jcm^{-2}) using a prototype LED device with blue light (wavelength $\lambda = 457$ nm).

Initial incubation of all cells for 2 h did not show any significant difference in cellular viability (data not shown), indicating the need for increasing the incubation time. Treatment of all cell lines with free curcumin without irradiation showed a dose dependent cellular toxicity referred to as dark toxicity **(Figure 17A, 17B, 17C; right graphs)**. This dark toxicity, however, could also be due to the presence of DMSO serving as a vehicle of free curcumin. Contrary to this, curcumin encapsulated liposomes didn't show any significant toxicity in the dark **(Figure 17A, 17B, 17C; left graphs)**, with all cell lines exhibiting 90-94% viability at maximal curcumin concentrations of 100 µmol/L. This data suggests that therapeutic toxicity can be abrogated by liposomal encapsulation and thus curcumin liposomes would remain non-toxic until illuminated by light of specific wavelengths.

Irradiation alone resulted in no significant cell death in any of the cell lines. It was noticed in all cell lines that a combined treatment of curcumin liposomes and light irradiation (PDT) had a significant impact on cellular viability resulting in light-dose dependent inhibition of cell proliferation as shown in **Figure 17** (all graphs). The half maximal inhibitory concentration (IC_{50}) value for each light dose was calculated by non-linear curve fitting. A gradual reduction in half maximal inhibitory concentration of liposomes was noticed with increasing light fluence. The maximal phototoxicity was observed at a maximum radiation fluence of 5 Jcm^{-2}. Since major effects were already seen at 3 Jcm^{-2}, this light fluence was used for subsequent experiments.

At the light fluence of 3 Jcm^{-2}, the IC_{50} values of curcumin liposomes for HeLa, UD-SCC-2 and VX2 cells were 9.52 µmol/L, 7.88 µmol/L and 20.70 µmol/L respectively. The observed PDT effect after illumination was curcumin dose-dependent and highly significant (p<0.001). These results are in accordance with previous reports pointing out a role of curcumin in the treatment of diverse maladies such as inflammatory diseases and cancer [93].

Similarly, López-Jornet et al. could demonstrate a synergistic effect of curcumin and ionizing irradiation on oral squamous cell carcinoma cells [180]. Feng and coworkers underlined the urgent need for specific curcumin formulations since the bioavailability of curcumin is very poor. Here the authors emphasized liposomal curcumin formulations as promising therapeutic vehicles [97]. Such curcumin loaded tetraether liposomes showed prominent therapeutic efficacy particularly when combined with PDT [104].

These observations are in agreement with a recent report using a curcumin-nanoemulsion in conjunction with PDT on HPV-16 E6 transduced A431 cells [178].
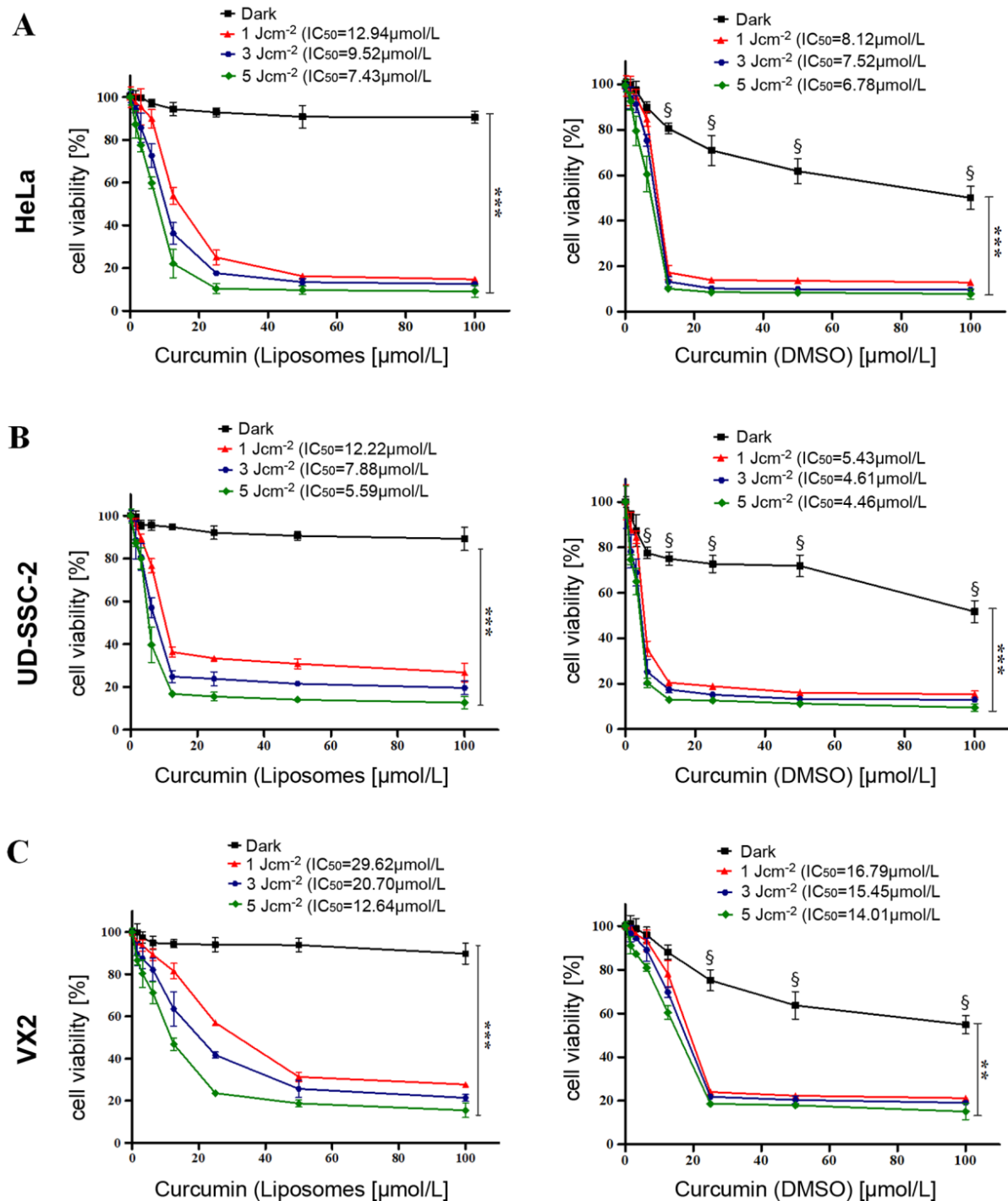

Figure 17. Evaluation of cellular viability in HeLa, UD-SCC-2 and VX2 cells. Cellular viability was assessed with the MTT assay to determine the dark toxicity and phototoxicity of curcumin loaded liposomes *(A, B and C left)* and free curcumin using DMSO as a vehicle *(A, B and C right)*. Dark toxicity

and phototoxicity were determined by incubation of curcumin liposomes and free curcumin for 4 hours in the concentration range of 0-100 μmol/L at light fluences of 1, 3 and 5 Jcm^{-2}. Dark refers to untreated cells (0 μmol/L curcumin) and cells treated with free curcumin or curcumin liposomes without PDT respectively. IC$_{50}$ values were calculated by non-linear curve fitting for each light fluence. All samples were measured in triplicates and the data was expressed as mean ± S.D.. Statistical significances are indicated as ***p<0.001, **p<0.01. §=Viability of cells treated with free curcumin (in DMSO) is significantly (p<0.001) lower than in the corresponding curcumin (liposomes) treated cells.

3.3.3   Evaluation of apoptosis as a cause of cell death

The underlying mechanism for inhibition of proliferation and cell death might be cellular apoptosis. Therefore the flow cytometry based Annexin V-FITC/PI assay was deployed to evaluate the rate of apoptosis in HeLa, UD-SCC-2 and VX2 cells after deploying various treatment modalities (mentioned in methods).

Flow cytometry analysis of HeLa cells (Figure 18A) showed that combined treatment of curcumin liposomes and PDT exhibited an increase in the percentage (49.4 ± 6.0%) of Annexin V (FITC) positive cells (consisting of early and late apoptotic or necrotic cells) when compared to cells irradiated with light only (7.4 ± 0.7%), cells incubated with curcumin liposomes only (7.4 ± 1.3%) and untreated (control) cells (1.8 ± 0.7%).

Flow cytometry analysis of UD-SCC-2 cells (Figure 18B) showed that the combined treatment of curcumin liposomes and PDT exhibited an increase in the percentage (33.7 ± 6.7%) of Annexin V (FITC) positive cells compared with cells irradiated with light only (5.8 ± 1.1%), cells incubated with curcumin liposomes only (8.7 ± 0.4%) and untreated cells (4.3 ± 0.5%).

Similarly, flow cytometry micrographs and graphical data of VX2 cells (Figure 18C) showed that the combined treatment of curcumin liposomes and PDT on cells exhibited an increase in the percentage (29.0 ± 4.6%) of Annexin V (FITC) positive cells when compared with cells irradiated with light only (1.1 ± 0.4%), cells incubated with curcumin liposomes only (6.5 ± 1.8%) and untreated cells (1.0 ± 0.2%).

Flow cytometry results therefore demonstrate for all cell lines that curcumin liposomes in combination with PDT promote significant cell death. Since early apoptotic cells (Annexin V-FITC positive and PI negative) did not show a significant rise, apoptosis could not be

unequivocally identified as the sole underlying cause of cell death in cells treated with curcumin liposomes and PDT.
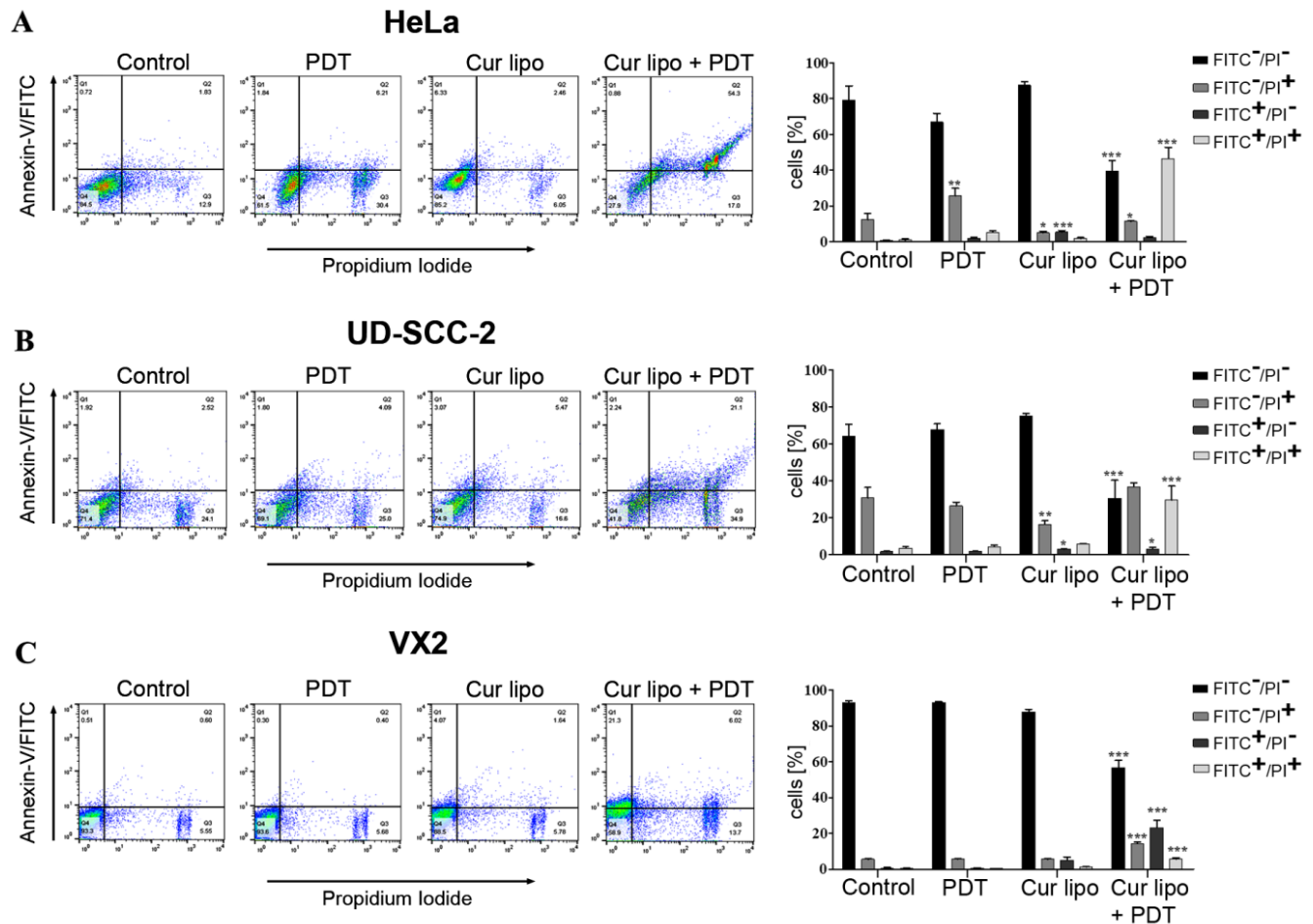
Figure 18. Evaluation of apoptosis as a cause of cell death in HeLa, UD-SCC-2 and VX2 cells after treatment with curcumin liposomes and PDT. All cells were incubated with curcumin liposomes for 4 h and subsequently irradiated with a light fluence of 3 Jcm^{-2}. After 24 h treatment, cells were co-stained with Annexin-V/FITC and PI. Representative FACS micrographs are shown for HeLa *(A)*, UD-SCC-2 *(B)* and VX2 *(C)* cells treated with PDT alone, curcumin liposomes alone or a combination of curcumin liposomes with PDT. Untreated cells were used as a control. Q1 represents early apoptotic cells, Q2 represents late apoptotic or necrotic cells, Q3 represents necrotic cells and Q4 represents live cells. Bar graphs represent the percentage of total apoptotic cells from at least three experiments. Data are shown as mean $\pm$ S.D. and statistical significances are indicated as ***p<0.001, **p<0.01, *p<0.05

3.3.4   Cell viability assessment via the SYTO9/PI live/dead assay

Live/dead assay was performed to differentiate between live and dead cells on the basis of cell membrane integrity [181]. HeLa (**Figure 19A**), UD-SCC-2 **(Figure 19B)** and VX2 **(Figure 19C)** cells were assayed using a dual staining procedure with SYTO9 and PI to determine the effects of light irradiation alone as well as curcumin liposomes with and without light irradiation (PDT) on cellular viability. During staining, SYTO9 enters cells regardless of their membrane integrity and binds to DNA and after excitation emits a green fluorescence while PI only enters cells with a disrupted membrane emitting a red fluorescence. Therefore SYTO9 stains all cells while PI stains necrotic and late apoptotic cells.
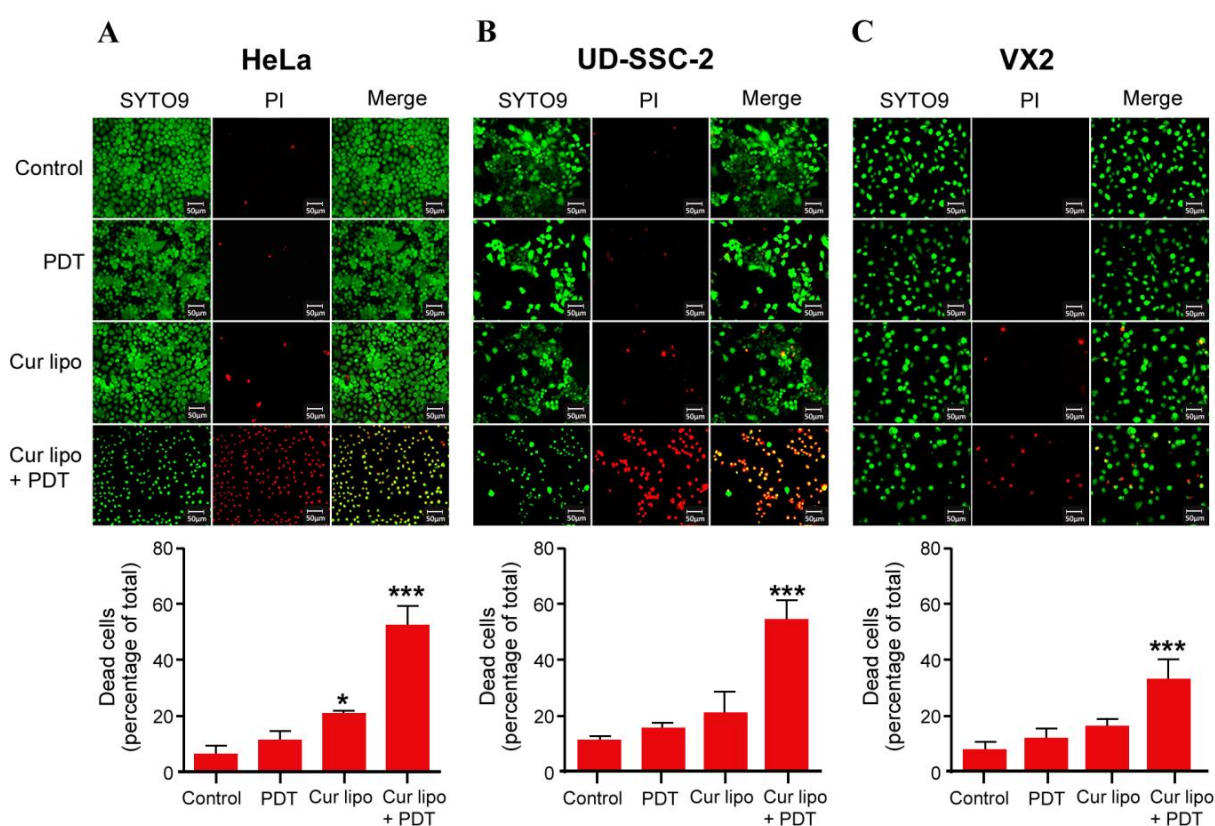
Figure 19. Live/dead staining of HeLa, UD-SCC-2 and VX2 cells. Cells were treated with light irradiation (PDT) only, with curcumin liposomes only or with curcumin liposomes in combination with PDT. Untreated cells were used as a control. All cells were stained with SYTO9 (green fluorescence) showing uniform green nuclei while PI only labeled non-viable or dead cells (red) representing late apoptotic or necrotic cells. Bar graphs represent the quantification of dead cells (percentage) in the different treatment groups. Treated cells were compared to untreated control cells. The values are shown as mean $\pm$ S.D. and statistical significances are indicated as ***p<0.001, *p<0.05.

Microscopic images of all cell lines demonstrate that cells without any treatment (control) and cells irradiated with light (PDT) only remained viable as indicated by the presence of green fluorescence. Cells treated with curcumin liposomes but without irradiation showed minor cell death (red fluorescence). In sharp contrast, treatment of cells with curcumin liposomes and PDT resulted in major cell death in all three cell lines. Interestingly, in a previous report the authors used curcumin loaded dextran micelles on C6 glioma cells. Here the authors observed major cell death when applying this formulation even in the absence of PDT [182]. In sharp contrast, in our study, using curcumin loaded liposomes without PDT; we only observed minor cell death which markedly rose after applying PDT **(Figure 19)**. This formulation therefore appears to be more suitable for the use *in vivo* since the toxic antitumor curcumin effect will be activated only after PDT.

3.3.5   Influence of PDT treatment on colony formation

Colony formation assay or clonogenic assay is an *in vitro* cellular method based on ability of formation of colony from a single cell. It is an assay to determine the effectiveness of various treatment modalities on cell survival and proliferation.

The effects of various PDT treatment strategies (as described in methds) on HeLa, UD-SCC-2 and VX2 cell colony formation were evaluated by a colony formation assay **(Figure 20)**. Cells without any treatment were considered as control. Colonies were evaluated 14 days after treatment.

HeLa cells exhibited a dramatically reduced (18%) ability to form colonies in cells treated with curcumin liposomes and PDT in comparison to control cells. Cells treated with curcumin liposomes alone reached 63% and cells treated with only PDT 77% of the colony formation level observed for control cells **(Figure 20A)**.

In UD-SCC-2 cells, the colony formation ability was reduced to 21% after combined treatment with curcumin liposomes and PDT compared with untreated control cells, while cells treated with curcumin liposomes alone and cells treated with irradiation alone showed a colony formation ability of 57% and 72%, respectively **(Figure 20B)**.

VX2 cells treated with curcumin liposomes and PDT showed the lowest number (27%) of colonies in comparison to control cells. In contrast, cells treated with curcumin liposomes showed 69% and cells exposed to light irradiation alone 89% colony formation ability **(Figure 20C)**.

Therefore colony formation assay results suggest that treatment of cell lines with a combination of curcumin liposomes and PDT could significantly reduce the number of colonies as compared to light irradiation only or curcumin liposomes alone.
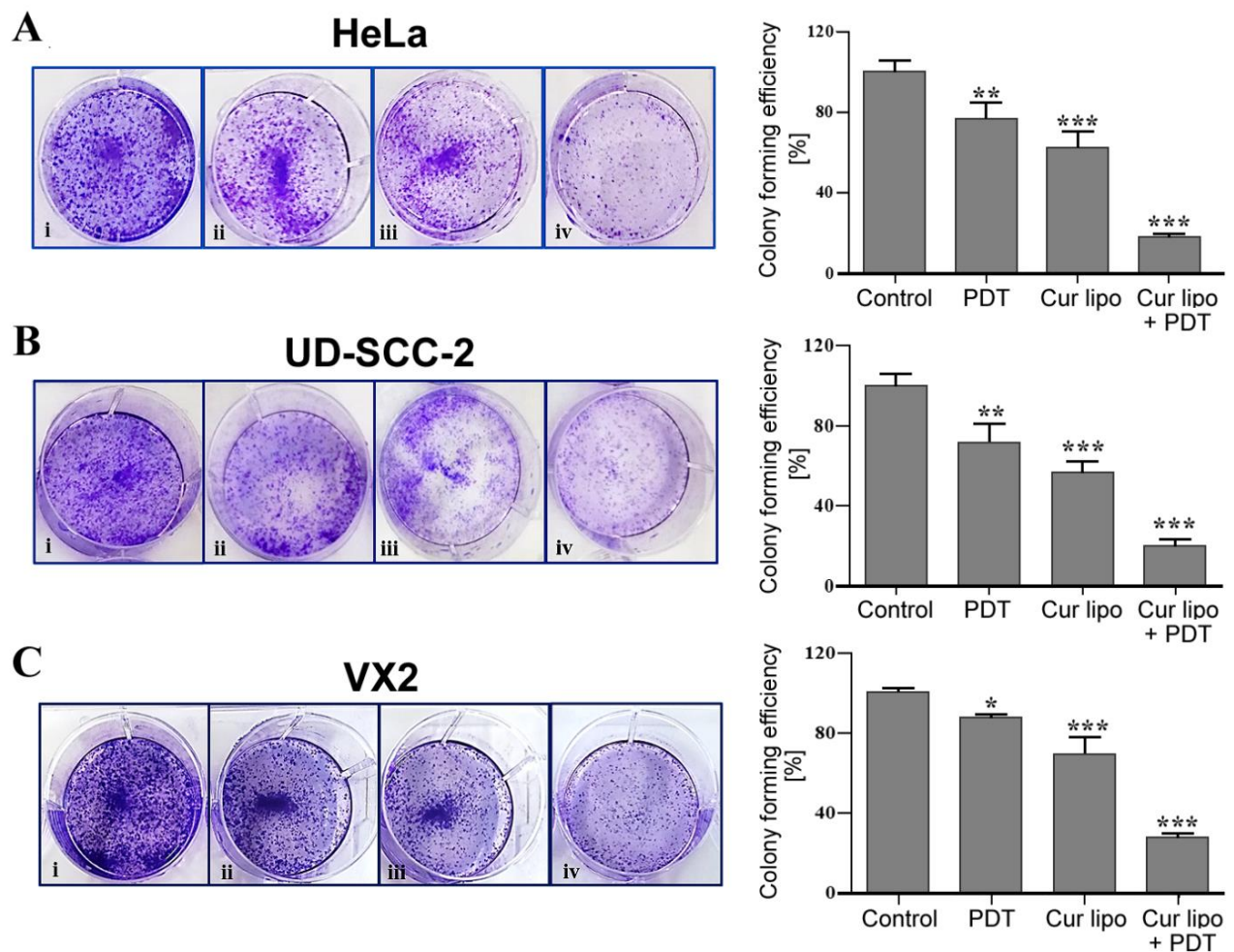
Figure 20. Colony formation assay with HeLa, UD-SCC-2 and VX2 cells. HeLa *(A)*, UD-SCC-2 *(B)* and VX2 *(C)* cells were exposed to PDT only *(ii)*, curcumin liposomes only *(iii)* or curcumin liposomes in combination with PDT *(iv)*. Untreated cells were used as a control *(i)*. Cell colonies of HeLa (A), UD-SCC-2 (B) and VX2 (C) cells were stained with 0.1% crystal violet dye. Graphical data represent the level (percentage) of colony formation after exposure to the various treatment modalities compared to control values. Values are presented as the mean ± S.D. and statistical significances are indicated as ***p<0.001, **p<0.01, *p<0.05.

3.3.6   Analysis of scratch cells migration

A major cause of cancer morbidity and mortality is cancer metastasis, which is responsible for 90% of cancer deaths. The migration of disseminated cancer cells into surrounding tissues is a primary step in tumor metastasis. Inhibition of cell migration can be potential target to prevent cancer metastasis [183] [184].

To investigate the role of photodynamic therapy in tumor metastasis, different treatment modalities were applied to HeLa, UD-SCC-2 and VX2 cells **(Figure 21)** followed by evaluation of tumor cell migration using the scratch (wound closure) assay. A significantly stronger inhibition of cell migration was observed microscopically in HeLa **(Figure 21A)**, UD-SCC-2 **(Figure 21B)** and VX2 **(Figure 21C)** cells treated with a combination of curcumin liposomes and light irradiation. Respective graphs at the right depict the percentage of cells migrating into the scratched area as observed at t = 24 h in HeLa **(Figure 21A)**, UD-SCC-2 **(Figure 21B)** and VX2 **(Figure 21C)** cells respectively.

In HeLa cells, the percentage of cells migrating towards the scratched area in untreated control cells, cells treated with PDT only, curcumin liposomes only and curcumin liposomes along with PDT were $99.0 \pm 0.2\%$, $76.9 \pm 2.1\%$, $59.5 \pm 4.5\%$ and $16.9 \pm 3.8\%$ respectively **(Figure 21A)**.

In UD-SCC-2 cells, the percentage of cells migrating towards the scratched area in untreated control cells, cells treated with PDT only, curcumin liposomes only and curcumin liposomes along with PDT were $90.4 \pm 0.8\%$, $71.2 \pm 1.8\%$, $62.8 \pm 2.2\%$ and $16.0 \pm 2.3\%$ respectively **(Figure 21B)**.

In VX2 cells, the percentage of cells migrating towards the scratched area in untreated control cells, cells treated with PDT only, curcumin liposomes only and curcumin liposomes along with PDT were $93.3 \pm 0.7\%$, $79.0 \pm 6.2\%$, $50.7 \pm 4.3\%$ and $10.7 \pm 4.5\%$ respectively **(Figure 21C)**.

Therefore, it becomes evident that curcumin liposomes photosensitized by light irradiation reduce cell migration and thereby could contribute to the inhibition of tumor cell metastasis.
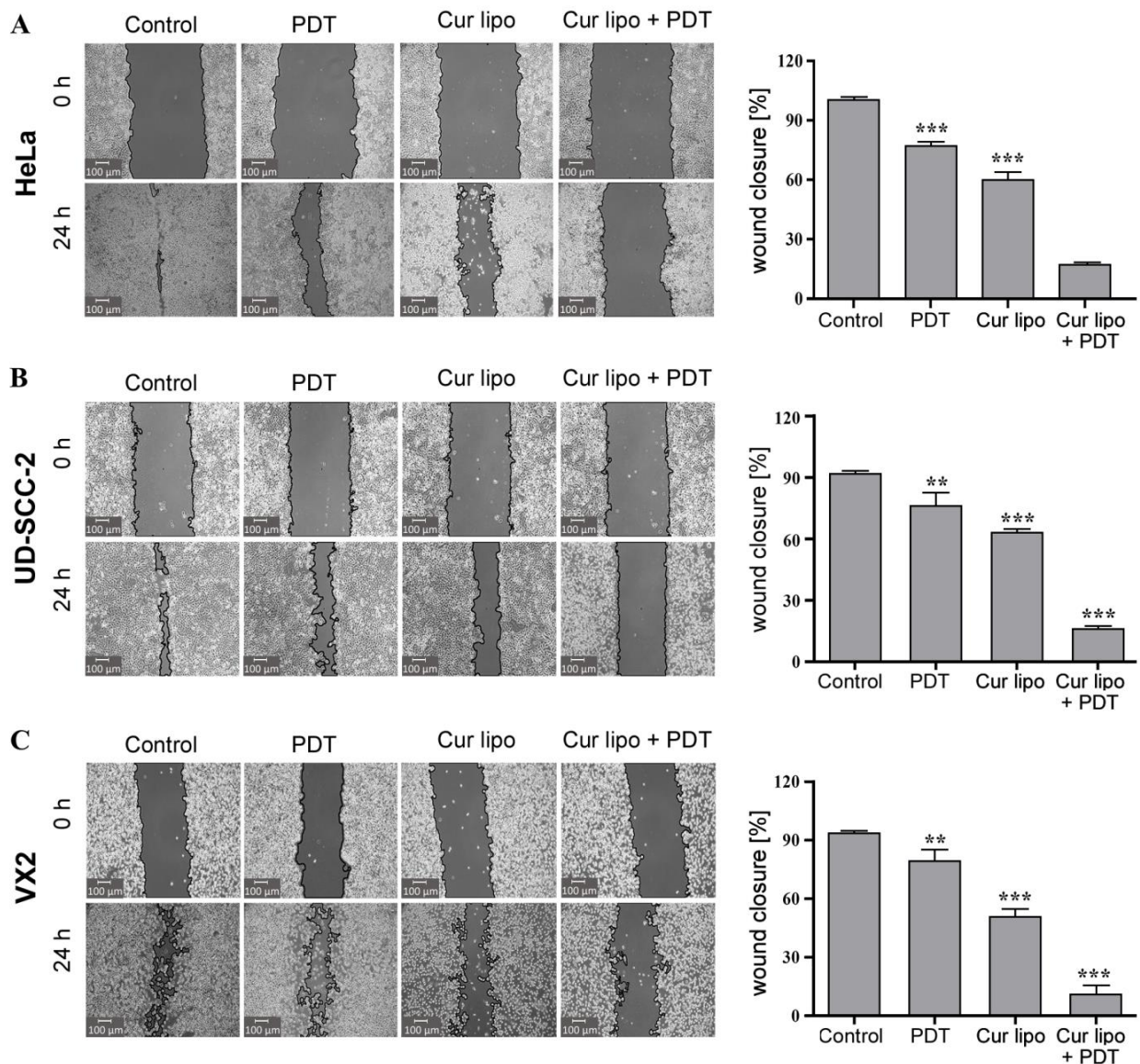
Figure 21. Cell migration (wound healing) assay in HeLa, UD-SCC-2 and VX2 cells. HeLa (A), UD-SCC-2 (B) and VX2 (C) tumor cells were treated with PDT only, curcumin liposomes only or curcumin liposomes in combination with PDT. Images were captured at t = 0 h directly after scratching the cell layer and t = 24 h to evaluate scratch (wound) closure that is indicative of cellular migration. The cell free area of the scratched region was measured with the MRI_wound healing tool used with the ImageJ analysis software [176]. The level of cell migration is presented as the percentage of scratch (wound) closure observed 24 h after treatment compared to control values. Controls indicate untreated cells. The values were expressed as the mean ± S.D. and statistical significances are indicated as ***p<0.001, **p<0.01.

3.3.7   Lysosomal disruption

Lysosome-dependent cell death has been shown to play an important role in cancer cell death and is primarily initiated by lysosomal membrane permeabilization (LMP) mechanism [185] [186]. It has been reported that photodynamic therapy elicit LMP with subsequent hydrolases leakage resulted in enhanced reactive oxygen species(ROS) production, apoptosis and necrosis led to cell death [51]. Various studies have suggested that PDT mediated LMP is mostly associated with photosensitizer that accumulates preferentially in lysosomes [187]. So in order to investigate the effects of various treatments on lysosomal membranes, Hela (**Fig 22A**), UDSSC-2 (**Fig 22B)** and VX2 (**Fig 22C)** cells were treated with light only, curcumin liposomes with and without light irradiation and stained with LysoTracker® red DND-99.

Microscopic images revealed that no lysosomal disruption was observed after the cells were treated with curcumin liposomes alone or light irradiation alone (similar fluorescence to untreated cells). Contrary to this, cells treated with curcumin liposomes in combination with PDT showed enhanced lysosomal disruption and a reduced fluorescence intensity of Lysotracker red as compared to other cells, suggesting a LMP effect induced by photosensitization of curcumin liposomes.
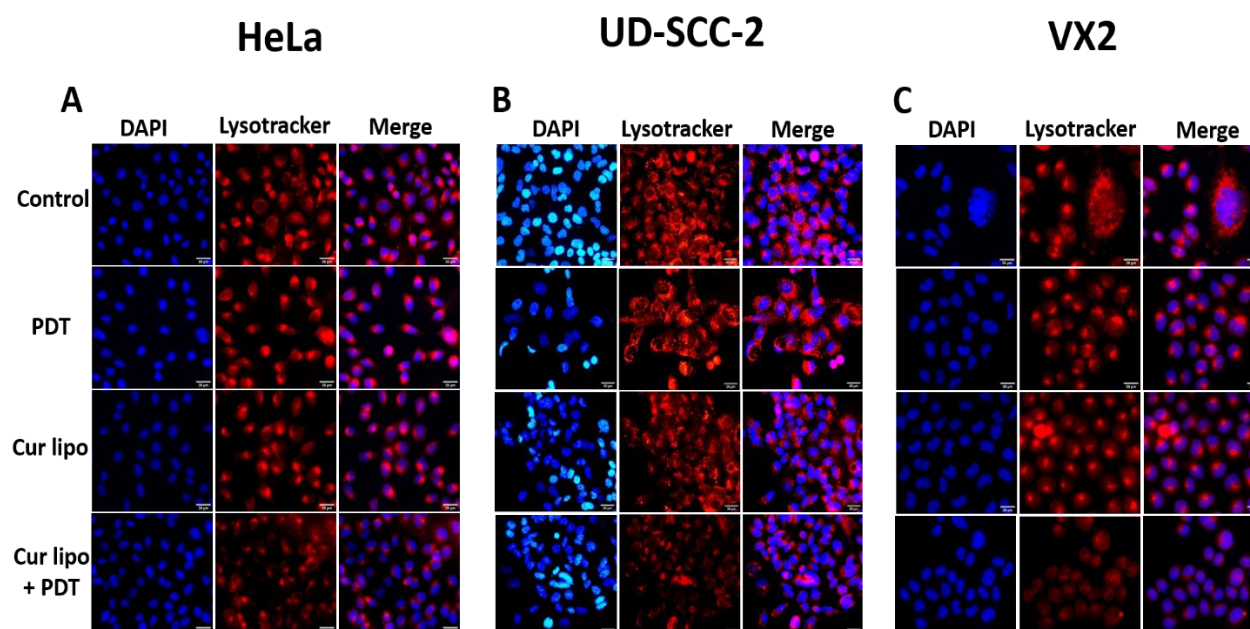
Figure 22. *Lysosomal disruption in Hela (A), UDSSC-2 (B) and VX2 (C) cells treated with PDT alone, curcumin liposomes alone and curcumin liposomes-PDT*. Blue (DAPI) fluorescence and red (Lyso-tracker Red) fluorescence correspond to nuclei and lysosomal staining respectively. Control represents untreated cells. Scale bar represents 50μm.

CHAPTER NO 4

Construction, and validation of CRPV E6 & E7 recombinant plasmids and their transient expression analysis in eukaryotic cells

4.1 *Aims and Objectives*

The first specific aim of this project was to generate recombinant DNA constructs containing CRPV E6 and E7 oncogenes using appropriate vectors and the second aim was transient expression of cloned CRPV E6 & E7 oncogenes and oncoproteins *in vitro*

Addressing the first aim:

i.   Full length CRPV E6 and E7 oncogenes from VX2 carcinoma were cloned into three plasmid vectors i.e. pcDNA 3.0, pEGFP-C1 and pDsRED-Monomer-C1

ii. Double restriction enzyme (RE) digestion and sequencing was done for sequence confirmation of the six recombinant plasmids

Addressing the second aim:

i.   The validated CRPV E6 & E7 expression plasmids were aimed to transfect into two eukaryotic cell lines i.e. COS-7 and VX2 using PEI based lipopolyplexes

ii.   The fluorescent reporter genes (GFP and RFP) in the respective recombinant plasmids would be helpful in assessing the transfection efficiency of cells using florescence microscopy before any chemical assay

iii. Expression of CRPV E6 & E7 oncogenes (mRNA) at transcript level was analyzed by RT-PCR after transient transfection of non-fluorescent recombinant genes into both cell lines

iv.   CRPV E6 and E7 oncoprotein expression was evaluated by western blot analysis after transfecting GFP and RFP E6 and E7 plasmids

v.   The use of fluorescent reporter tags has several advantages **a)** it will allow and help to study target protein localization **b)** detect candidate protein (CRPV E6 & E7) expression using anti-GFP or anti-RFP antibodies as there exist no commercially available antibodies directed against CRPV E6 and E7 protein

4.2 *MATERIALS & METHODS*

4.2.1   Recombinant Plasmid Generation

4.2.1.1   Primer design for cloning of the full-length CRPV E6 & E7 oncogene

The primers were designed to amplify full length coding sequences of CRPV E6 and E7 oncogenes from VX2 tumor derived RNA [117] [188]. The primer pairs used for the generation of E6 and E7 DNA constructs are summarized in **Table 9**.

Each of the forward primers contains an overhang of 6 bases (GATCGA) shown in blue to ensure restriction enzyme binding, specified and single cutter restriction enzyme sequence mentioned in red, Kozak sequence (GCCACC) mentioned in purple to enhance expression and translation of the GOI, start codon (ATG) followed by the sequence of the specific gene (coding sequence) to be amplified. Each of the reverse primers contains an overhang of 6 bases (AGCTAG) depicted in green, specific restriction enzyme sequence and a stop codon (TCA) followed by sequence of specific gene to be amplified.

Table 9. List of primer pairs for amplification of CRPV E6 & E7 full length genes

DNA construct	Direction	Primer Pair	Restriction sites	Base pair
E6_w	forward	GATCGA*AAGCTT*GCCACCATGGAGAACTGCCTGCC	HindIII	852
	reverse	AGCTAG*GAATTC*TCATCTAAATTCTGTGAAG	EcoRI	
E7_w	forward	GATCGA*GGATCC*GCCACCATGATAGGCAGAACTCCTAAG	BamHI	315
	reverse	AGCTAG*GAATTC*TCAGTTACAACACTCCGGGC	EcoRI	
E6_G/R	forward	GATCGA*CTCGAG*CTATGGAGAACTGCCTGCCACGC	XhoI	848
	Reverse	AGCTAG*GAATTC*TCATCTAAATTCTGTGAAG	EcoRI	
E7_G/R	Forward	GATCGA*CTCGAG*CTATGATAGGCAGAACTCCTAAG	XhoI	311
	Reverse	AGCTAG*GAATTC*TCAGTTACAACACTCCGGGC	EcoRI	

4.2.1.2   Conventional PCR

PCR was performed using the REDTaq® ReadyMix™ PCR Reaction Mix (Sigma-Aldrich, St. Louis, MO, USA) to generate full length E6 and E7 DNA constructs (E6_w, E7_w, E6_G/R, E7_G/R) for cloning into pcDNA3.0, pEGFP-C1, pDsRed-monomer-C1 vectors (Invitrogen Corporation, Carlsbad, CA, USA) using primers mentioned in **Table 9**. PCR reaction was carried according to manufacturer's instructions as shown in **Table 10**. For PCR reaction, RNA was obtained from the VX2 tumor and was prepared according to protocols mentioned in **section 2.2.4.4 (a-b).**

Table 10. PCR reaction mixture setup per sample for full length E6 & E7 DNA constructs

Reagents	Volume (µl)
RED Taq Ready mix	25
Forward Primer (50 µmol/L)	1
Reverse Primer (50 µmol/L)	1
cDNA	2
water	21
Total volume	50

PCR was performed with following cycling conditions:

   i.   Initial denaturation at 94° C for 5 min

   ii.   Denaturation at 96°C for 1 min

   iii.   Annealing temperature for primers is 35°C for 2 min   — 40x

   iv.   Extension at 72°C for 2 min

   v.   Final extension at 72°C for 5 min

Agarose gel electrophoresis was carried out as described by Sambrook [189]. The amplified DNA constructs along with Quick load 100 bp DNA ladder were run on a 2% agarose gel to separate DNA constructs on the basis of their size (length of each amplicon is shown in Table 8). The DNA amplicons were visualized by UV and subjected to purification using the QIAquick Gel Extraction

Kit (catalogue no 28706) (Qiagen, Hilden, Germany). DNA concentration of purified amplicons was measured with the NanoPhotometer® NP80 (IMPLEN, München, Germany).

4.2.1.3   Restriction enzyme (RE) digestion of PCR amplicons & backbone vectors with subsequent ligation

Double restriction enzyme digestion (37°C for 2 hours) of the purified DNA amplicons and vectors as mentioned in **Table 11** was done to produce linear amplicons and linear vectors with sticky ends. Each reaction mixture contained the following components:

  i.   1-2 µg of vector / 0.5-1 µg of purified and confirmed DNA
  ii.   4 µl of 10X cutsmart buffer (New England Bio Labs, MA, USA)
  iii.   2.5 µl of restriction enzyme 1 (RE1) for 5' site
  iv.   2.5 µl of restriction enzyme 2 (RE2) for 3' site
  v.   Water q.s to make final volume up to 40µl

Table 11. List of restrictions enzymes used for digestion of DNA amplicons and backbone vectors prior to ligation

PCR amplified gene inserts or Vectors	Restriction Enzymes	
	RE 1	**RE 2**
E6_w	HindIII	EcoRI
E7_w	BamH1	EcoRI
E6_ G/R	XhoI	EcoRI
E7_G/R	XhoI	EcoRI
pcDNA3.0	HindIII / BamH1	EcoRI
pDsRed-monomer-C1, EGFP-C1	XhoI	EcoRI

4.2.1.4   Ligation of DNA amplicons into the respective vector

For cloning, appropriate linearized vectors and digested DNA amplicons were added in molar ratio of 1:3. Each reaction mixture contains 10X T4 DNA ligase buffer (New England Bio Labs, MA, USA), T4 DNA ligase (New England Bio Labs, MA, USA), linearized DNA amplicons & linearized vector. This reaction mixture was incubated overnight at 16°C. Additionally, controls (vectors without DNA inserts) were also prepared for detection of background given by uncut or self-annealing vector itself.

4.2.1.5   Preparation of LB agar plates & LB Media

LB-agar solution & LB media were prepared by dissolving 20 g/L of LB-agar powder or 35 g/L of LB-broth (w/o agar) powder in water. Both media were autoclaved for 20 min at 121°C. LB agar media was allowed to cool down to 50°C followed by addition of appropriate antibiotics. Thereafter, the media was poured into petri dishes, allowed to settle for 20-30 min at RT. Three types of agar plates were prepared using kanamycin (30 µg/ml), kanamycin (50 µg/ml) and ampicillin (100 µg/ml). The LB media w/o agar was stored at 4°C without addition of antibiotics and would be further used during the transformation process.

4.2.1.6   Transformation

For transformation, 3-5 µl of each ligation mixture was added to 50 µl of pre-thawed DH5α competent cells (Invitrogen Corporation, Carlsbad, USA) followed by incubation on ice for 30 min. Subsequently, the reaction mixture was heat shocked at 42°C for 45 s and were incubated again on ice for 5 min. 1ml of pre-warmed LB media (w/o antibiotics) was added to each tube containing the transformation reaction and were incubation for a period of 1 hour at 37°C on a shaking incubator. Subsequently, the transformed cells containing different vectors were plated on respective agar plates as listed in **Table 12**. The agar plates were subjected to incubation at 37°C overnight for the formation of colonies. Approximately 5 colonies from each reaction agar plate were selected and streaked on seperate agar plates for overnight incubation at 37°C. In addition, colonies were also cultured overnight in 5 ml of LB media containing specified antibiotic as mentioned in **Table 12** using incubator shaker at 250 rpm.

Table 12. Overview of selection of agar plates on basis of vector in transformed cell.

Vector in Transformed cells	Antibiotics containing agar plates
pcDNA 3.0	Ampicillin (100 µg/ml)
pEGFP-C1	Kanamycin (30 µg/ml)
pDsRed-monomer-C1	Kanamycin (50 µg/ml)

4.2.1.7   Plasmid isolation and verification

QIA Mini preps (Cat 27104) (Qiagen, Hilden, Germany) were performed to isolate plasmids from overnight cultures of selected colonies. The isolated plasmids were subjected to gel electrophoresis after double restriction enzyme digestion. The digestion pattern obtained after using selective restriction enzymes was compared with predicted pattern to confirm DNA insert size, sequence and orientation.

After the confirmation of clones having a gene specific DNA of correct size. Plasmids were subsequently sent for sequence analysis (4base lab GmbH, Reutlingen). To ensure full sequence coverage, the sequencing primers were designed and selected so that they can read upstream and downstream of the gene insert.

Sequencing was performed to confirm that each recombinant plasmid contains the correct DNA insert, ligated at correct nucleotide position in the specified vector backbone. Sequencing results were evaluated using multiple sequence alignment and BioEdit software (v7.0.5.3). A list of primers including both customized and universal **(Table 13)** was used for sequencing of recombinant plasmids.

4.2.2   Formulation

The formulation used during this study is reported by Pinnapireddy et al [149]. Pinnapireddy et al, during the study has decribed generation and characterization of liposomes, polyplexes and lipopolyplexes.

Table 13. List of primers for sequencing of recombinant clones

Clones	Sequencing Primer	Primer sequences
E6_WT, GFP_E6	se6_r2_78-214	TCCAGATCCACCGGAGTTAG
	le6_f2_24-142	GCTAGAGAAGCTGCAGCAAA
E7_WT	T7	AATACGACTCACTATAGG
	sp6	ATTTAGGTGACACTATA
GFP_E7	pEGFP-C1-F	GAAGCGCGATCACATGGTC
	pEGFP-C1-R	CATTTTATGTTTCAGGTTCAGG
RFP_E6	pDsREDMonC1-1419L	GGAGGTGTGGGAGGTTT
	se6_f1_195-333	CTAACTCCGGTGGATCTGGA
	le6_r2_24-142	ATAGCCCCGTGCATTTGA
RFP_E7	e7_f2_152-250	CAGTGTCCGTGCCATGTAAG
	e7_r1_67-171	CTTACATGGCACGGACACTG

4.2.2.1   Preparation of liposomes

Briefly, liposomes were prepared by dissolving lipids such as DOPE, DPPC and cholesterol (70:15:15) in a mixture of chloroform: methanol (2:1) using 5ml round bottom flask containing 1ml of chloroform: methanol (2:1). The organic phase was evaporated at 40ºC using a rotary evaporator (Heidolph, Schwabach, Germany) to obtain thin film. Following rehydration of thin film with 20mM HEPES buffer (pH 7.4) and sonication in ultrasonic water bath, the liposomes were extruded through 200nm polycarbonate membrane using pre heated extruder (Avanti Polar Lipids, Alabaster, USA) for size reduction of liposomes. The liposomal formulations were filtered through 0.2 µm syringe prior to use.

4.2.2.2   Preparation of polyplexes

Polyplexes (PP) were prepared at N/P ratio of 9.5 (It is the ratio of nitrogen atoms in PEI to phosphate atoms in nucleic acids). For the preparation of polyplexes, equal volumes of pDNA and linear PEI (both diluted in opti-MEM) were mixed and incubated for 25 min under a laminar flow hood at room temperature.

4.2.2.3   Preparation of lipopolyplexes

For the preparation of lipopolyplexes (LPP), liposomes to PEI mass ratio (0.39 : 1) was used and accordingly equal volumes of liposomes (diluted in opti-MEM) and polyplexes were mixed with vigorous pipetting followed by incubation of the mixture for 1 hour at RT under the laminar flow hood (Labogene, Brigachtal, Germany). During this study, the resulting lipopolyplexes were used as transfection reagent for transient transfection of CRPV E6 and E7 recombinant plasmids.

4.2.3   Culturing of mammalian cells

COS-7 cells were cultivated in Dulbecco's Modified Eagle Medium (DMEM) supplemented with 10% fetal bovine serum (FBS), 2 mmol/L L-Glutamine, 50 μg/ml gentamicin, 100 U/ml penicillin and 100 μg/ml streptomycin at 37ºC, 5% CO_2 in a humidified atmosphere. VX2 cells were cultured in DMEM and Ham's F12 media (DMEM/ Ham`s F-12) with L-Glutamine supplemented with 10 % FBS, 50 μg/ml gentamicin, 100 U/ml penicillin/streptomycin and 50 μg/ml amphotericin under standard laboratory conditions (37ºC, 5% CO_2). All cells were grown in 100 mm tissue culture dishes and were passaged after reaching 80% confluency.

4.2.4   Transient Transfection via lipopolyplexes

For transfection experiments, $5\text{-}10 \times 10^5$ cells were seeded in each well of a 6 well plate so that they would be 70-80% confluent at the time of transfection. The lipopolyplexes were prepared as mentioned in *section 3.3.2*. Each individual well received 2 μg (in 200 μl) of plasmid and 800 μl of fresh media. After incubation of cells with complexes for 4 hours, additional fresh media (1 ml) was added. The cells were incubated for more 48 hours before analysis.

4.2.5   Transient gene expression

4.2.5.1   Confocal microscopy and image processing

For imaging, VX2 and COS-7 cells were grown on coverslips in 6 well plates and transfected with clones containing green fluorescent protein (GFP_E6, GFP_E7) and red fluorescent protein (RFP_E6, and RFP_E7) respectively. After 48 hours incubation period, cells were washed thrice with ice cold PBS containing Ca^{2+} and Mg^{2+} (pH 7.4) and fixed with ice cold methanol for 5 min. Afterwards, the coverslips were incubated with 0.1 µg/mL DAPI (Roche Diagnostics, Indianapolis, IN, USA) for 20 min to counterstain the nucleus of the cells. The coverslips were mounted face down on slides with Dako fluorescent mounting medium and sealed using transparent nail polish. The cells were subsequently analyzed with a confocal laser scanning microscope (Zeiss Axiovert 100M/LSM 510, Carl Zeiss GmbH, Jena, Germany).

4.2.5.2   Analytical and biochemical assays

4.2.5.2.1   Real time PCR analysis

For real time polymerase chain reaction analysis, VX2 and COS-7 cells were grown in 6 well plates and transfected with non-fluorescent clones (E6_WT and E7_WT). Cells were harvested after 48 hours of transfection. Total RNA derived from VX2 and COS-7 cells was isolated using the RNeasy Mini kit (Cat.74106) (Qiagen, Germany). 1.0 µg total RNA from each sample was used to prepare cDNA according to the protocol recommended by the Transcriptor First strand cDNA synthesis kit (Roche, Mannheim, Germany) using TProfessionalThermocycler (Biometra, Gottingen, Germany). Real time PCR analysis was done using PowerUp^{TM} Green Master Mix (Applied Biosystems, Vilnius, Lithuania) in combination with the respective primer pairs (Invitrogen, Germany) as listed in **Table 8**. GAPDH was used as housekeeping gene to normalize expression of oncogene transcripts in each sample. Quantitative measurement of CRPV E6 & E7 mRNA was carried out with the QuantStudio$^{®}$ TM5 system (Thermo Fisher Scientific, CA, USA). Non-transfected VX2 and COS-7 cells were used as a negative control.

4.2.5.2.2　　Western Blot Analysis

Western blot analysis was performed to analyze expression of recombinant proteins according to protocol mentioned in section. Briefly, VX2 and COS-7 cells were seeded in 6 well plates and transfected with plasmids encoding green fluorescent (GFP_E6, GFP_E7) and red fluorescent (RFP_E6, and RFP_E7) tagged oncoproteins. pEGFP-C1 and pDsRed-Monomer-C1 vectors without inserts were used as control.

Forty eight hours after transfection, cells were harvested and subjected to lysis in buffer containing 2 mmol/L ethylenediaminetetraacetic acid(EDTA), 1 % Nonidet P40, 137 mmol/L NaCl, 20 mmol/L Tris/HCl (pH8.0), 10 % glycerol supplemented with protease and phosphatase inhibitors (Sigma). SDS-PAGE was performed under standard conditions using a discontinuous 12 % acrylamide gel. Thirty-five µg of whole cell lysate protein was loaded per lane. The Precision Plus Protein™ Standard (161-0373) from Biorad (Hercules, CA, USA) was used for size comparison.

After SDS-PAGE, the proteins were transferred to nitrocellulose membranes. Subsequently, the membranes were blocked with 3 % nonfat dry milk/PBS followed by incubation overnight at 4°C with primary antibody: mouse monoclonal anti-GFP B-2 (SC-9996, 1:500, Santa Cruz Biotechnology); rabbit polyclonal anti-RFP (Living colors DsRed Polyclonal antibody) (632496, 1:1000, Takara). Then membranes were washed thrice in blocking buffer for 10 min and were incubated with an HRP-coupled secondary antibodies: mouse-IgGk BP-HRP, (SC516102, 1:2000, Santa Cruz Biotechnology); rabbit-IgGk HRP, (SC-2004, 1:2000, Santa Cruz Biotechnology) for 1 h at room temperature.

After incubation and three washes, proteins were visualized on X-ray film (Agfa, Cologne, Germany) using the enhanced chemiluminescence (ECL) method (Amersham Biosciences, Buckinghamshire, United Kingdom).

The online Expasy tool " compute PI / MW " was used to predict the molecular weight of recombinant proteins [190].

Table 14. Predicted molecular weights of clones with reporter genes

Recombinant Clones	Expected size (kDa)
GFP_E6	57.2
GFP_E7	37.8
RFP_E6	55.9
RFP_E7	36.6
pEGFP-C1	29.4
pDsRed-Monomer-C1	27.8

4.2.6   Statistical Analysis

All the experimental evaluations were performed in triplicates and the values were presented as a mean ± standard deviation. One-way ANOVA was performed to identify statistically significant differences using Graphpad prism 5. Dunnett's test was used for multi-comparison between the results and control. Probability values less than 0.05 were considered significant. Statistical significances are denoted as $*p < 0.05$, $**p < 0.01$, $***p < 0.001$, $****p < 0.0001$

4.3 *RESULTS & DISCUSSION*

4.3.1   Cloning

4.3.1.1   PCR Amplification of CRPV E6 and E7 oncogenes

VX2 tumor cDNA was used as a template for amplification of CRPV E6 and E7 oncogenes using end-time PCR. CRPV E6 and E7 full length genes were successfully amplified using primers listed in *Table 8*. Subsequent gel electrophoresis of the resulting amplicons (E6_w, E6_G/R, E7_w and E7_G/R) showed successful amplification of E6 and E7 genes with expected size as shown in **Figure 23**.

| Lane No	DNA amplicons with RE sites	Amplicon size (bp)
2	E6_w (HindIII / EcoRI)	852
3	E6 _ G/R (XhoI / EcoRI)	848
4	E7 _ G/R (XhoI / EcoRI)	311
5	E7_w (BamHI / EcoRI)	315
1	100 bp DNA ladder	
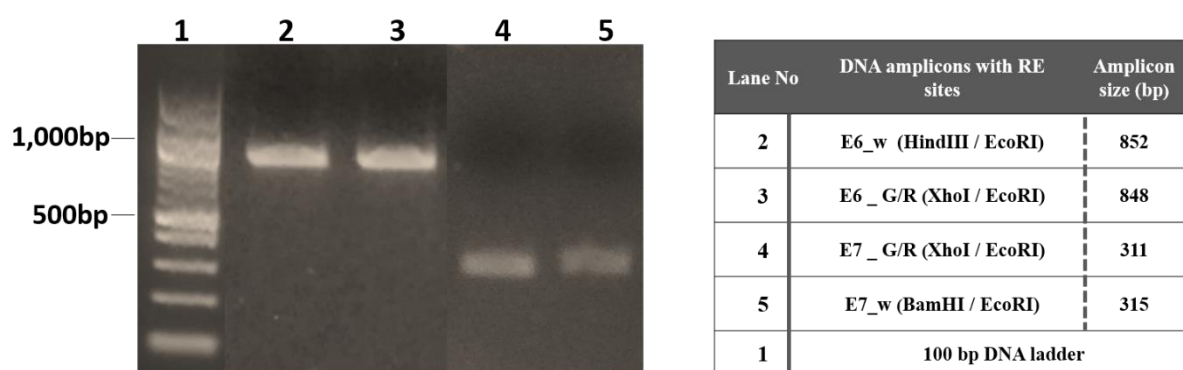
Figure 23. Gel electrophoresis of CRPV E6 and E7 amplicons. Agarose gel showing PCR amplification of full length gene products (E6 and E7 amplicons) containing different restriction sites for cloning into pcDNA 3.0, pEGFP-C1, and pDsRed-monomer-C1 vectors. Lane number, amplicons with restriction sites and their sizes are shown on the right.

4.3.1.2   Generation of recombinant plasmids

Following gel purification of PCR amplicons, double digestion was performed to produce DNA inserts and linear vectors with the sticky ends for ligation as described in **section 4.2.1.3**. The ligated products were used to transformation of DH5α competent cells and successful transformation resulted in colony formation on selective LB agar plate. Subsequently, plasmids were isolated and purified from overnight bacterial cultures of selected colonies from agar plate. Six different types of recombinant plasmids or clones were prepared during this study.

A brief description of each clone is mentioned as follow

4.3.1.2.a   Wild type E6 (E6_WT)

E6_WT clones as shown in **Figure 24** were generated by ligation of the CRPV E6 amplicons into the polylinker or multiple cloning site (MCS) of the mammalian expression vector pcDNA 3.0. For ligation, CRPV E6_w amplicon and pcDNA 3.0 were digested with *HindIII* and *EcoRI* endonucleases to produce sticky ends. Double restriction enzyme digestion of *E6_WT* recombinant plasmids yielded a DNA insert of expected size (852bp) for CRPV E6.
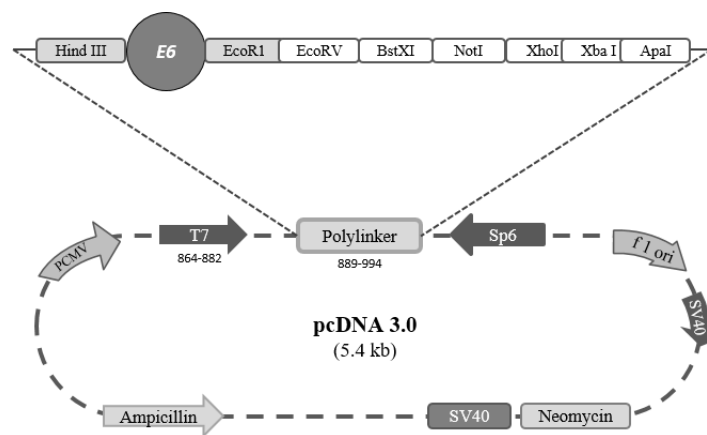

Figure 24. Schematic diagram of E6_WT clone. Recombinant plasmid is generated by cloning of DNA fragment containing CRPV E6 into pcDNA3.0 vector. Picture is designed by PlasMapper 2.0 software tool [191]

4.3.1.2.b   Wild type E7 (E7_WT)

E7_WT clones as shown in **Figure 25** were generated by ligation of CRPV E7 amplicons into the polylinker or multiple cloning site (MCS) of the mammalian expression vector pcDNA 3.0. *BamHI* and *EcoRI* endonucleases were used to produce sticky ends of E7_w amplicons and pcDNA 3.0 for ligation. Double restriction enzyme digestion of *E7_WT* recombinant plasmids yielded an insert of specific size (315bp) for E7. It also has to be noted that CRPV E7 in contrast to CRPV E6 contained HindIII restriction site in its sequence. Therfore, BamHI instead of HindIII was used for E7 cloning.
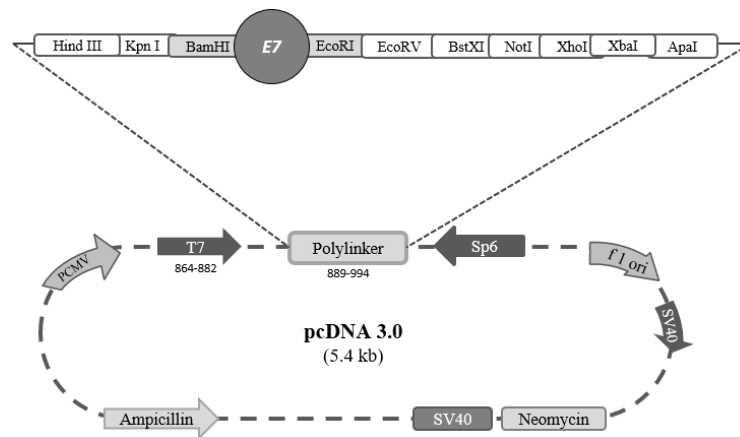
Figure 25. Schematic diagram of E7_WT clone. Recombinant plasmid is generated by cloning of DNA fragment containing CRPV E7 into pcDNA3.0 vector. Picture is designed by PlasMapper 2.0 software tool [191]

4.3.1.2.c   GFP_ E6 and GFP_ E7 clones

GFP_E6 and GFP_E7 clones as shown in **Figure 26** were generated by ligation of CRPV E6_G or E7_G amplicons into the multiple cloning site of the mammalian expression vector pEGF-C1. *XhoI* and *EcoRI* endonucleases were used to produce sticky ends in E6/E7_G amplicon and pEGFP-C1 prior to ligation. Double restriction enzyme digestion of GFP_E6 and GFP_E7 recombinant plasmids showed bands consistent with E6 (848bp) and E7 (311bp) respectively.
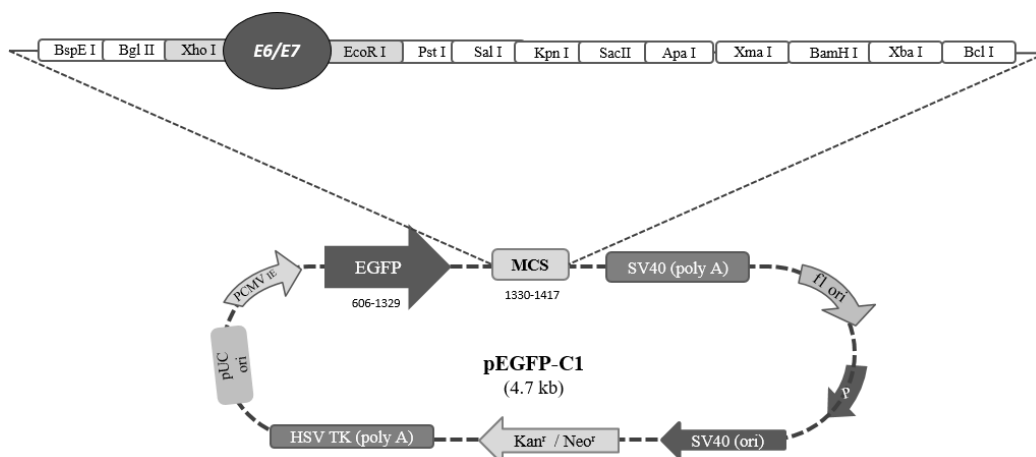

Figure 26. Schematic diagram of GFP E6/E7 clone. Recombinant plasmid is generated by cloning of DNA fragment containing CRPV E6 or E7 into pEGFP-C1 vector. Picture is designed by PlasMapper 2.0 software tool [191]

4.3.1.2.d   RFP_E6 and RFP_E7 clones

RFP_E6 and RFP_E7 clones as shown in **Figure 27** were generated by ligation of CRPV E6_R or E7_R amplicons respectively into the multiple cloning site of the mammalian expression vector pDsRed-Monomer-C1. *XhoI* and *EcoRI* endonucleases were used to produce sticky ends of E6/E7_G amplicons and pDsRed-Monomer-C1 prior to ligation. Double restriction enzymes digestion of RFP_E6 and RFP_E7 recombinant plasmids showed bands consistent with E6 (848bp) and E7 (311bp) respectively.
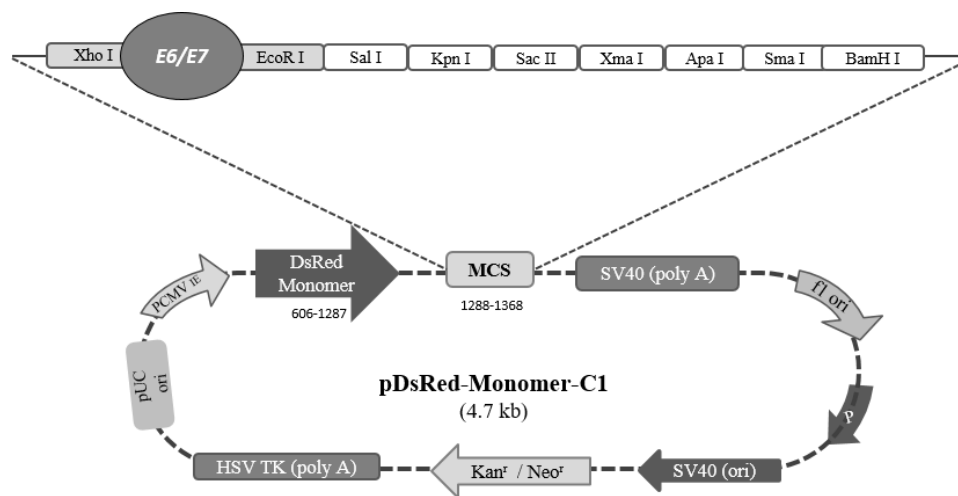
Figure 27. Schematic diagram of RFP E6/E7 clone. Recombinant plasmid is generated by cloning of DNA fragment containing CRPV E6/E7 into pDsRed-Monomer-C1 vector. Picture is designed by PlasMapper 2.0 software tool [191]

4.3.1.3   Validation of recombinant plasmids by RE digestion

The purified plasmids were subjected to double restriction enzyme digestion using the same two restriction enzymes deployed for cloning of the inserts to confirm DNA inserts of correct size. Double restriction enzyme digested recombinant and non-recombinant plasmids (control) were then run on a 0.8% agarose gel along with DNA ladder. Gel results revealed that non-recombinant plasmids gave a fragment at 5400bp or 4700bp consistent with for pcDNA3.0, pEGFP & pDsRed-Monomer-C backbone vectors while recombinant plasmids gave two fragments; large fragment for backbone vectors and the smaller fragment being consistent with the respective gene inserts (about 850bp for E6 and about 315bp for E7).
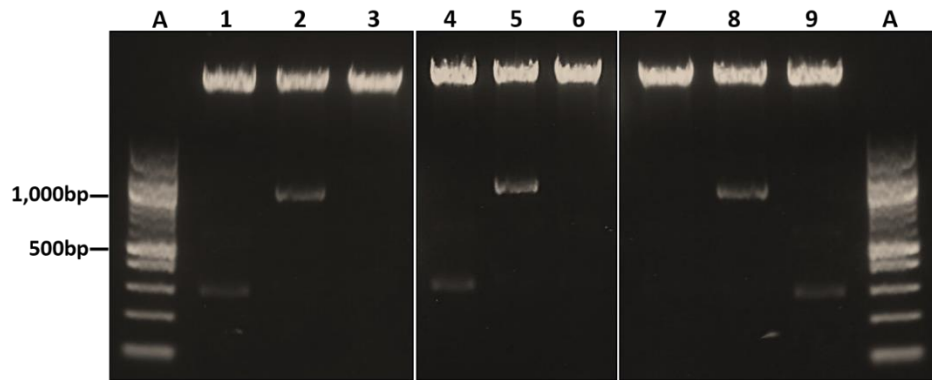
Figure 28. Validation of recombinant plasmids using restriction enzyme digestion.

Lane A: 100bp DNA ladder; *Lane 1*: HindIII and EcoRI digested E6_WT clone; *Lane 2*: BamHI and EcoRI digested E7_WT plasmid; *Lane 4*: XhoI and EcoRI digested GFP_E7 plasmid; *Lane 5*: XhoI and EcoRI digested GFP_E6 plasmid; *Lane 8*: XhoI and EcoRI digested RFP_E6 plasmid; *Lane 9*: XhoI and EcoRI digested RFP_E7 plasmid; Lane 3, 6, 7: RE digestion of non-recombinant plasmids without DNA inserts yield bands consistent with linearizedplasmids pcDNA 3.0, EGFP, DsRed-Monomer-C respectively.

4.3.1.4   Recombinant plasmid verification by sequence analysis

The obtained sequencing results were compared with CRPV E6 and E7 reference sequence (*NC_001541.1:154-975* and *NC_001541.1:1075-1359)*. The sequencing and alignment analysis showed that cloned CRPV E6 and E7 gene sequences were consistent with the reference sequence (see also appendix).

4.3.2   Fluorescence microscopy for evaluation of recombinant proteins expression

After establishment and validation of recombinant plasmids, transient transfection in COS-7 **(Figure 29A)** and VX2 cells **(Figure 29B)** was conducted for visual analysis of target (CRPV E6 and E7) proteins co-expressed with fluorescent proteins. 48 hours after transfection, the expression of GFP/RFF_E6 and GFP/RFF_E7 oncogenes was observed using confocal laser scanning microscopy (Zeiss Axiovert 100 M/LSM 510, Carl Zeiss Microscopy GmbH, Jena, Germany). Microscopic results revealed that CRPV E7 oncoproteins were highly expressed in both cell lines as compared to CRPV E6 oncoproteins. While comparing transfection efficiencies

of COS-7 and VX2 cells, it could be observed from microscopic images that COS-7 cells **(Figure 29A)** appeared to express higher levels of protein as compared to VX2 cells **(Figure 29B)**.
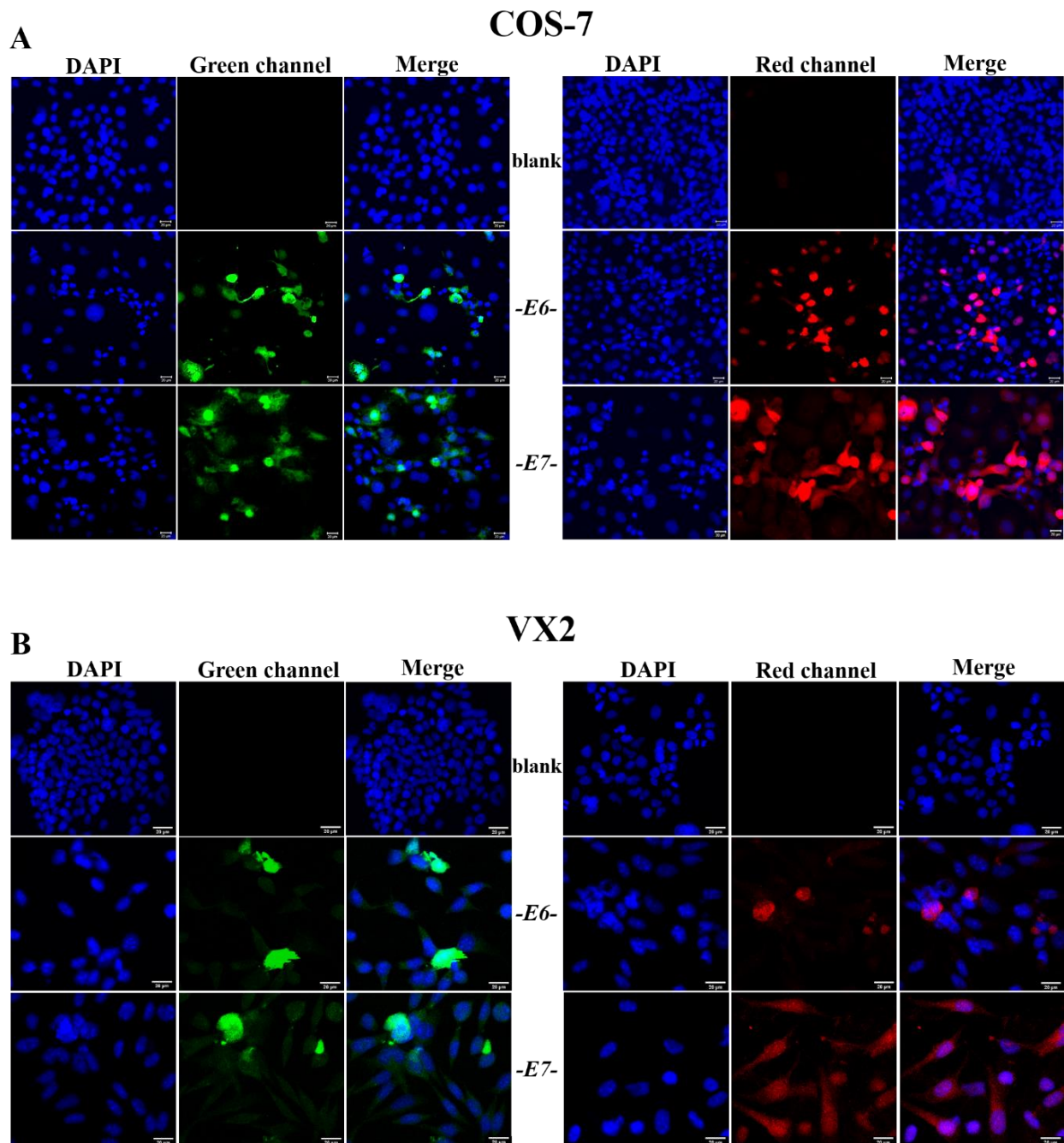
Figure 29. Florescence microscopic images of transiently expressed CRPV E6 and E7 recombinant proteins. (A) Images of COS-7 cells transfected with GFP_E6/E7 (left) and RFP_E6/E7 (right) recombinant plasmids. *(B)* Images of VX2 cells were taken accordingly. Non-transfected cells were used as blank to evaluate background staining. Red channel represents RFP expression and green channel represents GFP expression in cells. Scale bar represents 20 μm.

From the microscopic images, it can be seen that both COS-7 and VX2 cells transfected with RFP/GFP_E6 plasmids showed localization of CRPV-E6 protein predominantly in the nucleus and the perinuclear region which is consistent with various findings investigating localization of papilloma virus associated E6 and E6-AP [192] [193], while COS-7 and VX2 cells transfected with RFP/GFP_E7 plasmid showed a rather diffuse localization of the E7 protein both in the nucleus and cytoplasm and this characteristic of E7 protein matched other repeats of this viral oncoprotein [194] [195].

4.3.3 Quantitative PCR to evaluate expression levels of CRPV E6 & E7 mRNA

Real-time PCR was performed to evaluate expression levels of CRPV E6 and E7 recombinant transcripts in transiently transfected and non-transfected COS-7 (**Figure 30A)** and VX2 **(Figure 30B)** cells. Forty eight hours after transfection of E6_WT and E7_WT clones into COS-7 and VX2, cellular RNA were extracted for PCR analysis. As shown in **Figure 30A**, transfected COS-7 cells showed significantly higher levels of CRPV E6 and E7 mRNA expression with fold change ~ 29855.1 and ~ 18794.2 respectively (**** $p < 0.0001$, n=3) than seen in non-transfected COS-7 cells, which did not show any expression of CRPV E6 and E7 transcripts.

As reported during characterization of VX2 carcinoma derived cell line in 2nd chapter, VX2 cells already contained endogenous CRPV E6 and E7 transcripts. Upon transfecting VX2 cells with recombinant clones (E6_WT and E7_WT), we observed a significant increase in the expression of E6 and E7 relative to basal CRPV E6 & E7 mRNA levels. Relative differences in transcript levels of CRPVE6 and E7 in VX2 cells as depicted in *Figure 30B* demonstrate that transfected VX2 cells had a ~ 6565.47 fold higher expression of E6 mRNA (*** $p < 0.001$, n=3) and a ~ 3338.85 fold increased E7 mRNA expression levels (**** $p < 0.0001$, n=3) as compared to non-transfected VX2 cells containing basal E6 transcript level with fold change of ~ 97.56 and E7 transcript level with a fold change of ~ 80.86. These QPCR results suggest that wild-type CRPV E6 & E7 recombinant plasmids were successfully constructed, transcribed and suitable for further analysis.
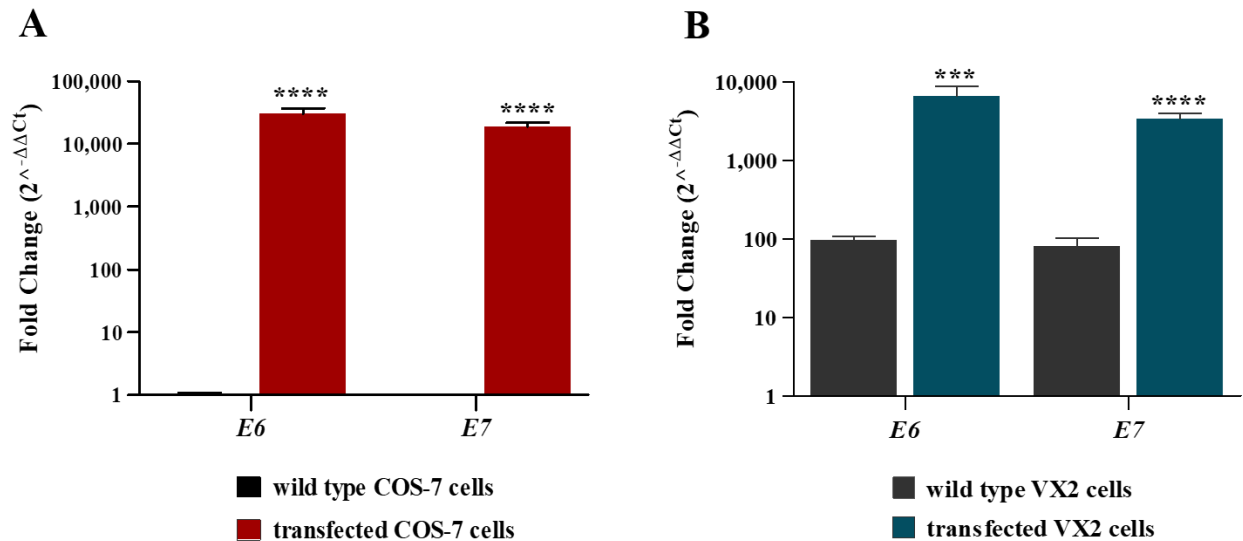
Figure 30. Comparison of gene expression level in transfected and non-transfected (wild-type) COS-7 cell and VX2 cells. Graph data shows relative fold change values for CRPV E6 and E7 mRNA level in transfected and non-transfected cells during quantitative PCR analysis. Values are represented as mean $\pm$ S.D. (n=3) and statistical significance is indicated as *** $p < 0.001$ and **** $p < 0.0001$.

4.3.4   Western blot analysis for recombinant proteins detection

The immunoblotting was performed to check expression of recombinant proteins in COS-7 and VX2 cells transiently transfected with green and red fluorescent clones of CRPV E6 and E7. The predicted molecular weights of CRPV E6 and E7 protein are 29.7 kDa and 10.5 kDa respectively, with the GFP tag adding 29.4 kDa and RFP tag adding 27.8 kDa for total of 57.2 kDa (GFP_E6), 37.8 kDa (GFP_E7), 55.9 kDa (RFP_E6) and 36.6 kDa (RFP_E7) respectively. Western blot analysis showed that the fusion proteins bands were consistent with expected molecular weights in case of GFP/RFP_E7 proteins, GFP_WT and RFP_WT both in COS-7 **(Figure 31A)** and VX2 **(Figure 31B)** cells. While GFP/RFP _E6 didn't show any band in any of the cell line.

The immunoblotting results demonstrate that GFP_E7 & RFP_E7 were successfully transcribed and translated in COS-7 and VX2 cells indicating that pEGFP_CRPV-E7 and pDsRed-Monomer_CRPV-E7 plasmids are suitable for further studies.

A

B

Recombinant proteins	Expected size (kDa)
GFP_E6	57.2
GFP_E7	37.8
RFP_E6	55.9
RFP_E7	36.6
GFP_WT	29.4
RFP_WT	27.8

C
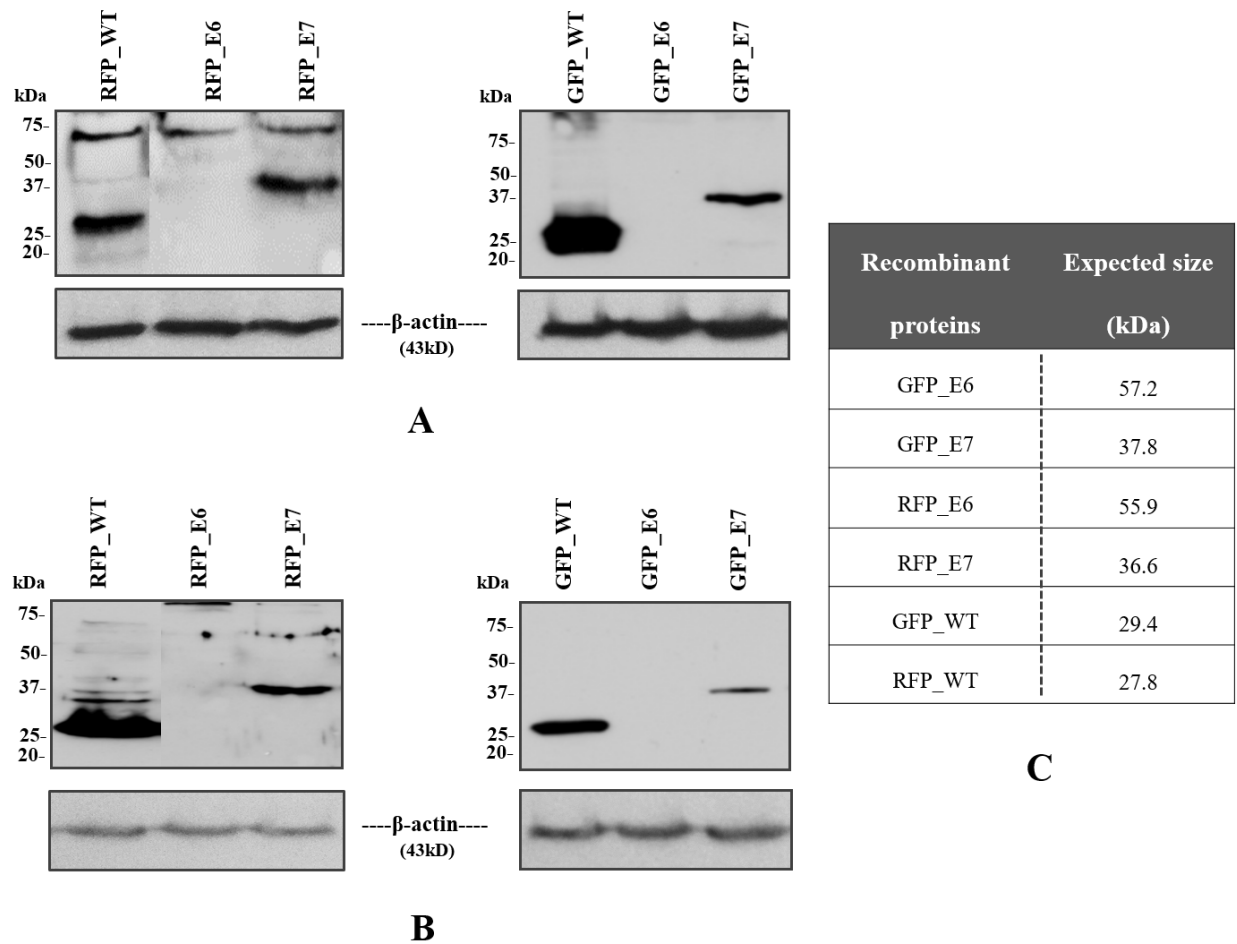
Figure 31. Western blot analysis for checking expression of recombinant proteins. GFP and RFP recombinant CRPV E6 and E7 protein expression in COS-7 cells **(A)** and in VX2 carcinoma derived cells **(B)**. Table showing predicted molecular weights of recombinant proteins in kDa. GFP_WT and RFP_WT refers to pEGFP and pDsRED-Monomer-C1 respectively **(C)**. Expression level of transiently expressed proteins was normalized by internal control β-actin.

84

CHAPTER NO 5

Summary and Outlook

5.1 *Summary and outlook*

This study focused on establishing an *in vitro* expression system for studying papillomavirus (cottontail rabbit papilloma virus, CRPV) associated rabbit squamous cell carcinomas. This system was chosen since the CRPV associated VX2 carcinoma of the New Zealand White rabbit is an established animal model for human head and neck squamous cell carcinoma (HNSCC). Literature research revealed several reports regarding VX2 carcinoma derived cell lines. Unfortunately, these cell lines were either discontinued or not readily available. This situation prompted us to generate our own VX2 cell line. Developing a VX2 carcinoma derived cell line would allow to perform *in vitro* studies thereby helping to reduce the number of animal experiments. The 2nd chapter of the thesis therefore deals with the development and characterization of a VX2 carcinoma derived cell line. It was presumed that this VX2 carcinoma cell line would help to conduct various experiments before performing tests in the VX2 rabbit animal model. VX2 cells were isolated from a VX2 tumor that was excised from the rabbit ear. Cells were allowed to grow and proliferate under standard laboratory conditions. The VX2 cell line survived for about 150 passages which is much longer than expected for cultures of normal cells, however, permanent cell growth could not be achieved. Immunostaining of VX2 cells at initial passages demonstrated the progressive loss of tumor associated fibroblasts giving rise to a VX2 cell line with a pronounced proliferative capacity. Flow cytometry results illustrated the presence of two VX2 cell populations, a small and a large one. Cell sorting, with subsequent cultivation for 5 days followed by western blot analysis favored the hypothesis that the larger VX2 cell population had the highest proliferative potential. Real time PCR was performed to analyze and confirm the presence of CRPV E6 and E7 oncogene transcripts in the VX2 cells using primers designed specifically to detect CRPV E6 and E7 transcripts. Expression of various proliferation markers, apoptosis related genes, EMT (epithelial mesenchymal transition) markers and CRPV E6 & E7 transcripts were consistently found in the VX2 carcinoma generated cell line as well as in the original VX2 tumor. Another objective, presented in the 3rd chapter of the thesis, was to evaluate therapeutic strategies in the VX2 carcinoma derived cell line. For this purpose, photodynamic therapy (PDT) was selected as a non-invasive treatment to investigate its biological effects on the VX2 carcinoma derived cells. Liposomal encapsulated curcumin was used as a photosensitizer. VX2 cells were treated with curcumin liposomes alone, PDT alone or a combination of curcumin liposomes and PDT. Cytotoxicity studies such as the MTT (3-(4,5-dimethylthiazol-2-yl)-2,5-diphenyltetrazolium bromide) assay showed that addition of PDT could

reduce the IC_{50} values of curcumin liposomes. Lysosomal disruption, live & dead staining and apoptosis assays were discussed in detail. A significant reduction in colony formation and cell migration was observed in cells exposed to both curcumin liposomes and PDT. In addition to the CRPV associated rabbit VX2 cell line, human papilloma virus (HPV) positive cell lines such as HeLa (HPV-18 positive cervical cancer cell line) and UD-SCC-2 (HPV-16 positive head and neck cancer cell line) were also included during this study to observe the therapeutic effects of curcumin loaded liposomes and PDT therapy. After assessing different parameters using PDT in papilloma virus associated cell lines, it could be concluded that a combination of curcumin liposomes along with PDT was significantly more effective when compared to a treatment with curcumin liposomes or PDT alone. The 4th chapter described an alternative approach for the *in vitro* study of CRPV oncogenes. Recombinant mammalian expression vectors containing CRPV E6 and E7 oncogenes with and without GFP and RFP reporter genes were successfully generated by PCR cloning using VX2 carcinoma derived RNA as a source. Recombinant clones were validated by restriction enzyme digestion and sequence analysis. Theses clones were transiently transfected in COS-7 & VX2 cells using polyethylenimine (PEI) based lipopolyplexes. The expression of CRPV E6 and E7 recombinant clones was assessed using different techniques. Microscopic results revealed successful expression of CRPV E6 & E7 genes by monitoring GFP and RFP reporter genes. Quantitative PCR demonstrated significant expression of E6 & E7 mRNA in transfected cell lines while western blot analysis demonstrated the expression of E7 recombinant proteins but not of E6 presumably due to failure of recombinant E6 proteins to dissolve sufficiently in the lysis buffer. The results presented in the 4th chapter provide an alternative platform for the study of anti-papillomavirus E6 and E7 therapeutic approaches. With this system, the consequences of targeted antiviral therapies could be easily evaluated by visual examination using fluorescence microscopy or quantitatively monitored in multiplate capable fluorescence detectors. The effect of experimental therapies on viral mRNA and protein expression levels could be measured via PCR and western blot analysis, e.g. by using anti-GFP or anti-RFP antibodies as no antibodies directed against CRPV E6 or E7 proteins are currently commercially available. In conclusion, this CRPV expression system could provide an *in vitro* platform for the evaluation of antiviral therapeutic approached prior to *in vivo* testing of e.g. promising therapeutic formulations in the CRPV positive rabbit VX2 carcinoma which serves as an animal model for human HNSCC

5.2 Zussamenfassung and Ausblick

Die vorliegende Studie konzentriert sich auf die Etablierung eines In-vitro-Expressionssystems zur Untersuchung eines Papillomavirus (*cottontail rabbit papilloma virus, CRPV*) assoziierten Kaninchen-Plattenepithelkarzinoms. Dieses System wurde gewählt, da das CRPV-assoziierte VX2-Karzinom des weißen Neuseelandkaninchens ein etabliertes Tiermodell für menschliche Plattenepithelkarzinome des Kopf- und Halsbereiches (*head and neck squamous cell carcinoma, HNSCC*) darstellt. Literaturrecherchen ergaben mehrere Berichte über von VX2-Karzinomen des Kaninchens abgeleitete Zelllinien. Leider wurden diese Zelllinien entweder abgesetzt oder waren nicht ohne weiteres verfügbar. Diese Situation veranlasste uns dazu, unsere eigene VX2-Zelllinie zu generieren, da die Entwicklung einer vom VX2-Karzinom abgeleiteten Zelllinie die Durchführung von In-vitro-Studien ermöglichen würde, wodurch die Anzahl der Tierversuche verringert werden kann. Das 2. Kapitel der Arbeit befasst sich daher mit der Entwicklung und Charakterisierung einer vom VX2-Karzinom abgeleiteten Zelllinie. Hierdurch wurde erhofft, dass diese VX2-Karzinomzelllinie dazu beitragen kann, verschiedene Experimente In-vitro durchzuführen, also noch bevor In-vivo Tests im VX2-Kaninchen-Tiermodell stattfinden. Hierzu wurden VX2-Zellen aus einem VX2-Tumor, welcher aus dem Kaninchenohr herausgeschnitten wurde, isoliert. Man ließ die Zellen unter Standardkulturbedingungen wachsen. Die so generierte VX2-Zelllinie überlebte etwa 150 Passagen, was für Kulturen normaler Zellen zwar länger ist als erwartet jedoch konnte kein permanentes Wachstum erreicht werden. Die Immunfärbung von VX2-Zellen bei initialen Passagen zeigte den fortschreitenden Verlust von Tumor-assoziierten Fibroblasten, was zu einer VX2-Zelllinie mit einer ausgeprägten Proliferationskapazität führte. Die Ergebnisse der Durchflusszytometrie wiesen auf das Vorhandensein von zwei VX2-Zellpopulationen, einer kleinen und einer großen. Nach Sortierung der 2 Zellpopulationen mittels Durchflusszytometrie mit nachfolgender Kultivierung für 5 Tage und anschließender Western-Blot-Analyse konnte gezeigt werden, dass die größere Zell-Subpopulation eine höhere Proliferation aufweist. Eine Echtzeit-PCR wurde durchgeführt, um das Vorhandensein von CRPV E6- und E7-Onkogen-Transkripten in den VX2-Zellen zu bestätigen und zu quantifizieren. Hierzu wurden Primer eingesetzt, die spezifisch zum Nachweis von CRPV E6- und E7-Transkripten geeignet sind. Die Expression verschiedener Proliferationsmarker, Apoptose-assoziierter Gene, EMT (Epitheliale Mesenchymale Transition)-Marker und CRPV E6 & E7-Transkripten wurde sowohl in der VX2-Karzinom-generierten Zelllinie als auch im ursprünglichen VX2-Tumor nachgewiesen. Ein weiteres Ziel, das im 3. Kapitel der Arbeit vorgestellt wird, war die Bewertung

therapeutischer Strategien in der generierten VX2-Zelllinie. Zu diesem Zweck wurde die photodynamische Therapie (PDT) als nicht-invasive Behandlungsmethode ausgewählt, um ihre biologischen Auswirkungen auf VX2-Karzinom Zellen zu untersuchen. Liposomal eingekapseltes Curcumin wurde als Photosensibilisator verwendet. VX2-Zellen wurden mit Curcumin-Liposomen allein, PDT allein oder einer Kombination von Curcumin-Liposomen und PDT behandelt. Zytotoxizitätsstudien wie der MTT (3- (4,5-Dimethylthiazol-2-yl) -2,5-diphenyltetrazoliumbromid) -Test zeigten, dass die Zugabe von PDT die IC_{50}-Werte von Curcumin-Liposomen verringern kann. Störungen der lysosomalen Integrität, Lebend- und Totfärbung und Apoptosetests wurden ausführlich diskutiert. Eine signifikante Verringerung der Koloniebildung und der Migrationsfähigkeit wurde in solchen Zellen beobachtet die sowohl Curcumin-Liposomen als auch PDT ausgesetzt waren. Zusätzlich zur CRPV-assoziierten Kaninchen-VX2-Zelllinie wurden ebenfalls humane Papillomavirus (HPV) -positive Zelllinien wie HeLa (HPV-18-positive Gebärmutterhalskrebs-Zelllinie) und UD-SCC-2 (HPV-16-positive Kopf- und Halskrebs-Zelllinie) in diese Studie einbezogen, um die therapeutischen Wirkungen von mit Curcumin beladenen Liposomen in Verbindung mit einer PDT zu beurteilen. Nach Bewertung verschiedener Parameter unter Verwendung von PDT in Papillomavirus-assoziierten Zelllinien konnte geschlossen werden, dass eine Kombination von Curcumin-Liposomen zusammen mit PDT im Vergleich zu einer Behandlung mit Curcumin-Liposomen oder PDT allein signifikant wirksamer war. Das 4. Kapitel beschreibt einen alternativen Ansatz für die In-vitro-Untersuchung von CRPV-Onkogenen. Rekombinante Säuger-Expressionsvektoren, die CRPV E6- und E7-Onkogene mit und ohne GFP- und RFP-Reportergenen enthielten, wurden erfolgreich durch PCR-Klonierung unter Verwendung von VX2-Karzinom-abgeleiteter RNA als Quelle erzeugt. Rekombinante Klone wurden durch Restriktionsenzymverdau und Sequenzanalyse validiert. Diese Klone wurden transient in COS-7- und VX2-Zellen unter Verwendung von Lipopolyplexen auf Polyethylenimin (PEI) -Basis transfiziert. Die Expression von rekombinanten CRPV E6- und E7-Klonen wurde unter Verwendung verschiedener Techniken bewertet. Mikroskopische Ergebnisse zeigten eine erfolgreiche Expression von CRPV E6- und E7-Genen durch Betrachtung von GFP- und RFP-Reportergenen. Die quantitative PCR zeigte eine signifikante Expression von E6- und E7-mRNA in transfizierten Zelllinien, während die Western-Blot-Analyse die Expression von rekombinanten E7- jedoch nicht von E6-Proteinen zeigte, vermutlich aufgrund des Unvermögens rekombinanter E6-Proteine, sich ausreichend im eingesetzten Lysispuffer zu lösen. Die im 4. Kapitel vorgestellten Ergebnisse bieten eine alternative Plattform für die Untersuchung von Therapieansätzen gegen virale Onkoproteine wie

E6 und E7. Mit diesem System könnten die Auswirkungen gezielter antiviraler Therapien durch visuelle Untersuchung unter Verwendung von Fluoreszenzmikroskopie bewertet oder in Multiwellplatten-fähigen Fluoreszenzdetektoren quantitativ gemessen werden. Die Wirkung experimenteller Therapien auf das Expressionsniveau viraler mRNA und Proteine könnte über PCR und Western-Blot-Analysen z.B. durch Verwendung von anti-GFP- oder anti-RFP-Antikörpern gemessen werden da derzeit keine gegen CRPV E6- oder E7-Proteine gerichteten Antikörper im Handel verfügbar sind. Zusammenfassend könnte dieses CRPV-Expressionssystem als eine In-vitro-Plattform für die Bewertung eines antiviralen Therapeutikums eingesetzt werden bevor ein In-vivo-Test im CRPV-positiven Kaninchen-VX2-Karzinom, welches als Tiermodell für menschliche HNSCC dient, durchgeführt wird.

CHAPTER NO 6

APPENDIX

6.1 *Sequence Alignments*

Following are the alignment results of cloned CRPV E6 and E7 gene plasmids against the reference E6 and E7 sequences of cottontail rabbit papilloma virus in GenBank with accession no. *NC_001541.1:154-975* and *NC_001541.1:1075-1359* respectively. The alignment data includes nucleotide sequences of T7, EGFP and Ds-Red-Monomer regions of the vector backbone. Therefore the alignment data provides information about each clone regarding its vector backbone and gene insert.

All alignments mentioned below contain the important sequence features

  i.   Start and stop codons are depicted in grey dotted boxes.
  ii.   Restriction enzymes are highlighted in grey solid boxes
  iii. All mismatched nucleotides are presented in red dotted box with " * " and base-pair deletion is represented by " # "

Figure i. Sequence alignment of E6_WT clone. Comparison of sequences to the predicted CRPV reference sequences (*NC_001541.1:154-975*) identified nucleotide mismatches at position

1014, 1675 & 1703 (marked by box with red dotted lines). Initiation and termination codons are mentioned in grey dotted box. Analysis also confirmed sequences of restriction sites. T7 promoter sequences provides confirmation of pcDNA 3.0 vector. One base-pair deletion was noted during analysis and marked with #.
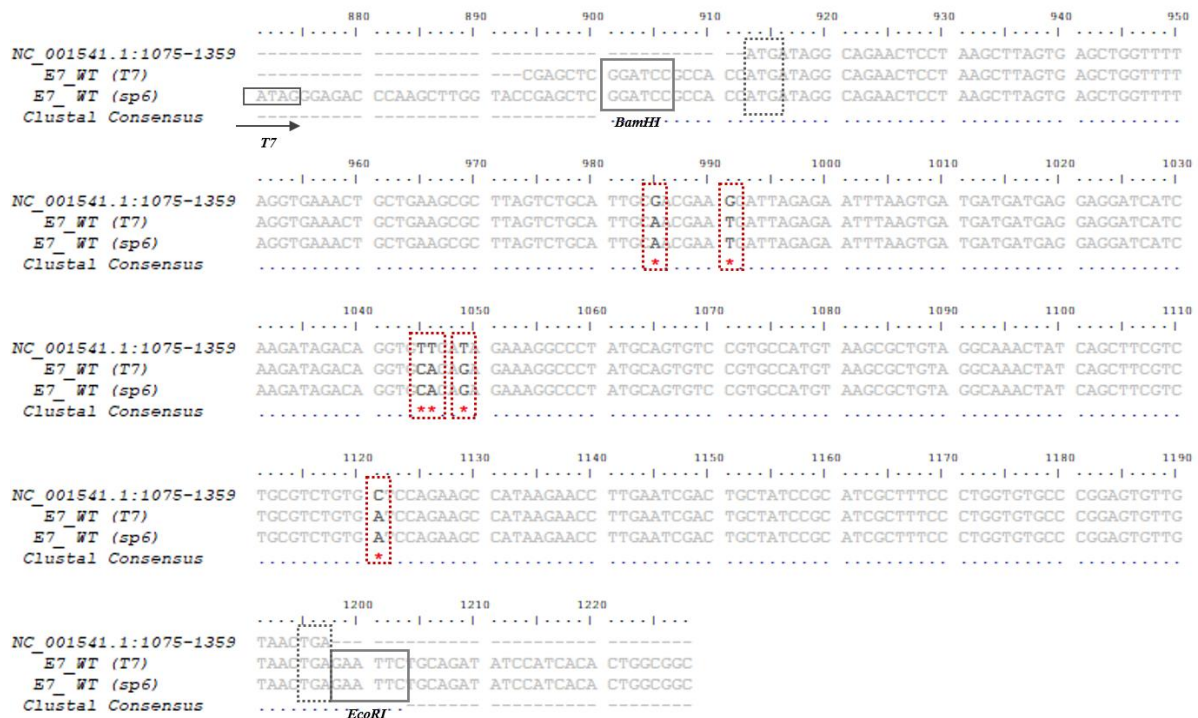
Figure ii- Sequence alignment of E7_WT clone. Comparison of sequences to the predicted CRPV reference sequences (*NC_001541.1:1075-1359*) identified nucleotide mismatches at position 985, 991, 1045, 1046, 1049 and 1121 (marked by box with red dotted lines). Analysis also confirmed sequences of restriction sites. T7 promoter sequences provides confirmation of pcDNA 3.0 vector. No base pair deletion observed in this sequence.
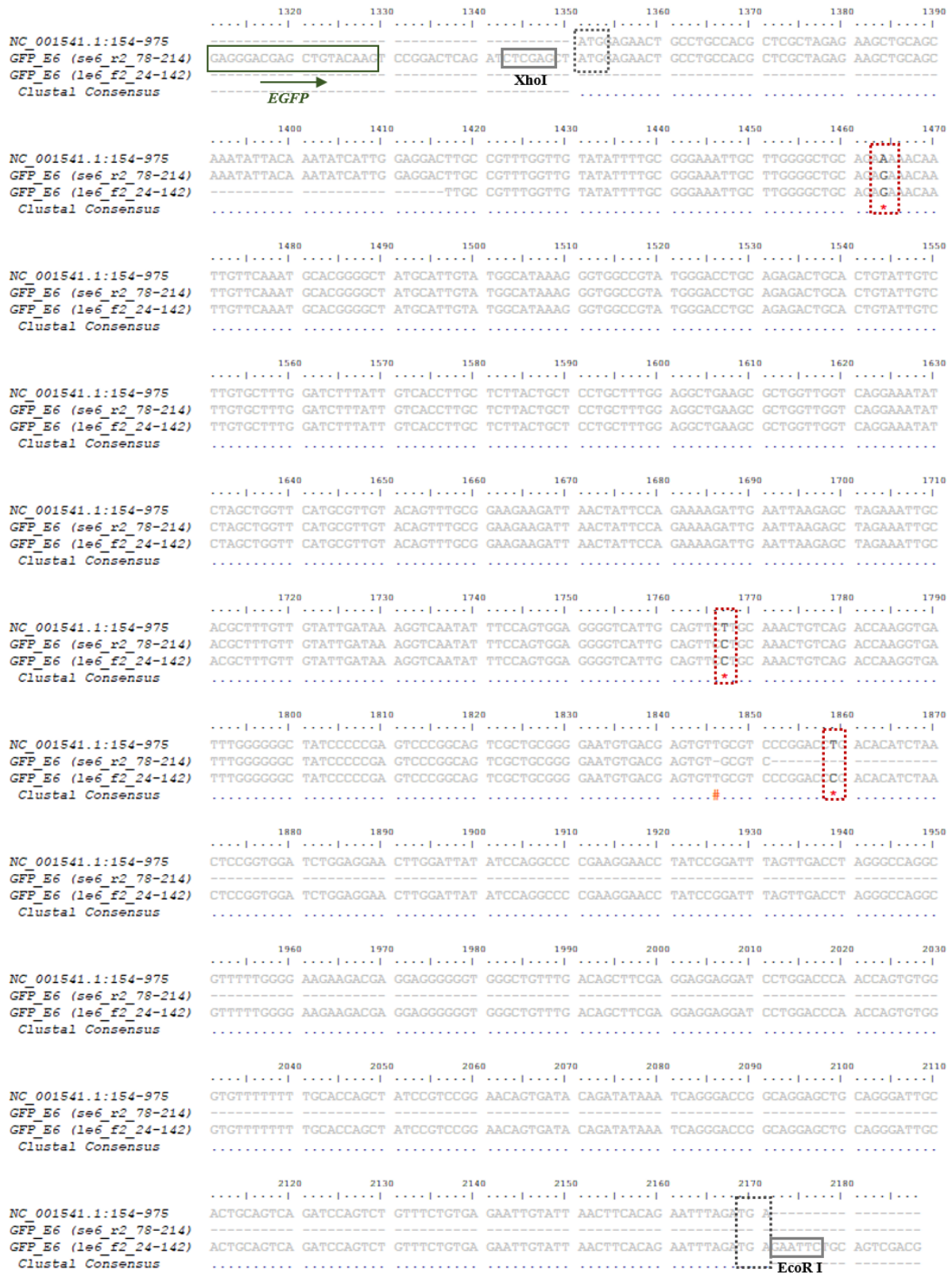
Figure iii - Sequence alignment of GFP_E6 clone. Comparison of sequences to the predicted CRPV reference sequence (*NC_001541.1:154-975*) identified nucleotide mismatches at position

1464, 1767 & 1859 (marked by box with red dotted lines). Start and stop codons are mentioned in grey dotted box. Analysis also confirmed sequences of restriction sites. EGFP promoter sequences provides confirmation of pEGFP-C1 vector. One base deletion observed and marked with #
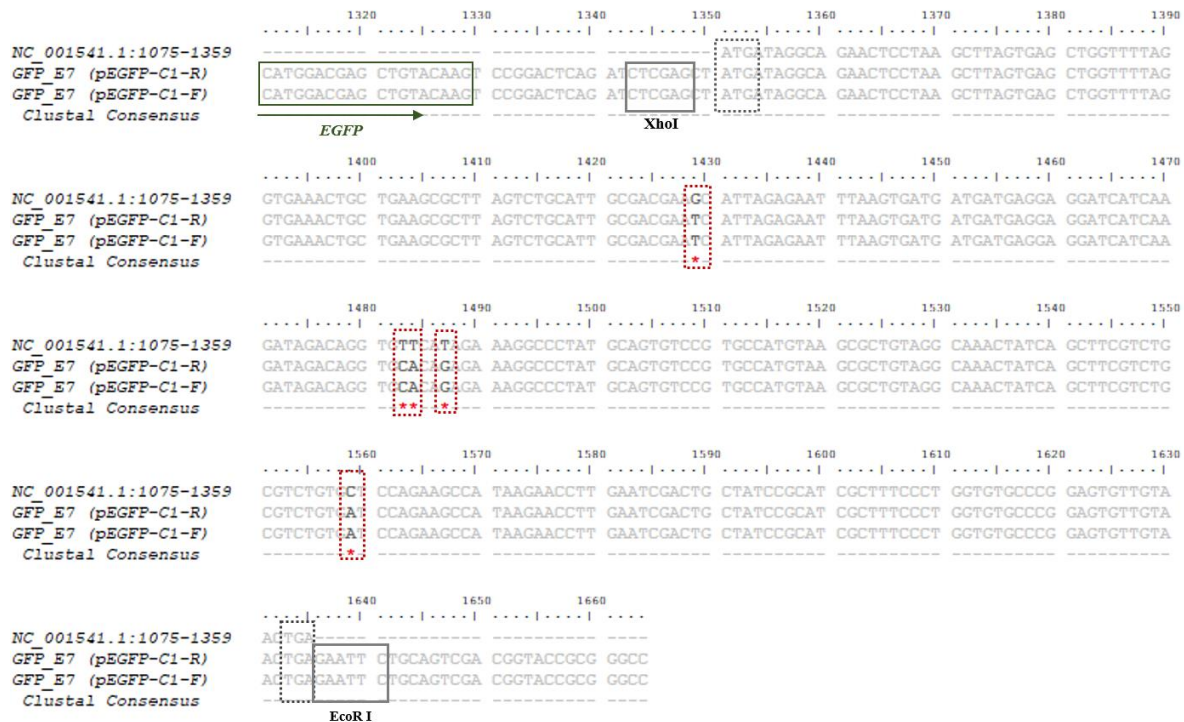

Figure iv- Sequence alignment of GFP_E7 clone. Comparison of sequences to the predicted CRPV reference sequence (*NC_001541.1:1075-1359*) identified nucleotide mismatches at position 1429, 1483, 1484, 1487, 1559 (marked by box with red dotted lines). Start and stop codons are mentioned in grey dotted box. Anlysis also confirmed sequences of restriction sites. EGFP promoter sequences provides confirmation of pEGFP-C1vector
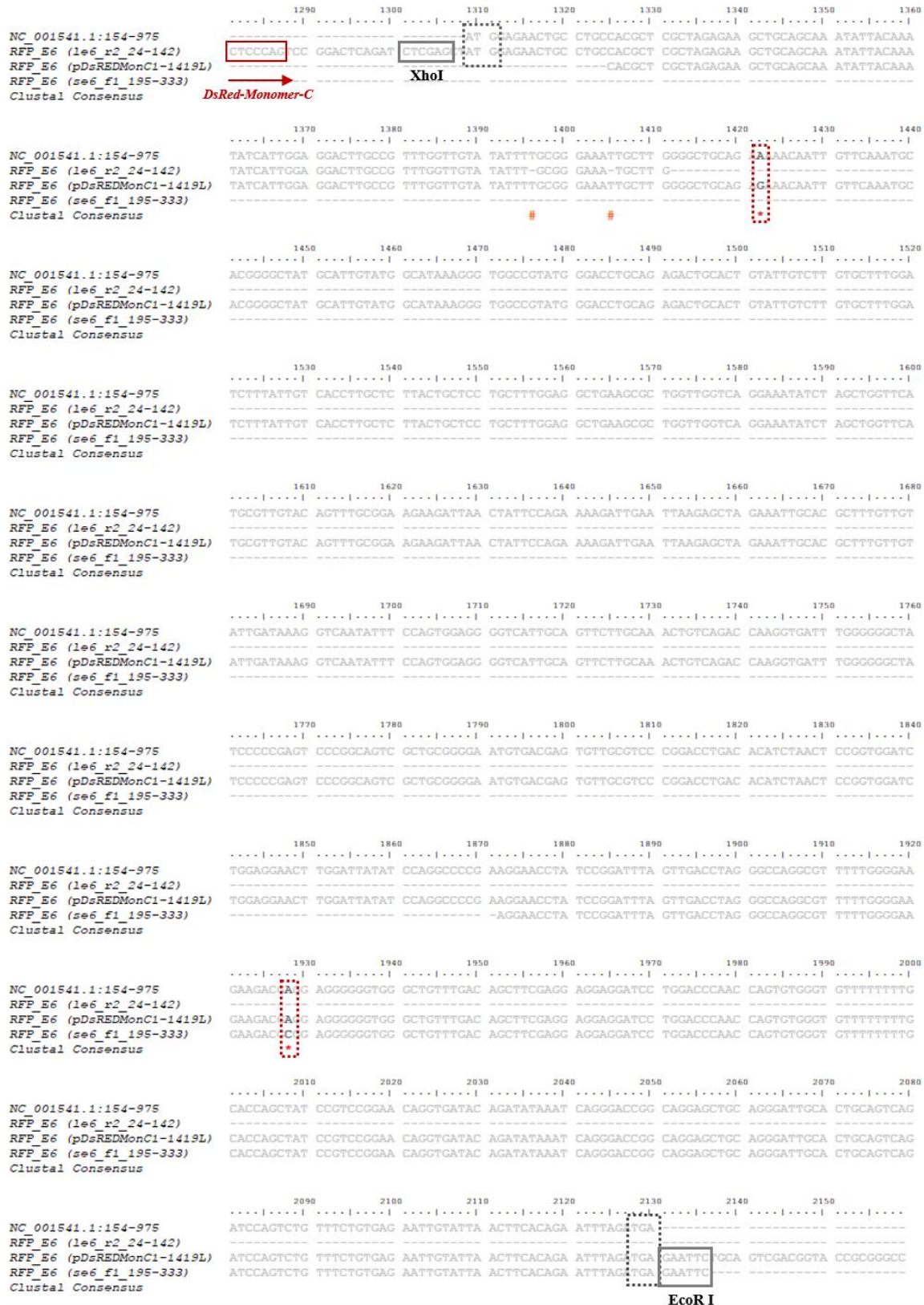
Figure v- Sequence alignment of GFP_E6 clone. Comparison of sequences to the predicted CRPV reference sequence (*NC_001541.1:154-975*) identified nucleotide mismatches at position

1422 & 1928 (marked by box with red dotted lines). Start and stop codons are mentioned in grey dotted box. Analysis also confirmed sequences of restriction sites. The promoter sequences provides confirmation of pDsRed-Monomer-C vector.
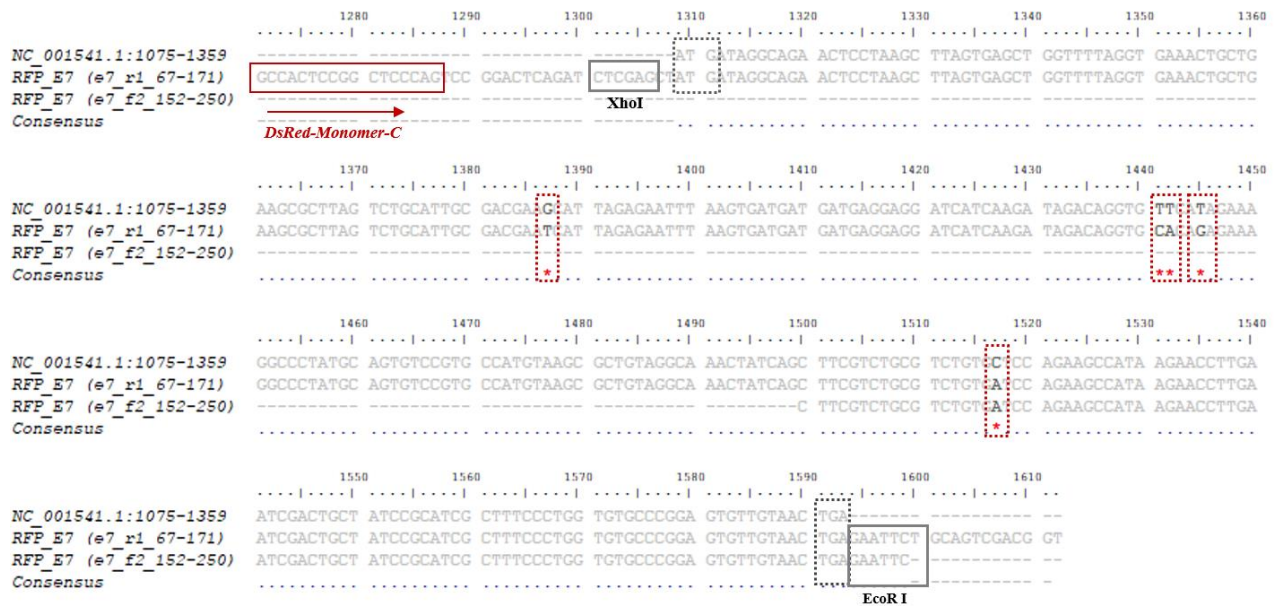
Figure vi- Sequence alignment of RFP_E7 clone: Comparison of sequences to the predicted CRPV reference sequence (*NC_001541.1:1075-1359*) identified nucleotide mismatches at position 1387, 1441, 1442, 1445 & 1517 (marked by box with red dotted lines). Start and stop codons are mentioned in grey dotted box. Analysis also confirmed sequences of restriction site. The promoter sequences provides confirmation of pDsRed-Monomer-C vector

6.2 *References*

1.   Chaikhoutdinov, I. & Goldenberg, D. Impact of Genetic Targets on Therapy in Head and Neck Squamous Cell Carcinoma. *Adv Exp Med Biol* **779**, 165–177 (2013).

2.   Ferlay, J. *et al.* Estimating the global cancer incidence and mortality in 2018: GLOBOCAN sources and methods. *Int J Cancer* **144**, 1941–1953 (2019).

3.   Goldberg, H. I., Lockwood, S. A., Wyatt, S. W. & Crossett, L. S. Trends and differentials in mortality from cancers of the oral cavity and pharynx in the United States, 1973-1987. *Cancer* **74**, 565–572 (1994).

4.   Werner, J. A., Dunne, A. A. & Myers, J. N. Functional anatomy of the lymphatic drainage system of the upper aerodigestive tract and its role in metastasis of squamous cell carcinoma. *Head Neck* **25**, 322–332 (2003).

5.   Harker, G. J. & Stephens, F. O. Comparison of intra-arterial versus intravenous 5-fluorouracil administration on epidermal squamous cell carcinoma in sheep. *Eur J Cancer* **28a**, 1437–1441 (1992).

6.   Den Otter, W. *et al.* Low doses of interleukin-2 can cure large bovine ocular squamous cell carcinoma. *Anticancer Res* **13**, 2453–2455 (1993).

7.   Steidler, N. E. & Reade, P. C. Experimental induction of oral squamous cell carcinomas in mice with 4-nitroquinolone-1-oxide. *Oral Surg Oral Med Oral Pathol* **57**, 524–531 (1984).

8.   Nauta, J. M., Roodenburg, J. L., Nikkels, P. G., Witjes, M. J. & Vermey, A. Comparison of epithelial dysplasia--the 4NQO rat palate model and human oral mucosa. *Int. J. Oral Maxillofac. Surg.* **24**, 53–8 (1995).

9.   Shklar, G. Experimental oral pathology in the Syrian hamster. *Prog Exp Tumor Res* **16**, 518–538 (1972).

10.   O'Malley Jr., B. W., Cope, K. A., Johnson, C. S. & Schwartz, M. R. A new immunocompetent murine model for oral cancer. *Arch Otolaryngol Head Neck Surg* **123**, 20–24 (1997).

11.   Hier, M. P., Black, M. J., Shenouda, G., Sadeghi, N. & Karp, S. E. A murine model for the immunotherapy of head and neck squamous cell carcinoma. *Laryngoscope* **105**, 1077–1080 (1995).

12.   Povlsen, C. O. & Rygaard, J. Heterotransplantation of human epidermoid carcinomas to the mouse mutant nude. *Acta Pathol Microbiol Scand A* **80**, 713–717 (1972).

13.   Lei, Z. G., Ren, X. H., Wang, S. S., Liang, X. H. & Tang, Y. L. Immunocompromised and immunocompetent mouse models for head and neck squamous cell carcinoma. *Onco Targets Ther* **9**, 545–555 (2016).

14.   Karanfilian, R. G., Rush Jr., B. F. & Murphy, T. Regional vs systemic effect of cis-dichlorodiammine platinum (II) on squamous cell carcinoma in rats. *Am Surg* **49**, 116–119 (1983).

15.   Schouwenburg, P. F., Van Putten, L. M. & Snow, G. B. External carotid artery infusion with single-and multiple-drug regimens in the rat. *Cancer* **45**, 2258–2264 (1980).

16.   Smith, L. P. & Thomas, G. R. Animal models for the study of squamous cell carcinoma of the upper aerodigestive tract: a historical perspective with review of their utility and limitations. Part A. Chemically-induced de novo cancer, syngeneic animal models of HNSCC, animal models of t. *Int J Cancer* **118**, 2111–2122 (2006).

17.   Méry, B. *et al.* Preclinical models in HNSCC: A comprehensive review. *Oral Oncology* vol. 65 51–56 (2017).

18.   Doorbar, J. Model systems of human papillomavirus-associated disease. *J Pathol* **238**, 166–179 (2016).

19.   Shope, R. E. A TRANSMISSIBLE TUMOR-LIKE CONDITION IN RABBITS. *J Exp Med* **56**, 793–802 (1932).

20.   Rothenberg, S. M. & Ellisen, L. W. The molecular pathogenesis of head and neck squamous cell carcinoma. *J Clin Invest*

122, 1951–1957 (2012).

21.   Spiotto, M. T., Pytynia, M., Liu, G. F., Ranck, M. C. & Widau, R. Animal models to study the mutational landscape for oral cavity and oropharyngeal cancers. *J Oral Maxillofac Res* **4**, e1 (2013).

22.   van Es, R. J., Dullens, H. F., van der Bilt, A., Koole, R. & Slootweg, P. J. Evaluation of the VX2 rabbit auricle carcinoma as a model for head and neck cancer in humans. *J Craniomaxillofac Surg* **28**, 300–307 (2000).

23.   Rous, P. & Beard, J. W. The Progression to Carcinoma of Virus-Induced Rabbit Papillomas (Shope). *J Exp Med* **62**, 523–548 (1935).

24.   Kidd, J. G., Beard, J. W. & Rous, P. Serological Reactions with a Virus Causing Rabbit Papillomas Which Become Cancerous : I. Tests of the Blood of Animals Carrying the Papilloma. *J Exp Med* **64**, 63–77 (1936).

25.   Kidd, J. G. & Rous, P. A TRANSPLANTABLE RABBIT CARCINOMA ORIGINATING IN A VIRUS-INDUCED PAPILLOMA AND CONTAINING THE VIRUS IN MASKED OR ALTERED FORM. *J Exp Med* **71**, 813–838 (1940).

26.   Greene, H. S. The heterologous transplantation V-2 rabbit carcinoma. *Cancer Res* **13**, 610–612 (1953).

27.   Rous, P., Kidd, J. G. & Smith, W. E. Experiments on the cause of the rabbit carcinomas derived from virus-induced papillomas. II. Loss by the Vx2 carcinoma of the power to immunize hosts against the papilloma virus. *J Exp Med* **96**, 159–174 (1952).

28.   Giri, I., Danos, O. & Yaniv, M. Genomic structure of the cottontail rabbit (Shope) papillomavirus. *Proc Natl Acad Sci U S A* **82**, 1580–1584 (1985).

29.   Belnap, D. M. *et al.* Conserved features in papillomavirus and polyomavirus capsids. *J. Mol. Biol.* **259**, 249–263 (1996).

30.   Wu, X., Xiao, W. & Brandsma, J. L. Papilloma formation by cottontail rabbit papillomavirus requires E1 and E2 regulatory genes in addition to E6 and E7 transforming genes. *J Virol* **68**, 6097–6102 (1994).

31.   Stubenrauch, F. & Laimins, L. A. Human papillomavirus life cycle: active and latent phases. *Semin Cancer Biol* **9**, 379–386 (1999).

32.   Schneider, M., Yigitliler, A., Stubenrauch, F. & Iftner, T. Cottontail Rabbit Papillomavirus E1 and E2 Proteins Mutually Influence Their Subcellular Localizations. *J Virol* **92**, (2018).

33.   Peh, W. L. *et al.* The viral E4 protein is required for the completion of the cottontail rabbit papillomavirus productive cycle in vivo. *J Virol* **78**, 2142–2151 (2004).

34.   Harry, J. B. & Wettstein, F. O. Transforming properties of the cottontail rabbit papillomavirus oncoproteins Le6 and SE6 and of the E8 protein. *J Virol* **70**, 3355–3362 (1996).

35.   Hu, J., Han, R., Cladel, N. M., Pickel, M. D. & Christensen, N. D. Intracutaneous DNA vaccination with the E8 gene of cottontail rabbit papillomavirus induces protective immunity against virus challenge in rabbits. *J Virol* **76**, 6453–6459 (2002).

36.   Christensen, N. D., Budgeon, L. R., Cladel, N. M. & Hu, J. Recent advances in preclinical model systems for papillomaviruses. *Virus Res* **231**, 108–118 (2017).

37.   Ganzenmueller, T. *et al.* The E7 protein of the cottontail rabbit papillomavirus immortalizes normal rabbit keratinocytes and reduces pRb levels, while E6 cooperates in immortalization but neither degrades p53 nor binds E6AP. *Virology* **372**, 313–324 (2008).

38.   Dunne, A. A. *et al.* Lymphogenic metastatic spread of auricular VX2 carcinoma in New Zealand white rabbits. *Anticancer Res* **22**, 3273–3279 (2002).

39.   Mandic, R. *et al.* Expression of MMP-3, MMP-13, TIMP-2 and TIMP-3 in the VX2 carcinoma of the New Zealand white

rabbit. *Anticancer Res* **22**, 3281–3284 (2002).

40. van Es, R. J. *et al.* The VX2 carcinoma in the rabbit auricle as an experimental model for intra-arterial embolization of head and neck squamous cell carcinoma with dextran microspheres. *Lab Anim* **33**, 175–184 (1999).

41. Amella, C. A. *et al.* Latent infection induced with cottontail rabbit papillomavirus. A model for human papillomavirus latency. *Am J Pathol* **144**, 1167–1171 (1994).

42. Easty, D. M. & Easty, G. C. Establishment of an in vitro cell line from the rabbit VX2 carcinoma. *Virchows Arch B Cell Pathol Incl Mol Pathol* **39**, 333–337 (1982).

43. Galasko, C. S. & Haynes, D. W. Survival of VX2 carcinoma cells in vitro. *Eur J Cancer* **12**, 1025–1026 (1976).

44. Shah, S. A. & Dickson, J. A. Preservation of enzymatically prepared rabbit VX2 tumour cells in vitro. *Eur. J. Cancer* **14**, 447–448 (1978).

45. Osato, T. & Ito, Y. In vitro cultivation and immunofluorescent studies of transplantable carcinomas Vx2 and Vx7. Persistence of a Shope virus-related antigenic substance in the cells of both tumors. *J Exp Med* **126**, 881–886 (1967).

46. Voelkel, E. F., Tashjian Jr., A. H., Franklin, R., Wasserman, E. & Levine, L. Hypercalcemia and tumor-prostaglandins: the VX2 carcinoma model in the rabbit. *Metabolism* **24**, 973–986 (1975).

47. Yoneda, T., Kitamura, M., Ogawa, T., Aya, S. & Sakuda, M. Control of VX2 carcinoma cell growth in culture by calcium, calmodulin, and prostaglandins. *Cancer Res.* **45**, 398–405 (1985).

48. Georges, E., Breitburd, F., Jibard, N. & Orth, G. Two Shope papillomavirus-associated VX2 carcinoma cell lines with different levels of keratinocyte differentiation and transplantability. *J. Virol.* **55**, 246–250 (1985).

49. Virmani, S. *et al.* Comparison of two different methods for inoculating VX2 tumors in rabbit livers and hind limbs. *J. Vasc. Interv. Radiol.* **19**, 931–936 (2008).

50. Nelke, K. H., Pawlak, W., Leszczyszyn, J. & Gerber, H. Photodynamic therapy in head and neck cancer. *Postepy Higieny i Medycyny Doswiadczalnej* vol. 68 119–128 (2014).

51. Agostinis, P. *et al.* Photodynamic therapy of cancer: An update. *CA. Cancer J. Clin.* **61**, 250–281 (2011).

52. Van Dyne, E. A. *et al.* Trends in Human Papillomavirus–Associated Cancers — United States, 1999–2015. *MMWR. Morb. Mortal. Wkly. Rep.* **67**, 918–924 (2018).

53. Lou, P.-J., Jones, L., Hopper, C. & Hopper FRCS, C. Clinical Outcomes of Photodynamic Therapy for Head-and-Neck Cancer www.tcrt.org. **2**, (2003).

54. Bredell, M. G., Besic, E., Maake, C. & Walt, H. The application and challenges of clinical PD-PDT in the head and neck region: A short review. *Journal of Photochemistry and Photobiology B: Biology* vol. 101 185–190 (2010).

55. Copper, M. P., Triesscheijn, M., Tan, I. B., Ruevekamp, M. C. & Stewart, F. A. Photodynamic therapy in the treatment of multiple primary tumours in the head and neck, located to the oral cavity and oropharynx. *Clin. Otolaryngol.* **32**, 185–189 (2007).

56. Daniell, M. D. & Hill, J. S. A HISTORY OF PHOTODYNAMIC THERAPY. *Australian and New Zealand Journal of Surgery* vol. 61 340–348 (1991).

57. Dolmans, D. E. J. G. J., Fukumura, D. & Jain, R. K. Photodynamic therapy for cancer. *Nature Reviews Cancer* vol. 3 380–387 (2003).

58. Abdel-kader, M. H. CHAPTER 1. The Journey of PDT Throughout History: PDT from Pharos to Present. in 1–21 (Royal Society of Chemistry, 2016). doi:10.1039/9781782626824-00001.

59.   Spikes, J. D. Photodynamic Action: From Paramecium to Photochemotherapy*. *Photochem. Photobiol.* **65**, 142S-147S (1997).

60.   Biologic Effects of Light 2001: Proceedings of a Symposium, Boston ... - Google Books. https://books.google.de/books?hl=en&lr=&id=wNW80YNZIlIC&oi=fnd&pg=PR11&dq=M.+F.+Holick+and+F.+Michael+,+Biologic+Effects+of+Light+,+Kluwer+Academic+publishers,+Norwell,+Massachusetts,+2001,+p.+3&ots=RKgt5cglcd&sig=dPDVXrXAnOD-XHlIWX4Z9h1fO38&redir_esc=y#v=onepage&q&f=false.

61.   Photodynamic Therapy - Google Books. https://books.google.de/books?hl=en&lr=&id=L73d4iPt3LAC&oi=fnd&pg=PA3&dq=J.+Moan+and+Q.+Peng+,+Photodynamic+therapy+'comprehensive+series+in+photochemical+and+photobiological+sciences'+,+2003,+p.+1&ots=XAoczXhSRs&sig=pzHqTxee8IwWw_JLS5zSO09Xwhw&redir_esc=y#v=onepage&q&f=false.

62.   Dougherty, T. J., Grindey, G. B., Fiel, R., Weishaupt, K. R. & Boyle, D. G. Photoradiation therapy. II. Cure of animal tumors with hematoporphyrin and light. *J. Natl. Cancer Inst.* **55**, 115–121 (1975).

63.   Kelly, J. F. & Snell, M. E. Hematoporphyrin derivative: a possible aid in the diagnosis and therapy of carcinoma of the bladder. *J. Urol.* **115**, 150–151 (1976).

64.   Detty, M. R., Gibson, S. L. & Wagner, S. J. Current clinical and preclinical photosensitizers for use in photodynamic therapy. *Journal of Medicinal Chemistry* vol. 47 3897–3915 (2004).

65.   Xiao, Q. *et al.* Discovery and Development of Natural Products and their Derivatives as Photosensitizers for Photodynamic Therapy. *Curr. Med. Chem.* **25**, 839–860 (2017).

66.   Abrahamse, H. & Hamblin, M. R. New photosensitizers for photodynamic therapy. *Biochemical Journal* vol. 473 347–364 (2016).

67.   Juarranz, Á., Jaén, P., Sanz-Rodríguez, F., Cuevas, J. & González, S. Photodynamic therapy of cancer. Basic principles and applications. *Clin. Transl. Oncol.* **10**, 148–154 (2008).

68.   Sato, K., Nagaya, T., Choyke, P. L. & Kobayashi, H. Near infrared photoimmunotherapy in the treatment of pleural disseminated NSCLC: Preclinical experience. *Theranostics* **5**, 698–709 (2015).

69.   Hamblin, M. R. & Newman, E. L. Photosensitizer targeting in photodynamic therapy I. Conjugates of haematoporphyrin with albumin and transferrin. *J. Photochem. Photobiol. B Biol.* **26**, 45–56 (1994).

70.   Kaščáková, S. *et al.* Somatostatin analogues for receptor targeted photodynamic therapy. *PLoS One* **9**, (2014).

71.   Luo, D., Carter, K. A., Miranda, D. & Lovell, J. F. Chemophototherapy: An Emerging Treatment Option for Solid Tumors. *Advanced Science* vol. 4 (2017).

72.   Kim, M. M. & Darafsheh, A. Light Sources and Dosimetry Techniques for Photodynamic Therapy. *Photochem. Photobiol.* **96**, 280–294 (2020).

73.   Rendon, A., Weersink, R. & Lilge, L. Towards conformal light delivery using tailored cylindrical diffusers: Attainable light dose distributions. *Phys. Med. Biol.* **51**, 5967–5975 (2006).

74.   Grossman, C. *et al.* Targeted laryngeal photodynamic therapy with a balloon diffusing light source. *Photodiagnosis Photodyn. Ther.* **7**, 158–161 (2010).

75.   Henderson, B. W. & Dougherty, T. J. HOW DOES PHOTODYNAMIC THERAPY WORK? *Photochemistry and Photobiology* vol. 55 145–157 (1992).

76.   Vrouenraets, M. B., Visser, G. W. M., Snow, G. B. & Van Dongen, G. A. M. S. Basic principles, applications in oncology and improved selectivity of photodynamic therapy. *Anticancer Research* vol. 23 505–522 (2003).

77.   Foote, C. S. DEFINITION OF TYPE I and TYPE II PHOTOSENSITIZED OXIDATION. *Photochemistry and*

Photobiology vol. 54 659–659 (1991).

78. Peng, Q., Moan, J. & Nesland, J. M. Correlation of subcellular and intratumoral photosensitizer localization with ultrastructural features after photodynamic therapy. *Ultrastructural Pathology* vol. 20 109–129 (1996).

79. Calixto, G. M. F. *et al.* Nanotechnology-based drug delivery systems for photodynamic therapy of cancer: A review. *Molecules* vol. 21 (2016).

80. Dougherty, T. J. *et al. REVIEW Photodynamic Therapy*. https://academic.oup.com/jnci/article-abstract/90/12/889/960771 (1998).

81. Mroz, P., Yaroslavsky, A., Kharkwal, G. B. & Hamblin, M. R. Cell death pathways in photodynamic therapy of cancer. *Cancers* vol. 3 2516–2539 (2011).

82. Li, W., Ma, Q. & Wu, E. Perspectives on the Role of Photodynamic Therapy in the Treatment of Pancreatic Cancer. *Int. J. Photoenergy* **2012**, (2012).

83. Fingar, V. H., Wieman, T. J. & Haydon, P. S. The Effects of Thrombocytopenia on Vessel Stasis and Macromolecular Leakage after Photodynamic Therapy Using Photofrin. *Photochem. Photobiol.* **66**, 513–517 (1997).

84. Fingar, V. H. *et al.* Analysis of acute vascular damage after photodynamic therapy using benzoporphyrin derivative (BPD). *Br. J. Cancer* **79**, 1702–1708 (1999).

85. Brackett, C. M., Owczarczak, B., Ramsey, K., Maier, P. G. & Gollnick, S. O. IL-6 potentiates tumor resistance to photodynamic therapy (PDT). *Lasers Surg. Med.* **43**, 676–685 (2011).

86. de Vree, W. J. A. *et al.* Evidence for an Important Role of Neutrophils in the Efficacy of Photodynamic Therapy in Vivo. *Cancer Res.* **56**, (1996).

87. Shishodia, S., Sethi, G. & Aggarwal, B. B. Curcumin: Getting back to the roots. in *Annals of the New York Academy of Sciences* vol. 1056 206–217 (Blackwell Publishing Inc., 2005).

88. Wilken, R., Veena, M. S., Wang, M. B. & Srivatsan, E. S. Curcumin: A review of anti-cancer properties and therapeutic activity in head and neck squamous cell carcinoma. *Molecular Cancer* vol. 10 (2011).

89. Mukhopadhyay, A., Bueso-Ramos, C., Chatterjee, D., Pantazis, P. & Aggarwal, B. B. Curcumin downregulates cell survival mechanisms in human prostate cancer cell lines. *Oncogene* **20**, 7597–7609 (2001).

90. Govindarajan, V. S. Turmeric—chemistry, technology, and quality. *C R C Crit. Rev. Food Sci. Nutr.* **12**, 199–301 (1980).

91. Wang, D. *et al.* Liposome-encapsulated curcumin suppresses growth of head and neck squamous cell carcinoma in vitro and in xenografts through the inhibition of nuclear factor κB by an AKT-independent pathway. *Clin. Cancer Res.* **14**, 6228–6236 (2008).

92. Wolzt, M. *et al.* Safety, tolerability and pharmacokinetics of liposomal curcumin (Lipocurc™) in healthy humans. doi:10.5414/CP202076.

93. Goel, A., Kunnumakkara, A. B. & Aggarwal, B. B. Curcumin as 'Curecumin': From kitchen to clinic. *Biochem. Pharmacol.* **75**, 787–809 (2008).

94. López-Jornet, P., Camacho-Alonso, F. & Gómez-Garcia, F. Effect of curcumin and irradiation in PE/CA-PJ15 oral squamous cell carcinoma. *Acta Odontol. Scand.* **69**, 269–273 (2011).

95. Koon, H. K., Leung, A. W. N., Yue, K. K. M. & Mak, N. K. Photodynamic effect of curcumin on NPC/CNE2 cells. *J. Environ. Pathol. Toxicol. Oncol.* **25**, 205–215 (2006).

96. Anand, P., Kunnumakkara, A. B., Newman, R. A. & Aggarwal, B. B. Bioavailability of curcumin: Problems and promises. *Molecular Pharmaceutics* vol. 4 807–818 (2007).

97.   Feng, T., Wei, Y., Lee, R. J. & Zhao, L. Liposomal curcumin and its application in cancer. *International Journal of Nanomedicine* vol. 12 6027–6044 (2017).

98.   Zylberberg, C. & Matosevic, S. Pharmaceutical liposomal drug delivery: a review of new delivery systems and a look at the regulatory landscape. *Drug Deliv.* **23**, 3319–3329 (2016).

99.   Gregoriadis, G. & Ryman, B. E. Lysosomal localization of -fructofuranosidase-containing liposomes injected into rats. *Biochem. J.* **129**, 123–133 (1972).

100.   Lasic, D. Doxorubicin in sterically stabilized. *Nature* vol. 380 561–562 (1996).

101.   Akbarzadeh, A. *et al.* Liposome: Classification, preparation, and applications. *Nanoscale Res. Lett.* **8**, 102 (2013).

102.   Bangham, A. D., Standish, M. M. & Watkins, J. C. Diffusion of univalent ions across the lamellae of swollen phospholipids. *J. Mol. Biol.* **13**, 238–252 (1965).

103.   Ozcetin, A., Mutlu, S. & Bakowsky, U. Archaebacterial tetraetherlipid liposomes. *Methods Mol. Biol.* **605**, 87–96 (2010).

104.   Duse, L., Pinnapireddy, S. R., Strehlow, B., Jedelská, J. & Bakowsky, U. Low level LED photodynamic therapy using curcumin loaded tetraether liposomes. *Eur. J. Pharm. Biopharm.* **126**, 233–241 (2018).

105.   Arber, W. & Linn, S. DNA Modification and Restriction. *Annu. Rev. Biochem.* **38**, 467–500 (1969).

106.   Smith, H. O. & Welcox, K. W. A Restriction enzyme from Hemophilus influenzae. I. Purification and general properties. *J. Mol. Biol.* **51**, 379–391 (1970).

107.   Shuman, S. DNA ligases: Progress and prospects. *Journal of Biological Chemistry* vol. 284 17365–17369 (2009).

108.   Griffith, F. The Significance of Pneumococcal Types. *J. Hyg. (Lond).* **27**, 113–159 (1928).

109.   Cohen, S. N., Chang, A. C. Y., Boyer, H. W. & Helling, R. B. Construction of biologically functional bacterial plasmids in vitro. *Proc. Natl. Acad. Sci. U. S. A.* **70**, 3240–3244 (1973).

110.   Hoseini, S. S. & Sauer, M. G. Molecular cloning using polymerase chain reaction, an educational guide for cellular engineering. *J. Biol. Eng.* **9**, 2 (2015).

111.   Rao, R. C. & Zacks, D. N. Cell and gene therapy. *Dev. Ophthalmol.* **53**, 167–177 (2014).

112.   Schleef, M. *Minicircle and miniplasmid dna vectors: the future of non-viral and viral gene transfer.* (John Wiley & Sons, 2013).

113.   Cohen, S. N., Chang, A. C. Y., Boyer, H. W. & Helling, R. B. Construction of Biologically Functional Bacterial Plasmids In Vitro. *Proc. Natl. Acad. Sci.* **70**, 3240–3244 (1973).

114.   Hardee, C. L., Arévalo-Soliz, L. M., Hornstein, B. D. & Zechiedrich, L. Advances in Non-Viral DNA Vectors for Gene Therapy. *Genes (Basel).* **8**, 65 (2017).

115.   Glover, D. J., Lipps, H. J. & Jans, D. A. Towards safe, non-viral therapeutic gene expression in humans. *Nat. Rev. Genet.* **6**, 299–310 (2005).

116.   A Quick Overview of Molecular Cloning | GoldBio. https://www.goldbio.com/articles/article/cloning-overview.

117.   Fernandez, J. M. & Hoeffler, J. P. *Gene expression systems: using nature for the art of expression.* (Elsevier, 1998).

118.   Demain, A. L. & Vaishnav, P. Production of recombinant proteins by microbes and higher organisms. *Biotechnol Adv* **27**, 297–306 (2009).

119.   Buck, P. M., Kumar, S. & Singh, S. K. Consequences of glycan truncation on Fc structural integrity. *MAbs* **5**, 904–916

(2013).

120.   Jacobs, P. P. & Callewaert, N. N-glycosylation engineering of biopharmaceutical expression systems. *Curr. Mol. Med.* **9**, 774–800 (2009).

121.   Lai, T., Yang, Y. & Ng, S. K. Advances in Mammalian cell line development technologies for recombinant protein production. *Pharm.* **6**, 579–603 (2013).

122.   Wurm, F. M. Production of recombinant protein therapeutics in cultivated mammalian cells. *Nat Biotechnol* **22**, 1393–1398 (2004).

123.   Zhu, J. Mammalian cell protein expression for biopharmaceutical production. *Biotechnol Adv* **30**, 1158–1170 (2012).

124.   Khan, K. H. Gene expression in Mammalian cells and its applications. *Adv. Pharm. Bull.* **3**, 257–263 (2013).

125.   Yasumura, Y. & Kawakita, Y. A line of cells derived from African green monkey kidney. *Nippon Rinsho* **21**, 1209–1210 (1963).

126.   Somia, N. & Verma, I. M. Gene therapy: trials and tribulations. *Nat Rev Genet* **1**, 91–99 (2000).

127.   Thomas, C. E., Ehrhardt, A. & Kay, M. A. Progress and problems with the use of viral vectors for gene therapy. *Nat Rev Genet* **4**, 346–358 (2003).

128.   Marshall, E. Gene therapy death prompts review of adenovirus vector. *Science (80-.).* **286**, 2244–2245 (1999).

129.   Kang, E. M. & Tisdale, J. F. The leukemogenic risk of integrating retroviral vectors in hematopoietic stem cell gene therapy applications. *Curr Hematol Rep* **3**, 274–281 (2004).

130.   Yin, H. *et al.* Non-viral vectors for gene-based therapy. *Nat Rev Genet* **15**, 541–555 (2014).

131.   Wolff, J. A. *et al.* Direct gene transfer into mouse muscle in vivo. *Science (80-.).* **247**, 1465–1468 (1990).

132.   Cevher, E., Demir, A. & Sefik, E. Gene Delivery Systems: Recent Progress in Viral and Non-Viral Therapy. in *Recent Advances in Novel Drug Carrier Systems* (InTech, 2012). doi:10.5772/53392.

133.   Bushman, F. D. Retroviral integration and human gene therapy. *Journal of Clinical Investigation* vol. 117 2083–2086 (2007).

134.   Lachmann, R. H. & Efstathiou, S. The use of herpes simplex virus-based vectors for gene delivery to the nervous system. *Molecular Medicine Today* vol. 3 404–411 (1997).

135.   Campos, S. & Barry, M. Current Advances and Future Challenges in Adenoviral Vector Biology and Targeting. *Curr. Gene Ther.* **7**, 189–204 (2007).

136.   Pillai, O. & Panchagnula, R. Polymers in drug delivery. *Current Opinion in Chemical Biology* vol. 5 447–451 (2001).

137.   Balazs, D. A. & Godbey, W. Liposomes for Use in Gene Delivery. *J. Drug Deliv.* **2011**, 1–12 (2011).

138.   Dufès, C., Uchegbu, I. F. & Schätzlein, A. G. Dendrimers in gene delivery. *Advanced Drug Delivery Reviews* vol. 57 2177–2202 (2005).

139.   Hofland, H. E. J., Shephard, L. & Sullivan, S. M. Formation of stable cationic lipid/DNA complexes for gene transfer. *Proc. Natl. Acad. Sci. U. S. A.* **93**, 7305–7309 (1996).

140.   Lin, M. T. S., Pulkkinen, L., Uitto, J. & Yoon, K. The gene gun: Current applications in cutaneous gene therapy. *International Journal of Dermatology* vol. 39 161–170 (2000).

141.   Kalli, C., Teoh, W. C. & Leen, E. Introduction of genes via sonoporation and electroporation. *Advances in Experimental*

Medicine and Biology vol. 818 231–254 (2014).

142. Ferrara, K. W. Driving delivery vehicles with ultrasound. *Advanced Drug Delivery Reviews* vol. 60 1097–1102 (2008).

143. Suda, T. & Liu, D. Hydrodynamic gene delivery: Its principles and applications. *Molecular Therapy* vol. 15 2063–2069 (2007).

144. Rezaee, M., Oskuee, R. K., Nassirli, H. & Malaekeh-Nikouei, B. Progress in the development of lipopolyplexes as efficient non-viral gene delivery systems. *J Control Release* **236**, 1–14 (2016).

145. Ewe, A. & Aigner, A. Cationic Lipid-Coated Polyplexes (Lipopolyplexes) for DNA and Small RNA Delivery. *Methods Mol Biol* **1445**, 187–200 (2016).

146. Bhavsar, D., Subramanian, K., Sethuraman, S. & Krishnan, U. M. 'Nano-in-nano' hybrid liposomes increase target specificity and gene silencing efficiency in breast cancer induced SCID mice. *Eur J Pharm Biopharm* **119**, 96–106 (2017).

147. Ewe, A. *et al.* Liposome-polyethylenimine complexes (DPPC-PEI lipopolyplexes) for therapeutic siRNA delivery in vivo. *Nanomedicine* **13**, 209–218 (2017).

148. Hadinoto, K., Sundaresan, A. & Cheow, W. S. Lipid–polymer hybrid nanoparticles as a new generation therapeutic delivery platform: a review. *Eur. J. Pharm. Biopharm.* **85**, 427–443 (2013).

149. Pinnapireddy, S. R., Duse, L., Strehlow, B., Schafer, J. & Bakowsky, U. Composite liposome-PEI/nucleic acid lipopolyplexes for safe and efficient gene delivery and gene knockdown. *Colloids Surf B Biointerfaces* **158**, 93–101 (2017).

150. Ganzenmueller, T. *et al.* The E7 protein of the cottontail rabbit papillomavirus immortalizes normal rabbit keratinocytes and reduces pRb levels, while E6 cooperates in immortalization but neither degrades p53 nor binds E6AP. *Virology* **372**, 313–324 (2008).

151. Haskell, K. M., Vuocolo, G. A., Defeo-Jones, D., Jones, R. E. & Ivey-Hoyle, M. Comparison of the binding of the human papillomavirus type 16 and cottontail rabbit papillomavirus E7 proteins to the retinoblastoma gene product. *J. Gen. Virol.* **74**, 115–119 (1993).

152. Schulz, S. *et al.* Treatment with ozone/oxygen-pneumoperitoneum results in complete remission of rabbit squamous cell carcinomas. *Int. J. Cancer* **122**, 2360–2367 (2008).

153. Handal, J. A. *et al.* Creation of rabbit bone and soft tissue tumor using cultured VX2 cells. *J Surg Res* **179**, e127-32 (2013).

154. Laemmli, U. K. Cleavage of structural proteins during the assembly of the head of bacteriophage T4. *Nature* **227**, 680–685 (1970).

155. Renart, J., Reiser, J. & Stark, G. R. Transfer of proteins from gels to diazobenzyloxymethyl-paper and detection with antisera: a method for studying antibody specificity and antigen structure. *Proc. Natl. Acad. Sci. U. S. A.* **76**, 3116–3120 (1979).

156. Towbin, H., Staehelin, T. & Gordon, J. Electrophoretic transfer of proteins from polyacrylamide gels to nitrocellulose sheets: procedure and some applications. *Proc Natl Acad Sci U S A* **76**, 4350–4354 (1979).

157. Giulietti, A. *et al.* An overview of real-time quantitative PCR: applications to quantify cytokine gene expression. *Methods* **25**, 386–401 (2001).

158. Grunert, S., Jechlinger, M. & Beug, H. Diverse cellular and molecular mechanisms contribute to epithelial plasticity and metastasis. *Nat Rev Mol Cell Biol* **4**, 657–665 (2003).

159. Turley, E. A., Veiseh, M., Radisky, D. C. & Bissell, M. J. Mechanisms of disease: epithelial-mesenchymal transition-- does cellular plasticity fuel neoplastic progression? *Nat Clin Pr. Oncol* **5**, 280–290 (2008).

160.   Rowley, T. Flow Cytometry - A Survey and the Basics. *Mater. Methods* **2**, (2012).

161.   Kupferman, M. E. *et al.* TrkB induces EMT and has a key role in invasion of head and neck squamous cell carcinoma. *Oncogene* **29**, 2047–2059 (2010).

162.   Canel, M. *et al.* Overexpression of focal adhesion kinase in head and neck squamous cell carcinoma is independent of fak gene copy number. *Clin Cancer Res* **12**, 3272–3279 (2006).

163.   Rubashkin, M. G. *et al.* Force engages vinculin and promotes tumor progression by enhancing PI3K activation of phosphatidylinositol (3,4,5)-triphosphate. *Cancer Res.* **74**, 4597–4611 (2014).

164.   Yamamura, M. *et al.* Functional analysis of Zyxin in cell migration and invasive potential of oral squamous cell carcinoma cells. *Int. J. Oncol.* **42**, 873–880 (2013).

165.   Georgescu, C. V, Saftoiu, A., Georgescu, C. C., Ciurea, R. & Ciurea, T. Correlations of proliferation markers, p53 expression and histological findings in colorectal carcinoma. *J Gastrointestin Liver Dis* **16**, 133–139 (2007).

166.   Sperry, R. B. *et al.* Zyxin controls migration in epithelial-mesenchymal transition by mediating actin-membrane linkages at cell-cell junctions. *J Cell Physiol* **222**, 612–624 (2010).

167.   Mise, N. *et al.* Zyxin is a transforming growth factor-beta (TGF-beta)/Smad3 target gene that regulates lung cancer cell motility via integrin alpha5beta1. *J Biol Chem* **287**, 31393–31405 (2012).

168.   Copper, M. P., Triesscheijn, M., Tan, I. B., Ruevekamp, M. C. & Stewart, F. A. Photodynamic therapy in the treatment of multiple primary tumours in the head and neck, located to the oral cavity and oropharynx. *Clin. Otolaryngol.* **32**, 185–189 (2007).

169.   Yamaguchi, S. *et al.* Photodynamic Therapy for Cervical Intraepithelial Neoplasia. *Oncology* **69**, 110–116 (2005).

170.   Kreider, J. W. & Bartlett, G. L. Shope rabbit papilloma--carcinoma complex. A model system of HPV infections. *Clin Dermatol* **3**, 20–26 (1985).

171.   Zhang, H. Thin-film hydration followed by extrusion method for liposome preparation. in *Methods in Molecular Biology* vol. 1522 17–22 (Humana Press Inc., 2017).

172.   Berridge, M. V., Herst, P. M. & Tan, A. S. Tetrazolium dyes as tools in cell biology: New insights into their cellular reduction. *Biotechnology Annual Review* vol. 11 127–152 (2005).

173.   Zelenin, A. V. *et al.* 7-amino-actinomycin D as a specific fluorophore for DNA content analysis by laser flow cytometry. *Cytometry* **5**, 348–354 (1984).

174.   Munshi, A., Hobbs, M. & Meyn, R. E. Clonogenic cell survival assay. *Methods Mol. Med.* **110**, 21–28 (2005).

175.   Rodriguez, L. G., Wu, X. & Guan, J. L. Wound-healing assay. *Methods Mol. Biol.* **294**, 23–29 (2005).

176.   Schneider, C. A., Rasband, W. S. & Eliceiri, K. W. NIH Image to ImageJ: 25 years of image analysis. *Nature Methods* vol. 9 671–675 (2012).

177.   Yue, P. Y. K., Leung, E. P. Y., Mak, N. K. & Wong, R. N. S. A Simplified Method for Quantifying Cell Migration/Wound Healing in 96-Well Plates. *J. Biomol. Screen.* **15**, 427–433 (2010).

178.   Bonfim, C. M. do *et al.* Antiviral activity of curcumin-nanoemulsion associated with photodynamic therapy in vulvar cell lines transducing different variants of HPV-16. *Artif. Cells, Nanomedicine Biotechnol.* **48**, 515–524 (2020).

179.   Mosmann, T. Rapid colorimetric assay for cellular growth and survival: Application to proliferation and cytotoxicity assays. *J. Immunol. Methods* **65**, 55–63 (1983).

180.   López-Jornet, P., Camacho-Alonso, F. & Gómez-Garcia, F. Effect of curcumin and irradiation in PE/CA-PJ15 oral

squamous cell carcinoma. *Acta Odontol. Scand.* **69**, 269–273 (2011).

181.   Berney, M., Hammes, F., Bosshard, F., Weilenmann, H.-U. & Egli, T. Assessment and Interpretation of Bacterial Viability by Using the LIVE/DEAD BacLight Kit in Combination with Flow Cytometry. *Appl. Environ. Microbiol.* **73**, 3283–3290 (2007).

182.   Raveendran, R., Bhuvaneshwar, G. S. & Sharma, C. P. Hemocompatible curcumin-dextran micelles as pH sensitive pro-drugs for enhanced therapeutic efficacy in cancer cells. *Carbohydr. Polym.* **137**, 497–507 (2016).

183.   Yamaguchi, H., Wyckoff, J. & Condeelis, J. Cell migration in tumors. *Current Opinion in Cell Biology* vol. 17 559–564 (2005).

184.   Guan, X. Cancer metastases: Challenges and opportunities. *Acta Pharmaceutica Sinica B* vol. 5 402–418 (2015).

185.   Dielschneider, R. F., Henson, E. S. & Gibson, S. B. Lysosomes as Oxidative Targets for Cancer Therapy. *Oxid. Med. Cell. Longev.* **2017**, 3749157 (2017).

186.   Halaby, R. Role of lysosomes in cancer therapy. *Res. Rep. Biol.* **6**, 147 (2015).

187.   Domagala, A. *et al.* Typical and atypical inducers of lysosomal cell death: A promising anticancer strategy. *International Journal of Molecular Sciences* vol. 19 2256 (2018).

188.   Kozak, M. An analysis of 5'-noncoding sequences from 699 vertebrate messenger RNAs. *Nucleic Acids Res* **15**, 8125–8148 (1987).

189.   Sambrook, J., Fritsch, E. F. & Maniatis, T. *Molecular cloning: a laboratory manual*. (Cold spring harbor laboratory press, 1989).

190.   ExPASy - Compute pI/Mw tool. https://web.expasy.org/compute_pi/.

191.   Dong, X., Stothard, P., Forsythe, I. J. & Wishart, D. S. PlasMapper: A web server for drawing and auto-annotating plasmid maps. *Nucleic Acids Res.* **32**, W660-4 (2004).

192.   Vaeteewoottacharn, K., Chamutpong, S., Ponglikitmongkol, M. & Angeletti, P. C. Differential localization of HPV16 E6 splice products with E6-associated protein. *Virol. J.* **2**, 50 (2005).

193.   Jackson, R., Togtema, M. & Zehbe, I. Subcellular localization and quantitation of the human papillomavirus type 16 E6 oncoprotein through immunocytochemistry detection. *Virology* **435**, 425–432 (2013).

194.   Laurson, J. & Raj, K. Localisation of human papillomavirus 16 E7 oncoprotein changes with cell confluence. *PLoS One* **6**, (2011).

195.   Dreier, K. *et al.* Subcellular localization of the human papillomavirus 16 E7 oncoprotein in CaSki cells and its detection in cervical adenocarcinoma and adenocarcinoma in situ. *Virology* **409**, 54–68 (2011).

196.   Dagona, A. G. BioEdit: a user-friendly biological sequence alignment editor and analysis program for Windows 95/98/NT. *Nucleic Acids Symp. Ser.*

197.   Primer designing tool. https://www.ncbi.nlm.nih.gov/tools/primer-blast/.

198.   Library, T. H. S. Research Guides: Mendeley Basics: Overview.

6.3 *Lists*

6.3.1   Lists of Abbreviation

APS	Ammoniumpersulphate
ATCC	American Type Culture Collection
BSA	Bovine serum albumin
Ca^{2+}	Calcium
CLSM	Confocal laser scanning microscopy
CRPV	Cottontail rabbit papilloma virus
Cur.lipo	Curcumin liposomes
DAPI	4',6'-diamidino-2-phenylindole
DMEM	Dulbecco's Modified Eagle Medium
DMSO	Dimethylsulfoxide
DOPE	1,2-dioleoyl-sn-glycero-3-phosphoethanolamine
DPPC	1,2-dipalmitoylphosphatidylcholine
DSPC	1,2-distearoyl-sn-glycero-3-phosphocholine
DSPG	1,2-Distearoyl-sn-glycero-3-phosphoglycerol
ECL	Enhanced chemiluminescence
EDTA	Ethylene diaminetetraacetic acid
EGFP	Enhanced green fluorescent protein
EMT	Epithelial to mesenhymal transition
FACS	Florescence activated cell sorting
E6-AP	E6 associated protein
FBS	Fetal bovine serum
FITC	Fluorescein isothiocyanate
FSC	Forward scatter
GFP	Green fluorescent protein
HEPES	4-(2-hydroxyethyl)-1-piperazineethanesulfonic acid
HNSCC	Head and neck squamous cell carcinoma
HPV	Human Papilloma Virus

HRP	Horseradish peroxidase
kDa	kilodalton
LB	Luria- Bertani
Mg^{2+}	Magnesium
MTT	3-(4,5-dimethylthiazolyl-2)-2,5-diphenyltetrazolium bromide
MW	Molecular weight
N/P ration	Nitrogen to Phosphate ratio
NZWR	New Zealand white rabbit
NP40	Nonidet P 40 substitute
pDNA	Plasmid DNA
PEI	Polyethylenimine
PI	Propidium iodide
PAGE	Polyacrylamide gel electrophoresis
PBS	Phosphate buffered saline
PDT	Photodynamic therapy
RE	Restriction enzyme
RFP	Red florescence protein
ROS	Reactive oxygen species
RT-PCR	Reverse transcriptase polymerase chain reaction
SCC	Squamous cell carcinoma
S.D	Standard deviation
SSC	Side scatter
WT	Wild type

6.4 *List of materials, devices and softwares*

Chemicals and Reagents

Reagents	Sources
Ampicillin	Sigma Aldrich Chemie GmbH, Taufkirchen, Germany
Agarose	Invitrogen Life Technologies, Scotland, UK
Agarose	Carl Roth GmbH & Co. KG, Karlsruhe, Germany
BSA	(PAA Laboratories, Pasching, Austria
Cholesterol	Sigma Aldrich Chemie GmbH, Taufkirchen, Germany
Curcumin	Sigma Aldrich Chemie GmbH, Taufkirchen, Germany
DAPI	Sigma Aldrich Chemie GmbH, Taufkirchen, Germany
DAPI	Roche Diagnostics, Indianapolis, IN, USA
DMSO $\geq$ 99%	Carl Roth GmbH & Co. KG, Karlsruhe, Germany
DOPE and DPPC	Gift samples from Lipoid AG, Steinhausen, Switzerland.
DSPC, DSPG	Lipoid GmbH, Ludwigshafen, Germany
Dulbecco's PBS	Biochrom AG, Berlin
ECL Westren Blotting substrate	Amersham Biosciences, Buckinghamshire, United Kingdom
EDTA	Roth, Karlsruhe, Germany
Ethanol	Carl Roth GmbH & Co. KG, Karlsruhe, Germany
Formaldehyde	Carl Roth, Karlsruhe, Germany
Formaldehyde	Sigma Aldrich Chemie GmbH, Steinheim, Germany
Fluorescent Mounting Medium	Dako, CA, USA
Glycerol	Carl Roth, Karlsruhe, Germany

HEPES Buffer	Sigma Aldrich Chemie GmbH, Taufkirchen, German
Hydrochlorid acid)	Merck, Darmstadt
Kanamycin	Sigma Aldrich Chemie GmbH, Taufkirchen, German
LB Agar & LB broth	Sigma-Aldrich, St. Louis, MO, USA
Medical X-ray film	Agfa, Cologne, Germany
Mercaptoethanol	Sigma-Aldrich, St. Louis, MO, USA
Methanol	Sigma-Aldrich, St. Louis, MO, USA
MilliQ® Water	Millipore Corporation, Billerica, USA
MTT dye	Sigma Aldrich Chemie GmbH, Taufkirchen, German
Nitrocellulose membrane	GE Healthcare, Germany
Non-fluorescent FluorSave™	Calbiochem Corporation, La Jolla, USA
Nonidet P40 Substitute (NP40)	Sigma-Aldrich, St. Louis, MO, USA
PEI MAX; Linear PEI 22 kDaa	Polysciences Europe GmbH, Hirschberg, Germany
pcDNA 3.0	Invitrogen Corporation, Carlsbad, CA, USA
pEGFP-C1 (PT 3028-5)	BD Biosciences Clontech, CA, USA
pDsRED-Monomer-C1 (PT 3796)	Clontech laboratories, CA, USA
Precision Plus Protein All Blue Standards	Bio-Rad Laboratories, München, Germany
Precision Plus Protein™ Standard (161-0373)	Biorad Hercules, CA, USA
Protease and phosphatase inhibitors	Sigma-Aldrich, Saint Louis, MO, USA
Propidium Iodide	Sigma-Aldrich, Saint Louis, MO, USA

Ribonuclease A	Sigma-Aldrich, St. Louis, MO, USA
SodiumDodecylsulfate (SDS)	Serva Electrophoresis, Heidelberg
Sodium-Chloride	Merck, Darmstadt, Germany
Sodiumhydroxide	Fisher Scientific, Leicestershire, UK
Skim milk powder	Merck, Darmstadt, Germany
Tetramethylethylenediamine (TEMED	Roth, Karlsruhe, Germany
Tris	Merck KG, Darmstadt, Germany
Tris-HCL	Roth, Karlsruhe, Germany
Tween-20	Roth, Karlsruhe, Germany

Media and supplements for cell culture

Materials	Sources
Amphotericin B	Biochrom AG, Berlin, Germany
DMEM	Capricon Scientific, Ebsdorfergrund, Germany
DMEM	PAA Laboratories, Pasching, Austria
DMEM/ Ham`s F-12	Capricon Scientific, Ebsdorfergrund, Germany
DMSO	Carl Roth, Karlsruhe, Germany
DMSO	Merck KG, Darmstadt, Germany
Fetal bovine serum	Capricon Scientific, Ebsdorfergrund, Germany
Fetal bovine serum	Biochrom AG, Berlin, Germany
Gentamicin	Biochrom AG, Berlin, Germany

Penicillin/ Streptomycin	Capricon Scientific, Ebsdorfergrund, Germany
Trypsin/ EDTA solution	Biochrom AG, Berlin, Germany
Trypsin/ EDTA solution	PAA, Laboratories, Pasching, Austria

Molecular biological and biochemical kits

Kits	Sources
Annexin V-FITC /PI kit	R&D Systems, Minneapolis, Canada
First strand cDNA-Synthesis Kit	Roche Diagnostics, Mannheim, Germany
Live/ Dead assay staining kit	Invitrogen™, Oregon, USA
Lyso® tracker red DND-99	Thermo Fischer Scientific, Dreieich, Germany
PowerUp™ SYBR® Green Master Mix	Applied Biosystems, Darmstadt, Germany
PowerUp™ SYBR® Green Master Mix	Thermo Fischer Scientific, Dreieich, Germany
PowerUp™ Green Master Mix	Applied Biosystems, Vilnius, Lithuania
QIAquick Gel Extraction Kit	Qiagen, Hilden, Germany
QIAprep spin Miniprep Kit	Qiagen, Hilden, Germany
QIAprep plasmid Midiprep Kit	Qiagen, Hilden, Germany
REDTaq® ReadyMix™ PCR Reaction Mix	Sigma-Aldrich, St. Louis, MO, USA

Consumables

Items	Sources
Microscopy Slides	Carl Roth GmbH & Co. KG, Karlsruhe, Germany

Petri Dishes; Tissue Culture grade	Sarstedt AG & Co., Nümbrecht, Germany
0.2 µm PES syringe filters	Sarstedt AG & Co. KG, Nümbrecht, Germany
18 mm cover slips	Gerhard Menzel B.V. & Co. KG, Braunschweig, Germany
6-well plates; TC Standard. F	(Sarstedt AG & Co. KG, Nümbrecht, Germany
96-well microtiter plates, Nunclon Delta	Thermo Fischer Scientific, Dreieich, Germany
96-well microtiter plates; CytoOne®	Starlab International GmbH, Hamburg, Germany
40µm nylon mesh	Becton Dickinson, Heidelberg, Germany
0.2 µmol/ L PES syringe filters	Whatman plc, Buckinghamshire, UK
0.2µmol/ L non-pyrogenic filters	Schleicher & Schuell, Dassel, Germany

Technical Instruments & devices

Devices	Manufacturer
Autoclave, Tuttnauer 3850 ELC,	Tuttnauer GmbH, Linden, Germany
Autoradiography cassette	Agfa, Köln, Germany
Bath sonicator; Transonic Digital S	Elmasonic P30H Schmidbauer GmbH, Singen, Germany
BD LSR II Flow cytometer	Becton Dickison, New Jersey, USA
Cell culture hood	Heraeus, Hanau, Germany
Cell counter R1	Olympus Corporation, Tokyo, Japan
Cell counting slides R1-SLI	Olympus Corporation, Tokyo, Japan
Centrifuge (Labofuge 400R)	Medifuge Heraeus, Hanau, Germany

Centrifuge universal (30 F)	Hettich, Tuttllingen
CO2 incubator, HeraCell	Heraus GmbH & Co. KG, Hanau, Germany
Confocal laser scanning microscope; (Zeiss Axiovert 100 M LSM 510)	Carl Zeiss Microscopy GmbH, Jena, Germany
Confocal laser scanning microscopy (Leica TCS SP2)	Leica Microsystems AG, Wetzlar, Germany
Extruder	Avanti Mini Avanti Polar Lipids Inc., Alabaster, USA
Freezer (-30°C)	PORRKA, Hollola, Finland
Freezer (-86°C)	Sanyo, Bad Neudorf
Hotblock for Tubes	HCL HBT 130, Kobe, Japan
Ice machine	Ziegra, Isernhagen
Incubator Shaker	New Brunswick Scientific, Edison, NJ, USA
Laborota 4000 Rotary Evaporator	Heidolph Instruments, Schwabach, Germany
Laminar Flow Hood; Labogene	LMS GmbH &Co.KG, Brigachtal, Germany
LED irradiator	Lumundus GmbH, Eisenach, Germany
Luminometer; FLUOstar® Optima	BMG Labtech, Ortenberg, Germany
Magnetic Stirrer; MCS 66	CAT Scientific, Paso Robles, USA
Microscope	CKX-53 Olympus, USA
MoFlo™ Astrios cell sorter	Beckman Coulter, Indiana, USA
NanoPhotometer® NP80	IMPLEN, Munchen, Germany
QuantStudio® TM5 System	Thermo Fischer, CA, USA

Refrigerator (+ 4°C)	PORRKA, Hollola, Finland
Shaking Incubator; IKA KS4000 IC	IKA Werke & Co. KG, Staufen, Germany
TProfesional Thermocycler	Biometra, Göttingen, Germany
Ultraviolet Transilluminator	UVP, Upland, CA, USA
Vacuum Pump; SC 920	KNF Neuberger GmbH, Freiburg, Germany
Water Bath	Kottermann GmbH & Co. KG, Hänigsen,

Softwares

- BD FACSDiva 7.0 software (Becton Dickison and Company, CA, USA
- FlowJo 10.6.2 (Ashland, OR, USA)
- Image J analysis software (MRI_ wound healing tool) (NIH, Maryland, USA)
- Multiple sequence alignment (MultAlin online, Tolouse, France)
- BioEdit software (v7.0.5.3) [196]
- NCBI/Primer-BLAST [197]
- ExPASy tool
- PlasMapper 2.0 software tool [191]
- Mendeley citation tool (Tauban Health science library, University of Michigan)[198]

6.4.1 List of Figures

6.4.2   List of Tables

6.4.3   Research Outputs

1. **Ambreen, G**.; Duse, L.; Tariq, I.; Ali, U.; Ali, S.; Pinnapireddy, S.R.; Bette, M.; Bakowsky, U.; Mandic, R. Sensitivity of Papilloma Virus-Associated Cell Lines to Photodynamic Therapy with Curcumin-Loaded Liposomes. *Cancers* **2020**, *12*, 3278.

2. Somaida, A.; Tariq, I.; **Ambreen, G**.; Abdelsalam, A.M.; Ayoub, A.M.; Wojcik, M.; Dzoyem, J.P.; Bakowsky, U. Potent Cytotoxicity of Four Cameroonian Plant Extracts on Different Cancer Cell Lines. *Pharmaceuticals* **2020**, *13*, 357

3. Tariq I, Ali MY, Janga H, Ali S, Amin MU, **Ambreen G**, Ali U, Pinnapireddy SR, Schäfer J, Schulte LN, Bakowsky U. Downregulation of MDR 1 gene contributes to tyrosine kinase inhibitor induce apoptosis and reduction in tumor metastasis: A gravity to space investigation. Int J Pharm. 2020 Oct 18; 591: 119993.

4. Ali S, Tariq I, Ali MY, Sohail F, Amin MU, **Ambreen G**, Schäfer J, Bakowsky U. Lipoparticles for synergistic chemo-photodynamic therapy to ovarian carcinoma cells: In vitro and in vivo assessments. 2020, submitted.

5. Saeed Ur Rashid Nazir**, Ghazala Ambreen,** Development and formulation of metformin (*Antidiabetic*) effervescen *Granules*: To increase patient compliance and its stability study. Pak. J. Pharm. Sci., Vol.27, No.4, July 2014, pp.763-766

6.4.4   Award

- DAAD Scholarship (April 2016- April 2020)

6.4.5   Abstracts/ Posters/ Oral Presentations

Didion J, **Ambreen G**, Ali U, Pinnapireddy SR, Stuck BA, Bakowsky U, Bette M, Mandic R. Evaluation of p21$^{CIP1/WAF1}$ expression and the appearance of γH2AX foci after photon based irradiation. 91st Annual Meeting of the German Society of Oto-Rhino-Laryngology, Head and Neck Surgery. 2020, Berlin, Germany. (*Conference paper*)

Ali U, **Ambreen G**, Pinnapireddy SR, Mohr E, Stuck BA, Bakowsky U, Bette M, Mandic R. Establishment and characterization of a VX2 carcinoma derived rabbit cell line for the study of human papilloma virus associated head and neck cancer. 90. Jahresversammlung 2019 "Topic-DIGITALISIERUNG IN DER HNO-HEILKUNDE". 2019, Berlin, Germany. (*Conference paper*)

Ambreen G, Ali U, Pinnapireddy SR, Bette M, Mandic R, Bakowsky U. Generation, validation and expression of cottontail rabbit papilloma virus E6 & E7 recombinant plasmids. 23rd Annual Meeting of Controlled Release Society, German Local Chapter (Functional Biomaterials and Release of Nucleic Acid Drugs. March 7-8, 2019, Leipzig, Germany. (*Oral presentation*)

Ambreen G, Ali U, Pinnapireddy SR, Mohr E, Stuck BA, Bakowsky U, Bette M, Mandic R. Targeting the E6 and E7 cottontail rabbit papillomavirus (CRPV) oncoproteins using low toxicity lipopolyplex enclosed siRNA as a paradigm for the treatment of human HPV-associated HNSCC. International Meeting on Precision Oncology and Personalized Medicine for Head and Neck Cancer. 18-19 January 2019, Heidelberg, Germany. (*Poster presentation*)

Mandic R, Bakowsky U, Ali U, **Ambreen G**, Franke N, Marquart A, Mack E, Stuck BA, Bette M. The VX2 carcinoma of the rabbit as a suitable animal model for papilloma virus associated head and neck squamous cell carcinomas. 2nd International Symposium on Tumor-Host Interaction in Head and Neck Cancer and 3rd International Symposium on HPV Infection in Head and Neck Cancer, 25–27 January 2018 in Essen, Germany. (*Poster presentation*)

Ambreen G, Ali U, Pinnapireddy SR, Mohr E, Bakowsky U, Bette M, Mandic R. Establishment and characterization of VX2 cell line. 21st Annual Meeting of Controlled Release Society, German Local Chapter "Future Trends in Nanomedicine" March 2-3, 2017, Marburg, Germany. (*Poster presentation*)

6.4.6 Curriculum Vitae

Personal Detail

Name	Ghazala Ambreen
Date of Birth	08 November 1984
Place of birth	Sargodha, Pakistan
Marital Status	Married (1 child)
Nationality	Pakistan

Professional Experience: Academic

2012-2014

Lecturer
University of Faisalabad, Punjab, Pakistan
Deliver various lectures on Pharmaceutical technology, Industrial Pharmacy, Pharmaceutical preparation, and Instrumental techniques at graduate level, Conduct internal & external practical exams.

2009-2010

Teaching Assistant
University Of Sargodha, Punjab, Pakistan
Conduct presentations on topics like cGMP, Role of QC & QA in industry, and Product Development, Assist teachers during Lab experiments & examinations

Professional Experience: Industrial

2010-2012

QC & QA Officer

Envoy Pharmaceutical Pvt Ltd.

QC testing of raw material/ intermediate/ finished products using UV-Vis Spectrophotometer, HPLC, Dissolution, Disintegration Apparatus.

Assist in preparing for and supporting external and internal audits.

Conducting various training programs i.e. "Good Laboratory Practices"

Feb-Sep 2009	**Production Pharmacist**
	Envoy Pharmaceutical Pvt Ltd.
	Responsible for generation of daily production report & IPC of tablets, capsules and powder for oral suspensions sections and maintaining BMR

Qualification:

2016- till date	**Ph.D (Pharmaceutical Technology)**
	Philipps-Universität Marburg
	Research Project: Establishment of *in vitro* expression system for CRPV as alternative approach to study HPV associated HNSCC
2009-2011	**M.Phil [Pharmaceutics]**
	University of Sargodha, Pakistan
	Research Project: "Development of formulation of Metformin effervescent granules and its pharmaceutical Characterization"
	CGPA=3.44/4
2003-2008	**Doctor of Pharmacy [Pharm-D]**
	University of Sargodha, Pakistan
	CGPA=3.24/4
2003	**F.Sc [Pre-medical]**
	Army Public School &College, Sargodha, Pakistan
	Grade A
2000	**Matriculation**
	Fauji Foundation Model School Sargodha, Pakistan
	Grade = A+

6.4.7 Acknowledgement

This research project was conceived by Prof. Dr. Udo Bakowsky, Institute of Pharmaceutical Technology and Biopharmacy, Philipps University Marburg with mutual affiliation of Prof. Dr. Robert Mandic, Universitätsklinikum Gießen und Marburg GmbH, Philipps-Universität Marburg and was performed from 2016 to 2020.

I would like to extend a special gratitude towards Prof. Dr. Udo Bakowsky for his immense guidance, support and thorough encouragement throughout the course of my doctoral studies. I would also like to thank profusely to Prof. Dr. Robert Mandic for his commitment, abundant motivation and great ideas to carry on this research work. A special note of appreciation for Prof. Dr. Michael Bette for his kind words of wisdom and uplifting encouragement.

I would like to tremendously appreciate and thanks Dr. Shashank Pinnapireddy for being an amazing group leader, for his guidance and technical support. A very special note of acknowledgement and gratitude for Imran Tariq, Sajid, Lili Duse, Umair Amin and Konrad Engelhardt for all the cooperation and support throughout the journey of this project. I am indebted to the kindness and guidance offered to me by Ms. Roswitha Peldszus, Ms. Grazyna Sadowski, Gavin Giel and Ms. Eva Maria Mohr by their technical support and knowledge. I would especially like to thank Julia Michaelis for ever being so understanding, humble and supportive.

I offer my deepest regards to my friends and colleagues Ms Uzma, Ms Bushra and Ms Tanzeela for being my pillars of strength and never letting me give up.

I am really greatful to HECpakistan and DAAD for providing me scholarship and make it possible for me to get higher education.

My heart is full of gratitude for my family members, my dear husband Mr. Shahid Ramzan, my sweet and lovely son Haider Sultan, very supportive and kind brothers Mr. Awais and Mr. Ubaid and above all my dearest mother Ms. Riffat Sultana for their unmatchable support, love, encouragement and keeping faith in me. This would not have been possible without them.

I dedicate this thesis to my late father.